UNIVERSIDADE FEDERAL DE SANTA CATARINA
DEPARTAMENTO DE ENGENHARIA MECÂNICA
PROGRAMA DE PÓS-GRADUAÇÃO EM ENGENHARIA MECÂNICA

TESE DE DOUTORADO

MANOEL KOLLING DUTRA

INVESTIGATION OF THE EFFECT OF HOT-WIRE, ELECTROMAGNETIC FIELD (EMF), AND DYNAMIC WIRE FEEDING TECHNIQUES ON WIRE-FEED LASER DIRECTED ENERGY DEPOSITION (L-DED)

FLORIANÓPOLIS
2026

Manoel Kolling Dutra

INVESTIGATION OF THE EFFECT OF HOT-WIRE, ELECTROMAGNETIC FIELD (EMF), AND DYNAMIC WIRE FEEDING TECHNIQUES ON WIRE-FEED LASER DIRECTED ENERGY DEPOSITION (L-DED)

Tese submetida ao Programa de Pós-Graduação em Engenharia Mecânica da Universidade Federal de Santa Catarina para obtenção do título de doutor em Engenharia Mecânica.

Orientador: Prof. Dr. Eng. Milton Pereira
Coorientador: Prof. Dr. Eng. Régis H. Gonçalves e Silva

Florianópolis
2026

Ficha catalográfica gerada por meio de sistema automatizado gerenciado pela BU/UFSC.
Dados inseridos pelo próprio autor.

Kolling Dutra, Manoel
INVESTIGATION OF THE EFFECT OF HOT-WIRE, ELECTROMAGNETIC FIELD (EMF), AND DYNAMIC WIRE FEEDING TECHNIQUES ON WIRE-FEED LASER DIRECTED ENERGY DEPOSITION (L-DED) / Manoel Kolling Dutra ; orientador, Milton Pereira, coorientador, Régis Henrique Gonçalves e Silva, 2026.
115 p.

Tese (doutorado) - Universidade Federal de Santa Catarina, Centro Tecnológico, Programa de Pós-Graduação em Engenharia Mecânica, Florianópolis, 2026.

Inclui referências.

1. Engenharia Mecânica. 2. Laser Directed Energy Deposition. 3. Wire feeding oscillation. 4. Induction heating. 5. Electromagnetic field. I. Pereira, Milton. II. Gonçalves e Silva, Régis Henrique. III. Universidade Federal de Santa Catarina. Programa de Pós-Graduação em Engenharia Mecânica. IV. Título.

Manoel Kolling Dutra

INVESTIGATION OF THE EFFECT OF HOT-WIRE, ELECTROMAGNETIC FIELD (EMF), AND DYNAMIC WIRE FEEDING TECHNIQUES ON WIRE-FEED LASER DIRECTED ENERGY DEPOSITION (L-DED)

O presente trabalho em nível de Doutorado foi aprovado, em 13 de abril de 2026, pela banca examinadora composta pelos seguintes membros:

Prof. Tiago Felipe de Abreu Santos, Dr. Eng.
Universidade Federal de Pernambuco

Prof. Walter Lindolfo Weingaertner, Dr. Ing.
Universidade Federal de Santa Catarina

Prof. Fabio Antônio Xavier, Dr. Eng.
Universidade Federal de Santa Catarina

Certificamos que esta é a versão final do trabalho de conclusão que foi julgado adequado para obtenção do título de Doutor em Engenharia Mecânica atribuído pelo Programa de Pós Graduação em Engenharia Mecânica.

ICP-Edu
Documento assinado digitalmente
Henrique Simas
Data: 16/04/2026 14:18:45-0300
CPF: ***.194.639-**
Verifique as assinaturas em https://v.ufsc.br

Coordenação do Programa de Pós-Graduação

ICP-Edu
Documento assinado digitalmente
Milton Pereira
Data: 16/04/2026 14:39:12-0300
CPF: ***.484.489-**
Verifique as assinaturas em https://v.ufsc.br

Prof. Milton Pereira, Dr. Eng. – Orientador

ICP-Edu
Documento assinado digitalmente
Regis Henrique Goncalves e Silva
Data: 16/04/2026 15:31:37-0300
CPF: ***.436.429-**
Verifique as assinaturas em https://v.ufsc.br

Prof. Régis Henrique Gonçalves e Silva, Dr. Eng. - Coorientador

Florianópolis, Abril de 2026

“A excelência nasce da disciplina aplicada diariamente às pequenas ações.”
Marco Aurélio

AGRADECIMENTOS

Ao meu orientador, Prof. Dr. Eng. Milton Pereira, pelo estímulo constante, atenção e colaboração decisiva ao longo de toda a evolução desta pesquisa. Milton, meu amigo, obrigado por acreditar e confiar em mim. Sem o seu apoio, este trabalho jamais teria sido concretizado.

Ao meu coorientador, Prof. Dr. Eng. Régis Henrique Gonçalves e Silva, pela valiosa colaboração no desenvolvimento desta pesquisa, especialmente no processamento e análise dos dados experimentais provenientes das filmagens de alta velocidade, bem como pela coautoria dos artigos científicos decorrentes deste trabalho.

Aos professores do Programa de Pós-Graduação em Engenharia Mecânica (POSMEC/UFSC), em especial ao Prof. Dr. Eng. Rolf Bertrand Schroeter e ao Prof. Dr. Eng. Fábio Antônio Xavier, pelos conhecimentos transmitidos, pelo incentivo à pesquisa e pela contribuição à minha formação acadêmica.

A toda a equipe do Laboratório de Mecânica de Precisão – LMP/UFSC, que foi minha segunda casa ao longo desta jornada, proporcionando inúmeras oportunidades de crescimento acadêmico e profissional.

Ao Laboratório de Eletromagnetismo e Compatibilidade Eletromagnética – MagLab/UFSC, pelo apoio e suporte nas análises e simulações magnéticas. Meus sinceros agradecimentos ao Prof. Dr. Eng. Adroaldo Raizer e ao amigo e colega Emanoel Pereira Elias.

Ao LABSOLDA/UFSC, por todo o apoio no desenvolvimento deste trabalho, em especial aos amigos Daniel Galeazzi e ao meu grande amigo Cláudio Marques Schaeffer, pelos cafés, pelas conversas inspiradoras e pelo companheirismo ao longo desta trajetória.

Aos meus amigos e colegas de trabalho do LMP/UFSC, que direta ou indiretamente contribuíram para a realização desta pesquisa: Tiago Faria Colvara, Gabriel Rogério, Felipe Lavaqui, Vitória Luise, Renato Panziera, Jurandir, Cassiano Bonin, Igor, Fernando Bordin, Erick Cardoso, Cláudio Abílio da Silveira, e tantos outros que, de alguma forma, colaboraram para que este trabalho se tornasse realidade. Meus sinceros agradecimentos.

À minha família, em especial à minha mãe, Cláudia Kolling, que esteve sempre presente e foi fundamental ao longo de todos esses anos. A Sarita Guarezi, pelo carinho, apoio e presença nos meses finais deste doutorado. Mesmo em tão pouco tempo, sua companhia trouxe leveza, motivação e equilíbrio nos cafés filosóficos.

Por fim, às instituições de ensino que marcaram minha trajetória acadêmica e pessoal: Colégio Visão (São José/SC), Centro Federal de Educação Tecnológica – CEFET-SC (Florianópolis/SC), Instituto Federal de Santa Catarina – IFSC (Florianópolis/SC) e Universidade Federal de Santa Catarina – UFSC (Florianópolis/SC).

RESUMO

A Deposição por Energia Direcionada a Laser alimentada por arame (L-DEDw) tem se destacado como uma tecnologia promissora de manufatura aditiva metálica para a fabricação e o reparo de componentes de médio e grande porte, em função de suas elevadas taxas de deposição, alta eficiência de utilização do material e flexibilidade geométrica. Entretanto, o processo ainda enfrenta desafios relevantes relacionados à instabilidade da transferência metálica, à dinâmica da poça de fusão, à formação de respingos e à elevada sensibilidade às variações de parâmetros operacionais, especialmente quando o arame é alimentado de forma contínua e em seu estado natural. Diante desse contexto, esta tese investiga os efeitos individuais e integrados das técnicas de aquecimento indutivo do arame (hot-wire), aplicação de campo eletromagnético externo (FEM) e alimentação dinâmica do arame no processo L-DED alimentado por arame, com o objetivo de aprimorar a estabilidade da transferência metálica, o comportamento da poça de fusão e a geometria dos cordões depositados. A hipótese central é que a integração dessas técnicas permite um controle mais eficiente da transferência de massa e energia, promovendo maior estabilidade do processo, redução do aporte térmico efetivo e ampliação da janela operacional. Para isso, foi desenvolvido um conceito inédito de alimentador de arame capaz de integrar pré-aquecimento indutivo, aplicação de campo eletromagnético e alimentação dinâmica por meio de oscilações controladas de avanço e recuo do arame. Os experimentos foram realizados utilizando arame ER70S-6 com diâmetro de 1,2 mm e substrato de aço SAE 1020, mantendo parâmetros controlados de potência do laser, velocidade de varredura e velocidade média de alimentação do arame. A caracterização do processo foi conduzida por meio de filmagens de alta velocidade para análise da transferência metálica e da dinâmica da poça de fusão, bem como por análises macrográficas das seções transversais dos cordões, com avaliação de altura, largura, penetração e diluição. Os resultados demonstraram que o aquecimento indutivo do arame altera o balanço térmico do processo, reduzindo a fração de energia do laser necessária para a fusão do material de adição e favorecendo a formação de uma ponte líquida mais estável. A aplicação do campo eletromagnético contribuiu para a estabilização da poça de fusão, reduzindo a ocorrência de respingos e promovendo maior uniformidade geométrica dos cordões, em função da atuação das forças de Lorentz no metal líquido. A alimentação dinâmica do arame introduziu uma modulação temporal controlada da transferência de massa e energia, influenciando diretamente a área da poça de fusão, o ângulo de molhamento e a estabilidade do processo. A análise dessas técnicas permite uma compreensão abrangente de suas influências individuais sobre o comportamento do processo, evidenciando seu potencial como estratégias independentes para a melhoria da estabilidade e da qualidade da deposição no L-DEDw. Adicionalmente, destaca-se que o desenvolvimento do sistema experimental proposto resultou na concepção, projeto e construção de uma infraestrutura inovadora de pesquisa, capaz de integrar aquecimento indutivo, aplicação de campo eletromagnético e alimentação dinâmica do arame em um único arranjo. Essa infraestrutura amplia significativamente as possibilidades de investigação no processo L-DED alimentado por arame, viabilizando a exploração de fenômenos e estratégias de controle anteriormente não acessíveis. Conclui-se que a integração das técnicas de hot-wire, campo eletromagnético e alimentação dinâmica constitui uma abordagem eficaz para o controle avançado do processo L-DED alimentado por arame, apresentando elevado potencial para aplicações industriais em manufatura aditiva metálica e revestimentos a laser.

Palavras-chave: Manufatura aditiva; Deposição por energia direcionada a laser; Alimentação de arame; Aquecimento indutivo; Campo eletromagnético; Transferência metálica.

ABSTRACT

Wire-fed Laser Directed Energy Deposition (W-LDED) has emerged as a promising metal additive manufacturing technology for the fabrication and repair of medium- and large-scale components, due to its high deposition rates, efficient material utilization, and geometric flexibility. Nevertheless, the process still faces significant challenges related to metal transfer instability, melt-pool dynamics, spatter formation, and strong sensitivity to process parameter variations, particularly when the filler wire is supplied continuously and without thermal or kinematic conditioning. In this context, this doctoral thesis investigates the individual and combined effects of inductive wire preheating (hot-wire), external electromagnetic field assistance (EMF), and dynamic wire feeding on the wire-fed L-DED process, aiming to improve metal transfer stability, melt-pool behavior, and deposited bead geometry. The central hypothesis is that the application of these techniques enables more effective control of mass and energy transfer, leading to enhanced process stability, reduced effective heat input, and an expanded operational window. To achieve this objective, a novel wire-feeding system was developed, capable of integrating inductive preheating, electromagnetic field application, and dynamic wire feeding through controlled forward–backward oscillations of the wire. Experimental investigations were conducted using ER70S-6 wire with a diameter of 1.2 mm deposited onto SAE 1020 steel substrates, under controlled laser power, scanning speed, and average wire feed rate. Process characterization was performed through high-speed imaging to analyze metal transfer behavior and melt-pool dynamics, as well as macrographic analysis of bead cross-sections to evaluate height, width, penetration, and dilution. The results demonstrate that inductive wire preheating modifies the thermal balance of the process, reducing the fraction of laser energy required to melt the filler material and promoting the formation of a more stable liquid bridge. Electromagnetic field assistance contributes to melt-pool stabilization, reducing spatter occurrence and improving bead geometric uniformity through the action of Lorentz forces on the molten metal. Dynamic wire feeding introduces a controlled temporal modulation of mass and energy transfer, directly influencing melt-pool area, contact angle, and overall process stability. The analysis of these techniques provides a comprehensive understanding of their individual influence on process behavior, highlighting their potential as independent strategies for improving stability and deposition quality in W-LDED. Additionally, the development of the experimental system enabled the conception, design, and construction of an innovative research infrastructure, capable of integrating inductive heating, electromagnetic field application, and dynamic wire feeding within a single setup. This infrastructure significantly expands the research possibilities in wire-based L-DED, enabling the investigation of phenomena and control strategies that were previously not accessible. It is concluded that the integration of hot-wire preheating, electromagnetic field assistance, and dynamic wire feeding constitutes an effective strategy for advanced process control in wire-fed L-DED, with strong potential for industrial applications in metal additive manufacturing and laser-based surface coating.

Key words: 3D Printing; Laser directed energy deposition; Wire feeding oscillation; Induction heating; Electromagnetic field; Metal transfer.

RESUMO EXPANDIDO

Introdução:

A deposição de energia direcionada a laser alimentada por arame (L-DEDw) tem se destacado como uma tecnologia promissora de manufatura aditiva metálica para fabricação e reparo de componentes de médio e grande porte, em função de suas elevadas taxas de deposição, alta eficiência energética e melhor aproveitamento do material quando comparada aos processos baseados em pó. Apesar dessas vantagens, o processo ainda enfrenta desafios significativos relacionados à instabilidade da transferência metálica, flutuações da poça de fusão, formação de respingos, elevada diluição e sensibilidade às variações de parâmetros operacionais. Esses fenômenos estão fortemente associados aos complexos mecanismos termo fluidodinâmicos que governam a interação entre o arame, a poça de fusão e o feixe laser.

Nos sistemas convencionais de L-DEDw, o controle do processo é majoritariamente passivo, limitado à definição de parâmetros fixos de potência do laser, velocidade de varredura e taxa de alimentação de arame. Tal abordagem restringe a capacidade de adaptação do processo frente às variações dinâmicas inerentes à deposição, especialmente durante regimes de ponte líquida e transições de transferência metálica. Nesse contexto, estratégias avançadas de controle térmico, eletromagnético e cinemático emergem como alternativas para ampliar a robustez e a estabilidade do processo.

A presente tese de doutorado propõe e investiga uma abordagem para o controle do processo L-DEDw, baseada na aplicação de três técnicas: aquecimento indutivo do arame (hot-wire), aplicação de campo eletromagnético externo (FEM) e alimentação dinâmica do arame. A hipótese central é que a atuação desses mecanismos permite controlar de forma mais eficaz a transferência metálica, a dinâmica da poça de fusão e a geometria do cordão depositado, ampliando a janela operacional do processo.

Objetivos:

O objetivo geral desta tese é investigar os efeitos individuais das técnicas de aquecimento indutivo do arame (hot-wire), aplicação de campo eletromagnético (FEM) e alimentação dinâmica do arame no processo de deposição por energia direcionada a laser alimentada por arame (L-DEDw), visando à melhoria da estabilidade da transferência metálica, do comportamento da poça de fusão e da geometria dos cordões depositados.

De forma específica, este trabalho busca:

I) desenvolver e caracterizar um sistema de aquecimento indutivo para pré-aquecimento do arame no processo L-DEDw;

II) avaliar a influência do campo eletromagnético aplicado na dinâmica da poça de fusão e na estabilidade da transferência metálica;

III) investigar o efeito da alimentação dinâmica do arame, por meio de oscilações controladas de avanço e recuo, sobre o comportamento da poça de fusão;

IV) analisar os efeitos da aplicação das três técnicas, baseado nos resultados individuais de cada técnica;

V) correlacionar os mecanismos físicos observados com a geometria final dos cordões depositados.

Materiais e métodos:

Os experimentos foram realizados em um sistema L-DEDw equipado com laser de fibra de alta potência, utilizando arame de aço carbono ER70S-6 com diâmetro de 1,2 mm, depositado sobre substrato de aço SAE 1020. O sistema experimental foi modificado para incorporar um dispositivo de aquecimento indutivo do arame, uma bobina geradora de campo eletromagnético estático na região da poça de fusão e um mecanismo de alimentação dinâmica do arame acionado por servomotor, que foram desenvolvidos no âmbito deste trabalho.

Os ensaios foram conduzidos mantendo parâmetros fixos de potência do laser, velocidade de varredura e velocidade média de alimentação do arame, de modo a isolar os efeitos das técnicas investigadas. A transferência metálica e o comportamento da poça de fusão foram analisados por meio de filmagens de alta velocidade, enquanto a geometria dos cordões foi avaliada por macrografia da seção transversal, com medições de altura, largura, penetração e diluição.

Foram realizadas comparações entre deposições convencionais (arame frio e alimentação contínua) e deposições assistidas individualmente por hot-wire, FEM e alimentação dinâmica.

Resultados e discussões:

Os resultados demonstraram que o aquecimento indutivo do arame promoveu uma modificação significativa no balanço térmico do processo, reduzindo a energia necessária para a fusão do arame e encurtando a distância entre o arame sólido e a poça de fusão. Esse efeito

favoreceu a formação de uma ponte líquida mais estável, resultando em cordões com menor altura e maior penetração.

A aplicação do campo eletromagnético externo mostrou-se eficaz na estabilização da poça de fusão, atuando na atenuação de instabilidades associadas à convecção de Marangoni e à tensão superficial. Observou-se uma redução na ocorrência de respingos e um aumento da uniformidade geométrica dos cordões, evidenciando a atuação das forças de Lorentz no metal líquido.

A alimentação dinâmica do arame introduziu uma modulação temporal controlada da transferência de massa e energia para a poça de fusão. A frequência de oscilação do arame mostrou-se um parâmetro crítico, influenciando diretamente a área da poça, o ângulo de molhamento e a estabilidade da ponte líquida. Foi identificada uma faixa de frequência operacional que equilibra estabilidade e flexibilidade do processo.

Com base na análise dos resultados obtidos individualmente para cada técnica, observa-se que a aplicação combinada apresenta potencial para gerar efeitos superiores àqueles observados isoladamente. Nesse sentido, o sistema híbrido tende a promover maior robustez operacional, controle mais preciso da geometria do cordão e maior estabilidade da transferência metálica, indicando a possibilidade de ampliação da janela de processamento do L-DEDw.

Considerações finais:

Esta tese demonstrou que a aplicação das técnicas de hot-wire indutivo, campo eletromagnético e alimentação dinâmica constitui uma abordagem eficaz para o controle avançado do processo L-DEDw. Os resultados evidenciam que o controle térmico, eletromagnético e cinemático atua de forma complementar sobre os mecanismos físicos da transferência metálica e da dinâmica da poça de fusão.

Do ponto de vista científico, o trabalho contribui para a compreensão aprofundada dos fenômenos envolvidos no L-DEDw, especialmente no regime de ponte líquida. Sob a perspectiva tecnológica, o sistema desenvolvido apresenta elevado potencial de aplicação industrial, oferecendo maior estabilidade, adaptabilidade e qualidade geométrica na deposição por laser com arame.

Palavras-chave:

Manufatura aditiva. Deposição de energia direcionada a laser. Alimentação de arame. Hot-wire. Campo eletromagnético. Transferência metálica.

LIST OF ABREVIATIONS AND ACRONYMS

Abbreviation	Description
AM	Additive Manufacturing
DED	Directed Energy Deposition
EMF	Electromagnetic Field
FEM	Finite Element Method
HW	Hot-Wire
IR	Infrared
L-DED	Laser Directed Energy Deposition
L-DEDw	Deposição por Energia Direcionada a Laser alimentada por arame
LC	Inductor–Capacitor
MA	Manufatura Aditiva
MOSFET	Metal-Oxide-Semiconductor Field-Effect Transistor
RMS	Root Mean Square
UFSC	Universidade Federal de Santa Catarina
W-LDED	Wire-Laser Directed Energy Deposition
ZVS	Zero Voltage Switching

LIST OF SYMBOLS

ARTICLE I – INDUCTIVE HOT-WIRE ASSISTANCE

Symbol	Unit	Description
δ	[mm]	Skin depth
B	[T]	Magnetic flux density
H	[A/m]	Magnetic field intensity
I	[A]	Electric current
N	[–]	Number of turns
f	[Hz]	Frequency
ρ	[Ω·m]	Electrical resistivity
σ	[S/m]	Electrical conductivity
μ	[H/m]	Magnetic permeability
μ_0	[H/m]	Vacuum magnetic permeability
μ_r	[–]	Relative magnetic permeability
$\dot{q}$	[W]	Heat generation rate
$\dot{q}$_conv	[W]	Convective heat dissipation
$\dot{q}$_rad	[W]	Radiative heat dissipation
A	[m²]	Heat exchange surface area
T	[°C]	Temperature
t	[s]	Time
c	[J/(kg·°C)]	Specific heat capacity
m	[kg]	Mass
L	[m]	Length of the coil

ARTICLE II – ELECTROMAGNETIC FIELD ASSISTANCE

Symbol	Unit	Description
B	[T]	Magnetic flux density
H	[A/m]	Magnetic field intensity
J	[A/m²]	Current density
F_L	[N]	Lorentz force
σ	[S/m]	Electrical conductivity
v	[m/s]	Fluid velocity
∇T	[K/m]	Temperature gradient
γ	[N/m]	Surface tension
θ	[°]	Contact angle

ARTICLE III – DYNAMIC WIRE FEEDING

Symbol	Unit	Description
f_osc	[Hz]	Wire oscillation frequency
A_osc	[mm]	Wire oscillation amplitude
v_w	[m/min]	Wire feed speed
t_adv	[s]	Wire advancing time
t_ret	[s]	Wire retracting time
θ	[°]	Contact angle
A_mp	[mm²]	Melt pool area
h	[mm]	Bead height
w	[mm]	Bead width
d	[mm]	Penetration depth

CONTENTS

1 INTRODUCTION 19
1.1 MOTIVATION 20
1.2 FUNDAMENTAL QUESTION 22
1.3 HYPOTHESES 22
1.4 OBJECTIVES 23
1.4.1 Specific Objectives 23
2 INTEGRATION OF THE SCIENTIFIC ARTICLES 24
2.1 ARTICLE I – INDUCTIVE HOT-WIRE ASSISTANCE IN WIRE-LASER DIRECTED ENERGY DEPOSITION 25
2.2 ARTICLE II – ELECTROMAGNETIC FIELD ASSISTANCE FOR METAL TRANSFER STABILIZATION 26
2.3 ARTICLE III – DYNAMIC WIRE FEEDING AS AN ACTIVE PROCESS CONTROL STRATEGY 27
3 EVALUATION OF MAGNETIC FIELD BEHAVIOR AND HEATING EFFICIENCY OF AN INDUCTIVE PREHEATING COIL FOR WIRE-BASED LASER ENERGY DEPOSITION (L-DED) 29
3.1 INTRODUCTION 30
3.2 SYSTEM DESCRIPTION 32
3.2.1 Inductive coil configuration 32
3.2.2 LC Resonant circuit characteristics 33
3.3 ELECTROMAGNETIC ANALYSIS 35
3.3.1 Analytical modeling 36
3.3.1.1 Magnetic field and magnetic induction generation 36
3.3.1.2 Induced current, skin depth and skin effect 36
3.3.1.3 Power dissipation and heat generation in the wire 38
3.3.1.4 Analytical results 39

3.4 FINITE ELEMENT MODELING OF THE MAGNETIC FIELD AND POWER DISSIPATION 39
3.4.1 Simulation setup 40
3.4.2 Simulation results 42
3.5 THERMAL ANALYSIS 44
3.5.1 Heat dissipation by convection 44
3.5.2 Heat dissipation by radiation 46
3.5.3 Thermal balance and temperature elevation 47
3.6 FINITE ELEMENT MODELING OF THE THERMAL DISSIPATION 49
3.6.1 Simulation setup 49
3.6.2 Simulation results 49
3.7 CONCLUSIONS 51
3.8 ACKNOWLEDGEMENTS 52
3.9 REFERENCES 52
4 EFFECT OF THE MAGNETIC FIELD GENERATED BY COIL ON METAL TRANSFER BEHAVIOR IN WIRE-LASER DIRECTED ENERGY DEPOSITION ... 56
4.1 INTRODUCTION 57
4.2 MAGNETIC FIELD GENERATION COIL 59
4.2.1 Design Aspects of the Coil 59
4.2.2 Electromagnetic Simulation 60
4.2.3 Electromagnetic Characterization of the Field Generation Coil 61
4.3 HIGH-SPEED VIDEOGRAPHY ANALYSIS OF METAL TRANSFER 62
4.3.1 Metal Transfer without EMF Assistance 65
4.3.2 Metal Transfer with EMF Assistance 66
4.3.3 Discussion of Physical Mechanisms 71
4.3.4 Melt pool behavior under electromagnetic field assistance 72
4.4 RESULTS AND DISCUSSION 73
4.4.1 Wire Misalignment and Melt Pool Interaction 74

4.5 BEAD GEOMETRY AND DILUTION 77
4.6 CONCLUSIONS 78
4.7 ACKNOWLEDGEMENTS 79
4.8 REFERENCES 80
5 INFLUENCE OF DYNAMIC WIRE FEEDING ON METAL TRANSFER IN LASER-DIRECTED ENERGY DEPOSITION (L-DED) **83**
5.1 INTRODUCTION 84
5.2 DYNAMIC WIRE FEEDING SYSTEM 85
5.2.1 Bench Experiments of the Dynamic Wire Feeder **87**
5.3 HIGH-SPEED VIDEOGRAPHY ANALYSIS OF METAL TRANSFER 89
5.3.1 Continuous Wire Feeding **90**
5.3.2 Dynamic Wire Feeding **92**
5.3.3 Effect of Dynamic Feeding Frequency **93**
5.3.4 Contact Angle Behavior under Dynamic Wire Feeding **94**
5.4 RESULTS AND DISCUSSION 96
5.4.1 Melt-Pool Geometry and Stability **96**
5.4.2 Influence of Feeding Frequency **97**
5.4.3 Contact Angle and Wetting Behavior **98**
5.4.4 Comparative Discussion **98**
5.4.5 Bead Geometry with and without Dynamic Feeding **98**
5.5 CONCLUSIONS 99
5.6 ACKNOWLEDGEMENTS 101
5.7 REFERENCES 101
6 CONCLUSIONS **104**
6.1 SUGGESTIONS FOR FUTURE WORK 108
7 COMPLEMENTARY REFERENCES **110**

1 INTRODUCTION

Laser technology has emerged as a tool of great relevance for industry, particularly in the metal-mechanical sector, often serving as a key instrument for enhancing competitiveness, productivity, and quality (DASS; MORIDI, 2019). Metal additive manufacturing (AM) using laser energy sources is a clear example of this scenario. With the continuous development of laser sources, one of the methods that has gained increasing prominence in metal AM is Laser Directed Energy Deposition (L-DED), which establishes a new paradigm for the production, repair, and design of complex components in various applications, such as automotive, aerospace, medical equipment, naval, and oil and gas industries (GISARIO *et al.*, 2019). In this process, the laser beam is used as a focused energy source, and the deposited material is delivered to a focal point where it is melted and deposited layer by layer (DING *et al.*, 2015; THOMPSON *et al.*, 2015).

When the L-DED method is employed as an AM process for metallic materials, two different types of feedstocks are commonly used: wire and powder (DING *et al.*, 2015). The main advantage of wire-fed L-DED processes is their high material utilization efficiency (DASS; MORIDI, 2019; DING *et al.*, 2015; POOLPERM; NAKKIEW; NAKSUK, 2021). This makes the process particularly advantageous for the production of large-scale and high-volume components. However, wire-fed L-DED processes also present several operational challenges.

To fabricate complex structures, multiple adjacent layers must be deposited side by side (DASS; MORIDI, 2019; DING *et al.*, 2015). During processing, the previously deposited material undergoes multiple heating and cooling cycles, while the feed wire material is subjected to a sequence of heating, melting, solidification, and rapid cooling. The amount of heat supplied to the material strongly influences its final properties (DING *et al.*, 2015).

Compared to conventional wire deposition methods, the use of dynamic wire feeding, hot-wire, and electromagnetic force (EMF) assistance during deposition has demonstrated significant potential to alter metal transfer modes, particularly by transitioning from more turbulent transfer regimes to more stable ones. This transition directly affects the quality of the deposited bead and improves control over metal transfer behavior (HUANG *et al.*, 2021a; HUANG *et al.*, 2014; PENG *et al.*, 2015; RODRIGUES *et al.*, 2020).

Therefore, this doctoral research aims to investigate the effects of hot-wire (LIU *et al.*, 2014; VOIGT, 2019; ZHANG; KONG; KOVACEVIC, 2020), electromagnetic force (EMF) (BACHMANN *et al.*, 2014; CORRADI *et al.*, 2020; NIE *et al.*, 2020), and dynamic wire feeding (DING *et al.*, 2015; POOLPERM; NAKKIEW; NAKSUK, 2021; RODRIGUES *et al.*, 2020) techniques on the wire-fed L-DED process, with the objective of evaluating process behavior and achieving a significant improvement in process stability compared to currently available results. In addition, it is hypothesized that the integration of these techniques into the process enables additive manufacturing with reduced thermal input, improved stability, and enhanced control of metal transfer.

The wire-fed L-DED process integrating hot-wire, EMF, and dynamic wire feeding remains scarcely explored, and the number of studies in additive manufacturing employing these combined techniques is still limited. The advancement of metallic component fabrication through layer-by-layer deposition represents one of the potential applications of this innovative "hybrid" process, which currently lacks comprehensive scientific development. These characteristic positions the present research proposal as a scientific and technological advancement that may foster future investigations. Improving this processing technique and addressing this gap in the existing literature constitute an original and substantial contribution of this doctoral thesis. It is expected that the development of this work will lead to technical and scientific results capable of generating publications in high-impact journals and potentially supporting the filing of a patent application for the developed device

1.1 MOTIVATION

Wire-fed Laser Directed Energy Deposition (W-LDED) has attracted increasing interest due to its high deposition rates, efficient material utilization, and suitability for manufacturing and repairing large-scale metallic components (DING *et al.*, 2015; DASS and MORIDI, 2019). However, despite these advantages, the process remains strongly limited by instabilities in metal transfer and melt-pool dynamics, which often result in spatter formation, irregular bead geometry, and excessive dilution, compromising process robustness and deposition quality (DING *et al.*, 2015; THOMPSON *et al.*, 2015).

One of the main challenges in W-LDED lies in achieving stable liquid-bridge transfer under practical processing conditions. Metal transfer behavior is highly sensitive to thermal gradients, surface tension forces, and wire–pool interaction, making the process susceptible to oscillations and transfer mode transitions (PENG *et al.*, 2015; FU *et al.*, 2024). These effects are further intensified in multilayer depositions, where cumulative thermal input and geometric tolerances amplify instability (GHASEMPOUR-MOUZIRAJI *et al.*, 2024).

Several auxiliary techniques have been proposed to mitigate these limitations. Wire preheating using hot-wire technology has been shown to reduce the laser energy required for wire melting, improving thermal efficiency and reducing dilution (PENG *et al.*, 2015; KISIELEWICZ *et al.*, 2021). Nevertheless, hot-wire alone does not fully suppress melt-pool oscillations or spatter when disturbances occur.

More recently, the application of electromagnetic fields (EMF) has emerged as a promising strategy to influence melt-pool behavior in laser-based deposition processes. Studies have demonstrated that Lorentz forces generated by external magnetic fields can damp Marangoni-driven convection, stabilize molten metal flow, and reduce dilution (BACHMANN *et al.*, 2014; CORRADI *et al.*, 2020; NIE *et al.*, 2020). However, most investigations have focused on powder-based systems or isolated EMF effects, leaving wire-fed processes comparatively underexplored.

In parallel, dynamic wire feeding strategies, based on periodic modulation of wire advancement and retraction, have been proposed as an effective means to control melt-pool geometry and metal transfer behavior (DING *et al.*, 2015; SONG *et al.*, 2023; LI *et al.*, 2022). These studies indicate that dynamic feeding can actively redistribute energy between the wire and the substrate, influencing wetting behavior and deposition stability. Nonetheless, dynamic feeding has typically been investigated independently, without considering its interaction with electromagnetic or thermal assistance.

Therefore, although hot-wire preheating, electromagnetic field assistance, and dynamic wire feeding have individually demonstrated potential to improve W-LDED performance, the use of a system capable of integrating these three techniques remains scarcely explored in the literature. The lack of systematic experimental studies addressing the combined effects of these techniques represents a clear scientific gap. Addressing this gap is essential for advancing

process stability, reducing sensitivity to disturbances, and enabling more robust industrial implementation of wire-based laser additive manufacturing.

1.2 FUNDAMENTAL QUESTION

Based on the current state of the art and the identified scientific gap, the following fundamental research question is formulated:

How can the application of hot-wire preheating, electromagnetic field assistance, and dynamic wire feeding improve metal transfer stability, melt-pool behavior, and deposition quality in wire-fed Laser Directed Energy Deposition?

1.3 HYPOTHESES

To address the fundamental question, the following central hypothesis is proposed:

The application of inductive hot-wire preheating, electromagnetic field assistance, and dynamic wire feeding promotes more stable metal transfer and improved melt-pool control in W-LDED by reducing thermal gradients, damping surface-tension-driven instabilities, and synchronizing mass and energy transfer, thereby enhancing bead quality and process robustness.

To support and validate this hypothesis, the following scientific hypotheses are implicitly tested throughout this thesis:

- Hot-wire preheating reduces the laser energy required for wire melting, leading to lower dilution and improved thermal efficiency;
- Electromagnetic forces generated by a dedicated coil stabilize liquid-bridge transfer by damping Marangoni-driven convection and delaying droplet detachment;
- Dynamic wire feeding enables controlled modulation of melt-pool geometry and wetting behavior through periodic wire advancement and retraction;
- Each technique, when applied independently, produces measurable improvements in metal transfer stability, melt-pool dynamics, and bead geometry.

1.4 OBJECTIVES

The main objective of this doctoral thesis is to investigate and demonstrate the effects of hot-wire preheating, electromagnetic field assistance, and dynamic wire feeding can enhance metal transfer stability, melt-pool behavior, and deposition quality in wire-fed Laser Directed Energy Deposition.

1.4.1 Specific Objectives

In order to achieve the main objective, the following specific objectives are defined:

- To investigate the individual effects of hot-wire preheating, electromagnetic field assistance, and dynamic wire feeding on metal transfer behavior in W-LDED using high-speed imaging and quantitative analysis;
- To design and develop an integrated hybrid wire-feeding head capable of incorporating hot-wire, EMF, and dynamic feeding functionalities;
- To develop and validate an inductive heating system for controlled wire preheating;
- To implement an electromagnetic coil and switching circuit capable of generating controlled magnetic fields during deposition;
- To implement a control strategy capable of synchronizing wire motion, electromagnetic excitation, and thermal input;
- To evaluate the impact of these techniques on melt-pool geometry, bead morphology, dilution, and process stability.

2 INTEGRATION OF THE SCIENTIFIC ARTICLES

This doctoral thesis is structured in the form of three scientific articles that together constitute a coherent and integrated investigation into metal transfer stabilization and process control in wire-fed Laser Directed Energy Deposition (W-LDED). Each article addresses a specific aspect of the proposed hybrid deposition approach, while collectively contributing to the overarching objective of improving process stability, deposition quality, and robustness through the integration of hot-wire preheating, electromagnetic field assistance, and dynamic wire feeding.

The integration of the articles follows a logical and progressive structure, in which fundamental process characterization is first established, followed by the investigation of electromagnetic and thermal assistance, and finally by the assessment of dynamic wire feeding as an active control strategy. This approach allows a systematic exploration of individual mechanisms as well as their combined effects within the W-LDED process.

The first article establishes the experimental and analytical foundations of the research by characterizing metal transfer behavior and melt-pool dynamics under baseline conditions and under the application of inductive wire preheating. The results demonstrate that hot-wire preheating reduces the laser energy required for wire melting, alters the thermal balance between wire and substrate, and directly influences melt-pool geometry and dilution. High-speed imaging reveals changes in liquid-bridge formation and stability, providing quantitative evidence of the role of thermal assistance in controlling metal transfer mechanisms.

Building upon this foundation, the second article investigates the influence of an externally applied electromagnetic field on metal transfer behavior and melt-pool stability in W-LDED. In this study, a dedicated electromagnetic coil is integrated into the deposition system to generate controlled Lorentz forces acting on the molten metal. The experimental results show that electromagnetic field assistance significantly stabilizes the liquid bridge, suppresses spattering, and promotes more uniform bead geometry. The analysis highlights the role of electromagnetic forces in damping surface-tension-driven instabilities and modifying melt-pool flow patterns, thereby enhancing deposition robustness under identical processing conditions.

The third article extends the scope of the investigation by introducing dynamic wire feeding as an active and time-dependent control strategy. By periodically modulating wire advancement and retraction, the study demonstrates that dynamic feeding enables controlled redistribution of energy and mass transfer during deposition. The results indicate that wire oscillation frequency plays a critical role in melt-pool stability, wetting behavior, and bead geometry. Furthermore, when combined with thermal and electromagnetic assistance, dynamic wire feeding provides additional flexibility in tailoring the deposition process and mitigating instabilities associated with continuous feeding.

Taken together, the three articles demonstrate that the individual application of hot-wire preheating, electromagnetic field assistance, and dynamic wire feeding already yields measurable improvements in W-LDED performance. The coordinated use of thermal, electromagnetic, and kinematic control mechanisms enables a more stable metal transfer regime, improved control over melt-pool behavior, and enhanced deposition quality.

Therefore, this integration of articles provides a comprehensive and unified framework for understanding and advancing hybrid control strategies in wire-based laser additive manufacturing. The results presented throughout the thesis contribute both scientifically and technologically to the development of more robust W-LDED processes, supporting future research and potential industrial implementation.

2.1 ARTICLE I – INDUCTIVE HOT-WIRE ASSISTANCE IN WIRE-LASER DIRECTED ENERGY DEPOSITION

Article published in The International Journal of Advanced Manufacturing Technology, Volume 141, 2025, Pages: 1879-1892, DOI: https://doi.org/10.1007/s00170-025-16829-5

The first scientific article focuses on the development and evaluation of an inductive hot-wire preheating system applied to the wire-fed Laser Directed Energy Deposition (W-LDED) process. This article establishes the thermal foundation of the thesis by investigating how controlled wire preheating influences energy distribution, metal transfer behavior, and bead geometry during deposition.

In this study, an inductive heating system was designed, implemented, and experimentally characterized to preheat the filler wire prior to its interaction with the laser-

induced melt pool. Compared to conventional resistive heating, inductive heating promotes a surface-concentrated thermal profile due to the skin effect, which is particularly advantageous for enhancing laser absorption and controlling melting at the wire tip. Electrical parameters, thermal response, and heating efficiency were systematically analyzed, allowing the relationship between supplied electrical power and resulting wire temperature to be quantified. Infrared thermography and electrical measurements were employed to validate the stability and controllability of the heating system.

Experimental depositions demonstrated that inductive hot-wire preheating reduces the fraction of laser energy required for wire melting, thereby modifying the thermal balance between the wire and the substrate. As a consequence, changes in bead geometry, penetration depth, and dilution were observed when compared to conventional cold-wire deposition. High-speed imaging revealed that preheated wire conditions affect liquid-bridge formation and metal transfer stability by reducing the thermal gradient at the wire tip.

Within the context of the thesis, this first article provides the fundamental thermal framework upon which the subsequent studies are built. By demonstrating that wire preheating can actively influence energy input and transfer mechanisms, it establishes hot-wire assistance as a key component of the proposed hybrid W-LDED process.

2.2 ARTICLE II – ELECTROMAGNETIC FIELD ASSISTANCE FOR METAL TRANSFER STABILIZATION

Article published in The International Journal of Advanced Manufacturing Technology, Volume 141, 2026, Pages: 1879-1892, DOI: https://doi.org/10.1007/s00170-026-17569-w

The second scientific article investigates the effect of an externally applied electromagnetic field on metal transfer behavior and melt-pool stability in wire-fed Laser Directed Energy Deposition. This work builds directly upon the thermal control strategies introduced in Article I, extending the investigation toward electromagnetic control of molten metal dynamics.

A custom-designed electromagnetic coil was developed and integrated into the W-LDED setup to generate a controlled static magnetic field acting on the wire–melt pool

interaction zone. Analytical calculations, finite element simulations, and experimental measurements were conducted to characterize the magnetic field distribution and ensure reproducible electromagnetic excitation during deposition.

High-speed imaging was employed to capture transient metal transfer phenomena under both reference conditions and electromagnetic field assistance. The results demonstrate that the applied magnetic field significantly stabilizes liquid-bridge transfer, delays droplet detachment, and reduces spatter formation. Quantitative cross-sectional analysis further showed improvements in bead geometry, including increased height, reduced dilution, and enhanced robustness against wire misalignment.

The observed stabilization effects were attributed to Lorentz forces arising from the interaction between the applied magnetic field and electrically induced currents within the molten metal. These forces act as an electromagnetic damping mechanism, suppressing Marangoni-driven convection and promoting a more uniform thermal and fluid-flow distribution in the melt pool.

In the overall structure of the thesis, Article II introduces electromagnetic force assistance as a non-contact and highly controllable strategy for improving metal transfer stability. It complements the thermal control achieved through hot-wire preheating and demonstrates that electromagnetic fields play a critical role in stabilizing W-LDED processes.

2.3 ARTICLE III – DYNAMIC WIRE FEEDING AS AN ACTIVE PROCESS CONTROL STRATEGY

Article published in The International Journal of Advanced Manufacturing Technology, Volume 142, 2026, Pages: 1879-1892, DOI: https://doi.org/10.1007/s00170-026-17735-0

The third scientific article addresses dynamic wire feeding as an active and time-dependent control strategy for wire-fed Laser Directed Energy Deposition. This study expands the scope of the thesis by introducing kinematic modulation of wire delivery as a means to actively influence melt-pool behavior and energy distribution.

A servo-driven wire feeding system capable of controlled forward–backward oscillations was developed and integrated into the deposition setup. The system enabled precise

control of oscillation frequency and wire displacement, allowing systematic investigation of dynamic feeding regimes under constant laser power and average wire feed rate.
High-speed videography and quantitative analysis of melt-pool area, contact angle, and bead cross-sections were used to compare continuous and dynamic feeding conditions. The results show that dynamic wire feeding introduces controlled fluctuations in melt-pool geometry by intermittently altering the interaction between the wire, laser, and substrate. Lower oscillation frequencies favored melt-pool expansion due to longer retraction intervals, while higher frequencies limited energy accumulation and reduced pool size.

These findings demonstrate that dynamic wire feeding provides an additional degree of freedom for controlling metal transfer and melt-pool dynamics. Although continuous feeding offers high geometric stability, dynamic feeding enables adaptive modulation of energy input and wetting behavior, particularly when combined with thermal and electromagnetic assistance. Within the framework of the thesis, Article III completes the hybrid control concept by incorporating kinematic modulation as a complementary strategy to thermal and electromagnetic control. Together, the three articles establish a comprehensive approach for enhancing stability, controllability, and performance in wire-based laser additive manufacturing.

3 EVALUATION OF MAGNETIC FIELD BEHAVIOR AND HEATING EFFICIENCY OF AN INDUCTIVE PREHEATING COIL FOR WIRE-BASED LASER ENERGY DEPOSITION (L-DED)

Manoel Kolling Dutra[1], Caio Linhares Prujansky[1], Milton Pereira[1],
Régis Henrique Gonçalves e Silva[1], Adroaldo Raizer[2], Emanoel Pereira Elias[2]

[1]Department of Mechanical Engineering, Federal University of Santa Catarina, Delfino Conti Street, Florianópolis, 88040-900, Santa Catarina, Brazil.
[2]Department of Electrical and Electronic Engineering, Federal University of Santa Catarina, Conti Street, Florianópolis, 88040-900, Santa Catarina, Brazil.

Abstract

Laser Directed Energy Deposition (L-DED) is an additive manufacturing technique that fabricates metallic parts by melting and depositing material layer by layer. In wire-based L-DED, controlling the wire temperature is essential to ensure deposition stability, minimize defects, and improve component quality. A promising approach is inductive preheating, where an electromagnetic coil increases the wire temperature before it enters the melt pool, reducing thermal gradients and enhancing process robustness. This work presents the analytical modeling and simulation of a low-frequency electromagnetic heating system for wire preheating in L-DED. Mathematical models were developed to estimate the magnetic field, induced current, heat generation, and temperature rise in the wire. These models provide insight into the system's physical behavior and guide the design of the coil. The coil, conceived for laboratory experiments, was evaluated using both analytical methods and finite element simulations. The electromagnetic analysis considered the interaction between the coil's alternating magnetic field and the induced currents in the wire, which generate heat through resistive losses. Subsequently, a thermal analysis estimated the resulting temperature rise. Although simplifications were adopted, such as neglecting temperature-dependent magnetic properties, the models yielded useful approximations of the heating system's behavior. The developed system will be applied in future studies to improve the L-DED process by enabling

consistent wire preheating, thereby enhancing deposition stability, reducing variability, and improving overall part quality. Additionally, the modeling approach can be adapted to different wire materials, feed rates, and ambient conditions, demonstrating the versatility of the proposed system for diverse applications.

Keywords: Coil design, Induction heating, L-DED, Wire pre-heating.

3.1 INTRODUCTION

Laser Directed Energy Deposition (L-DED) is a category of Additive Manufacturing (AM) in which a focused laser beam melts material during deposition, enabling precise material addition and achieving control over part geometry [1–3]. In metallic L-DED, two primary types of feedstock materials are commonly utilized: wire and powder, each offering distinct advantages in terms of process efficiency, material utilization, and application suitability [4]. Wire laser deposition involves feeding the material to be deposited in the form of a wire, which is melted using a laser energy source and precisely manipulated over the deposition volume [2, 5]. This process offers several advantages compared to powder-based systems, including a cleaner processing environment, lower environmental impact from wire production, negligible material waste, and higher deposition rates [6]. However, wire deposition presents challenges, such as the need for precise alignment of the wire into the laser focus, ensuring simultaneous melting of the wire and base metal, and achieving uniform and controlled deposition [7].

A technique gaining increasing attention for enhancing process stability is wire preheating, commonly referred to as the hot-wire method [8]. In the inductive wire preheating electromagnetic fields and forces have been proposed as complementary tools to improve the deposition process by influencing melt pool dynamics [9]. Steady magnetic fields are known to have a damping effect on melt flow, resulting in improved process stability [10], while low-frequency magnetic fields can provide surface forces that mitigate weld sagging in laser-induced melt pools [11, 12]. Moreover, low-frequency magnetic fields have been shown to beneficially impact melt pool dilution, acting as a pulsating force that periodically damps melt flow perpendicular to the field lines [13]. Despite these advances, the role of the magnetic field generated by inductive heating coils in L-DED remains underexplored.

Inductive heating coils, commonly used to preheat feedstock materials, generate complex magnetic fields that influence not only the heating efficiency but also the melt pool behavior and material properties during deposition. A detailed understanding of the magnetic field distribution and its interaction with the process environment is crucial for optimizing both inductive heating and the overall deposition process.

The magnetic field generated by the induction coil has a direct influence on the deposition environment during the L-DED process. The preheating of the wire significantly reduces the thermal gradient between the wire and the melt pool, facilitating a more stable and continuous metal transfer, as also reported in recent studies on hot-wire-assisted processes [5, 13]. This reduction in thermal gradients promotes the formation of a stable liquid bridge between the wire tip and the melt pool, resulting in fewer spatters, reduced droplet rejection, and improved deposition stability. The influence of magnetic field oscillation can be clearly seen in the supplementary high-speed footage (see Supplementary Video S1[1]). Furthermore, the alternating magnetic field generated by the coil can induce Lorentz forces on the electric charges within the molten pool, modifying the fluid flow behavior, as demonstrated by Huang *et al.* [8] and Gatzen, Tang and Vollertsen [10]. Similar effects have been reported with alternative modulation strategies, such as dynamic laser beam polarization, which influenced melt pool stirring and improved surface morphology during welding [14].

This paper focuses on the magnetic analysis of an inductive heating coil specifically designed for the L-DED process. The primary objective is to characterize the magnetic field generated by the coil and evaluate its influence on the deposition environment. By leveraging simulation and experimental techniques, the study provides insights into the coil's magnetic behavior, contributing to the development of more efficient and controlled L-DED systems. The findings aim to support process optimization for additive manufacturing applications, particularly those involving electromagnetic fields and inductive heating.

[1] Supplementary Video S1 can be accessed online at: Video S1 .

3.2 SYSTEM DESCRIPTION

This section presents the structural characterization of the induction heating coil employed in the L-DED process. The approach includes a systematic analysis of the coil design parameters, material selection criteria, and power circuit design strategies.

3.2.1 Inductive coil configuration

The heating coil used in this study was specifically designed and developed by the authors to meet the requirements of wire preheating in the L-DED process. The coil was built with 1 *mm* copper wire, 56 *mm* length, 17 *mm* diameter, and 11 turns. Its resistance and inductance were measured with an impedance analyzer, as show in Table 3.1.

Table 3.1 - Measured resistance and inductance of the coil.

Frequency	Resistance	Inductance
20 Hz	14.8 mΩ	1.22 μH
100 Hz	58.8 mΩ	0.93 μH

The wire fixation support was designed to ensure feeding stability, with a rigid, easy-to-assemble structure that maintains wire alignment during the process. Figure 3.1 shows the wire feeding system, including the heating coil and fixation support.

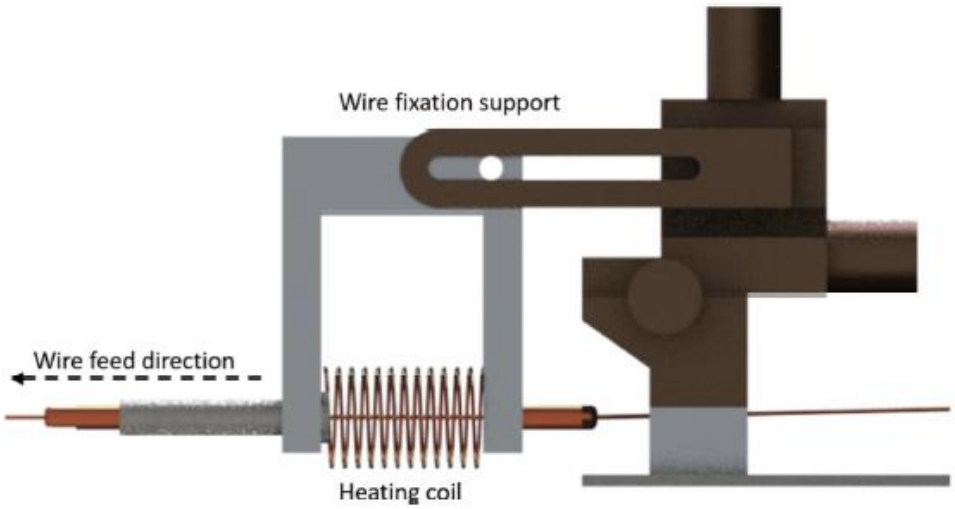


Figure 3.1 - Wire feeding model developed with the heating coil and wire feed support, showing wire feed direction.

The proposed system leverages the principles of electromagnetic induction to achieve efficient preheating of the additional wire during the L-DED process. A Low- Frequency 105 *kHz* alternating current is applied to a coil encircling the feed wire, generating a time-varying magnetic field in accordance with Ampère's Law. This dynamic magnetic field induces eddy currents, also known as Foucault currents, within the conductive material of the wire. The interaction between these induced currents and the wire's electrical resistance produces localized heating through the Joule effect, where electrical energy is dissipated as heat.

This design is original and developed in-house by the authors, differing from conventional induction heating coils described in the literature. To contextualize, similar approaches to coil-based heating in welding and additive manufacturing have been reported, for instance, by Voigt *et al.* [15] in GTAW applications and by Rudnev *et al.* [16] in the design principles of induction heating systems.

3.2.2 LC Resonant circuit characteristics

The heating coil is powered through a center tap, as illustrated in Figure 3.2, with alternating current. This current is supplied by an LC resonant converter with transistor switching. The schematic diagram of the converter circuit is also shown in Figure 3.2.

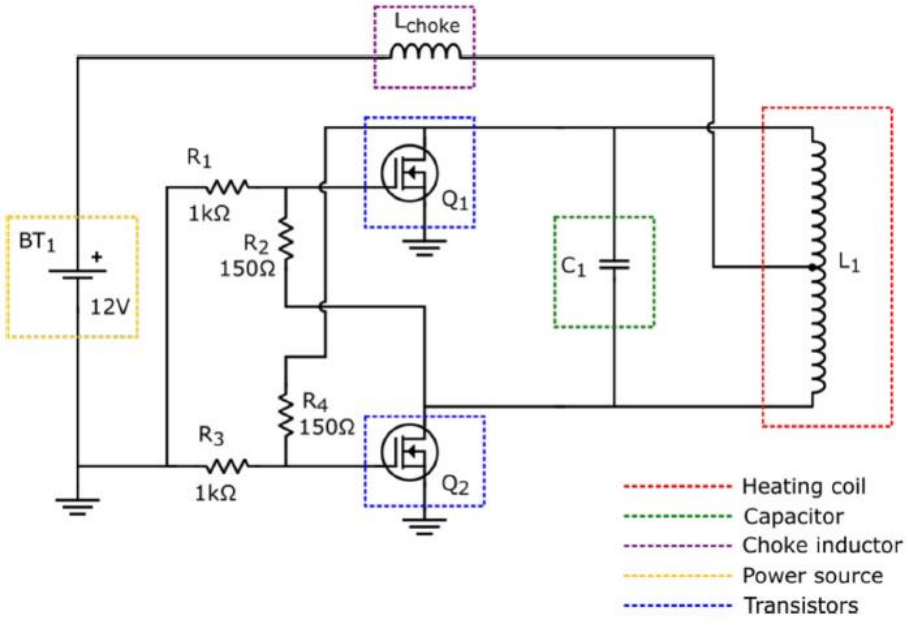


Figure 3.2 - Electronic LC resonant converter circuit designed to generate alternating current for heating coil.

Figure 3.2 shows the LC resonant converter circuit used to power the heating coil. This circuit consists of a 12*V* DC power supply (*BT*1), which feeds the center tap of the heating coil (*L*1). A choke inductor (*Lchoke*) is connected in series between the power supply and the center tap and is used to prevent the return of alternating current to the source. A capacitor (*C*1) is connected in parallel with the heating coil and is responsible for establishing the voltage oscillation that enables the transistors' switching.

In the circuit, two MOSFET transistors (*Q*1 and *Q*2) are used to invert the reference point of the input voltage and allow current oscillation through a switching process known as Zero Voltage Switching (ZVS), which reduces losses in the transistors [17]. The transistor model used is the IRFZ444N.

The capacitor's charging and discharging process enables the alternate switching of transistors *Q*1 and *Q*2, thereby inverting the voltage reference and reversing the direction of the current through the inductor. This cycle repeats continuously, producing a low-frequency oscillation of approximately 105 kHz. The resulting rapid oscillations generate a time-varying magnetic field in the inductor. Figure 3.3 shows the current signal measured by the oscilloscope.

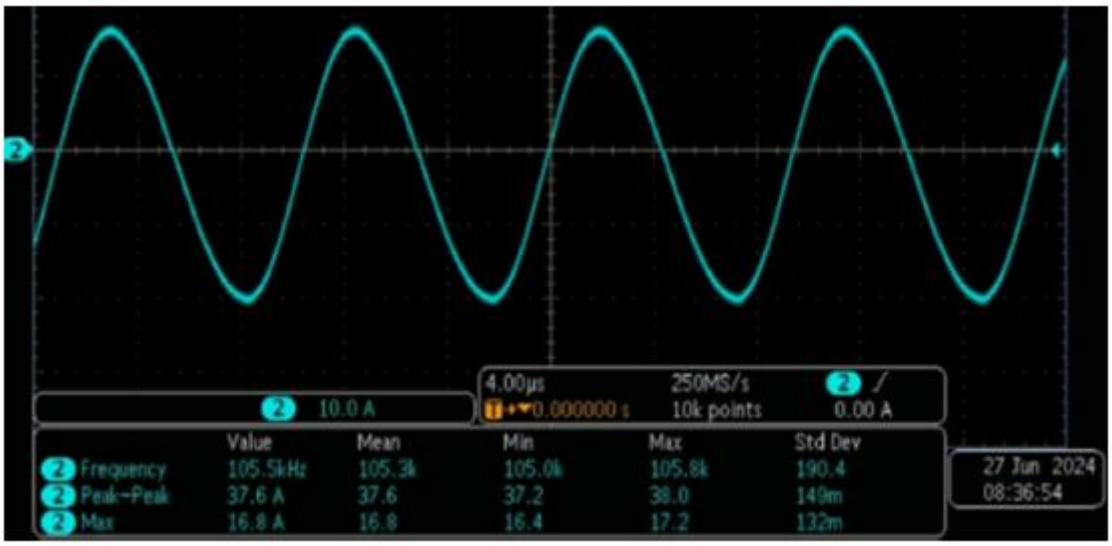


Figure 3.3 - Current signal as measured by the oscilloscope. Circuit's mean frequency measured at 105.3 *kHz*, with mean peak current of 18.8 *A*.

It is observed that the sinusoidal electric current shown in Figure 3.3 exhibits a magnitude offset. When corrected based on the peak-to-peak current (37.6 A), a peak current of 18.8 A is obtained, corresponding to an RMS (Root Mean Square) value of 13.3 A.

The alternating magnetic field induces eddy currents within the wire, resulting in resistive heating according to Joule's Law. The operating frequency of the LC oscillator is a critical factor, as it must be compatible with the skin depth and the wire diameter to ensure a proper distribution of the eddy current. An inadequate choice of frequency can lead to magnetic saturation of the material, reducing the efficiency of inductive heating. Maintaining an appropriate frequency ensures effective energy transfer and uniform heating of the wire.

The low-frequency (LF) operation is particularly advantageous in mitigating edge effects and ensuring that the heating mechanism uniformly affects the wire's cross-section. This efficiency is essential for pre-heating applications in laser directed energy deposition (L-DED) processes, where consistent wire temperature significantly influences deposition quality and process stability.

After the development of the low-frequency oscillation system for heating and the construction of a coil capable of providing adequate heat for laboratory experiments, it became essential to gain a deeper understanding of the physical dynamics of the process. This includes evaluating the coil's limitations, its performance, and the amount of heat generated. To achieve this, a mathematical analysis of the problem was carried out, taking into account electromagnetic and thermal aspects.

The objective of this analysis is to identify the main factors that influence the behavior of the coil, contributing to the assessment of its effectiveness and limitations in practical applications.

3.3 ELECTROMAGNETIC ANALYSIS

This section analyzes the coil's electromagnetic behavior, focusing on magnetic field distribution and power transfer to the wire, based on classical electromagnetism equations [18, 19] and validated by numerical simulation using the parameters from Section 3.2.

3.3.1 Analytical modeling

Through analytical methods, the coil's ability to generate magnetic field and induction will be evaluated, as well as the influence of the skin effect on the induced current.

3.3.1.1 Magnetic field and magnetic induction generation

The current flowing through the coil will create a magnetic field at its center, which can be calculated using analytical methods. The magnetic field inside a long solenoid carrying a steady current can be expressed by Equation 3.1, where the magnetic induction can be obtained by Equation 3.2 [18, 19].

$$H = \frac{N.I}{L} \quad (3.1)$$

$$B = \mu_0.\mu_r.H \quad (3.2)$$

Where H is the magnetic field inside the coil (A/m), N is the number of turns, I is the current flowing through the coil (A), L is the length of the coil (m), B is the magnetic induction inside the coil (T), μ_0 is the magnetic permeability of vacuum (H/m), and μ_r is the relative permeability of the medium. Since the medium inside the coil is air, μ_r can be reasonably assumed to be approximately 1.

3.3.1.2 Induced current, skin depth and skin effect

The alternating magnetic field generated by the coil induces eddy currents in the wire, producing heat by the Joule effect, a process known as induction heating. Due to the skin effect, current density concentrates near the surface of the conductor and decreases toward the center, a behavior characteristic of materials with homogeneous electromagnetic properties [20].

This phenomenon, known as the skin effect, occurs in any alternative current system and is particularly relevant in inductive heating, as it concentrates induced currents near the surface, limiting heat penetration [21]. Studies on billet heating confirm this behavior, showing maximum current density at the outer layer, decreasing toward the core [22].

The skin effect plays a crucial role in the concentration of eddy currents within the surface layer of the workpiece. Because of the circular (circumferential) nature of these eddy currents in a solid cylinder, no current flows at the center of the conductor (Figure 3.4). Experimental studies and simulations confirm this behavior, showing that approximately 86 %

of the total power dissipated as heat is confined to the skin depth [20]. Higher frequencies reduce skin depth, further concentrating current near the surface.

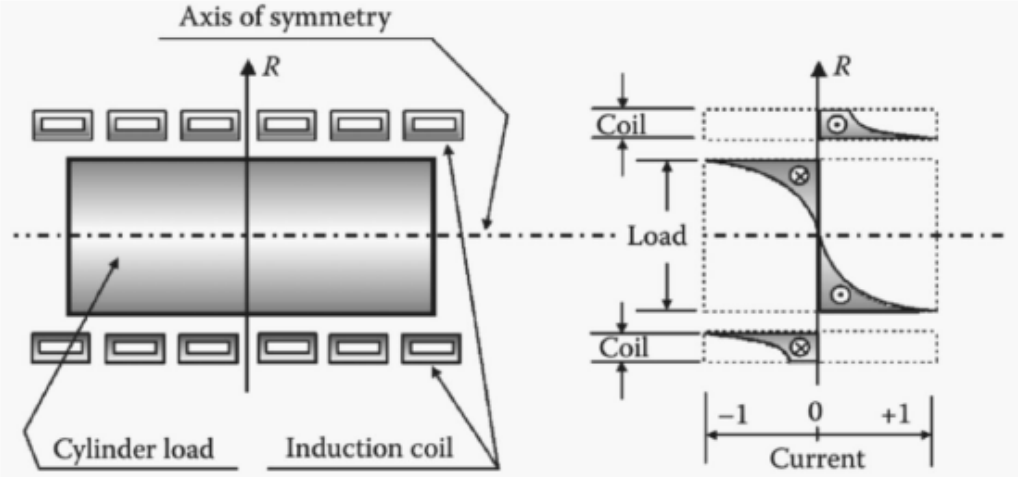


Figure 3.4 - Instantaneous distribution of AC currents in "wire-to-workpiece" system. The wire dimensions relative to the coil were modified for a better understanding of the phenomenon [20].

The induced current distribution defines the effective heating depth, known as skin depth (δ), corresponding to the distance where power density drops to 14 % of its surface value [20]. The skin depth of the electromagnetic field in a conductive material can be determined using Equation 3.3 [19].

$$\delta = \frac{1}{\sqrt{\pi . f . \mu . \sigma}} \qquad (3.3)$$

Where δ is the skin depth (m), f is the frequency of the electromagnetic field (Hz), σ is the material conductivity (S/m), and μ is the magnetic permeability of the material (H/m).

During the heating cycle, the electrical resistivity of most metals can increase by a factor of four to six relative to its initial value. As a result, even in nonmagnetic metals, the skin depth can increase significantly during the heating process. For most induction heating applications, due to the skin effect and other electromagnetic phenomena, the current density distribution is inherently nonuniform. Furthermore, thermal gradients within the heated workpiece cause variations in both electrical resistivity (ρ) and relative magnetic permeability (μr), leading to additional complexities in the current and power density profiles. Since estimating the

material's relative magnetic permeability is challenging due to its dependence on temperature variations, Simpson [23] proposed a nomogram to estimate the skin depth based on the workpiece resistivity and the characteristics of the induction coil, as shown in Figure 3.5. To estimate the skin depth, it is necessary to know the applied magnetic field (*H*), which is calculated using Equation 3.1, considering the RMS (Root Mean Square) value of the current (*I)* in the coil.

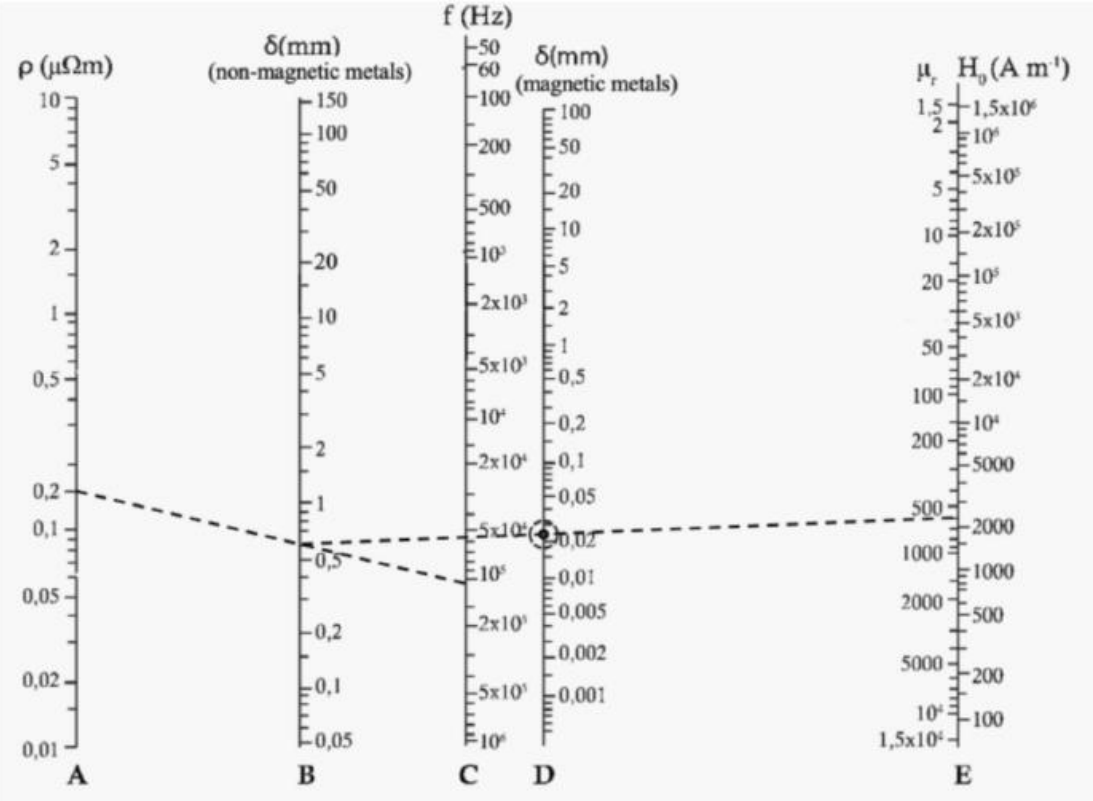


Figure 3.5 - Nomogram to calculate reference depth. For nonmagnetic materials, connect resistivity (A) to frequency (C); intersect at (B) for depth. For magnetic materials, connect (A) to (C), then (B) to *H*0 or permeability (E); intersection at (D) gives depth. Adapted from [13].

To correctly use the nomogram, it is also necessary to know the heated material resistivity ρ ($\mu\Omega.m$) and the system's current frequency f (Hz).

3.3.1.3 Power dissipation and heat generation in the wire

The power dissipated as heat in the wire due to the eddy currents induced by the magnetic field of the coil was derived by Simpson [23]. It depends on the interaction between

the electromagnetic field and the physical properties of the wire. This power dissipation can be described by the Equation 3.4.

$$q_{gen} = \frac{I^2.N^2.\rho.\pi.d.10^{-6}}{\delta.L} \quad (3.4)$$

Where q_{gen} (W) is the power dissipated in the wire, I (A) the RMS current in the coil, N the number of turns, ρ ($\mu_.m$) the electrical resistivity of the heated wire, d (mm) the diameter of the wire, δ (mm) the skin depth and L (m) the length of the coil.

3.3.1.4 Analytical results

Considering the characteristics of the heating coil presented in Section 3.2, the peak current 18.8 A, and the magnetic permeability of vacuum $\mu 0 = 4\pi 10^{-7}$ H/m, the magnetic field of 3693 A/m and the magnetic flux density of 4.64mT inside the coil are determined. The corresponding RMS values are 2611 A/m and 3.28 mT, respectively.

In this work, ER70S-6welding wire was used. This wire is a low- to medium-strength carbon steel with a carbon content of up to 0.15 %, and it is classified as a magnetic material for nomogram analysis. Its electrical resistivity is 0.2 $\mu\Omega.m$, which is consistent with typical values for low-carbon steels. Based on the nomogram (Figure 3.5) and the magnetic field value, the skin depth for the system is determined to be 0.024 mm. Given that the diameter of the heated wire is 1.2 mm, it is evident that the skin effect is significant, causing most of the power dissipation to occur within a thin layer near the wire's surface. The nomogram also allows for the estimation of the system's relative permeability, which is found to be approximately 600.

Using Equation 3.4, and considering the skin depth obtained from the nomogram, along with the characteristics of the coil and the welding wire, the total power dissipation was found to be 9.6 W.

3.4 FINITE ELEMENT MODELING OF THE MAGNETIC FIELD AND POWER DISSIPATION

In this work, the magnetic field generated by the current applied to the coil was analyzed using analytical calculations. However, to validate these results and investigate effects that are difficult to model analytically, such as spatial variations in the magnetic field and the

distribution of induced current in the heating wire, a numerical simulation will be performed using software based on the Finite Element Method (FEM) for electromagnetic analysis [24]. This approach provides a more detailed solution to the problem, enabling direct comparisons with the theoretical results previously obtained.

The electromagnetic analysis of the system described in Section 3.2 was performed using Maxwell, from Ansys' Electronics simulation platform [24].

3.4.1 Simulation setup

The coil geometry was modeled according to the specifications presented in Section 3.2.1. Figure 3.6 shows the 3D models of the coil, its support, and the wire used in the FEM simulation. In (a), the front view highlights the model components, while (b) shows an isometric view of the simulation model, emphasizing the two through-holes in the upper part of the support, which are used to secure it and provide greater stability to the coil.

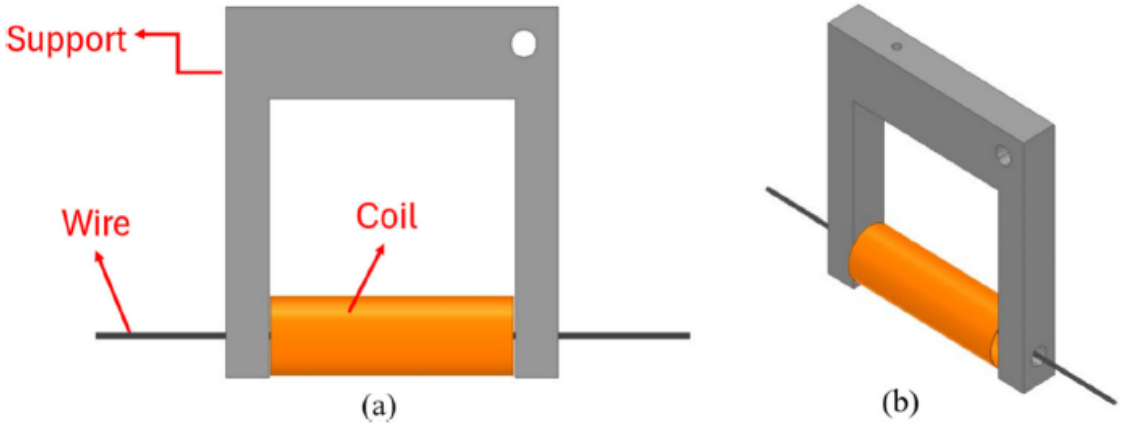


Figure 3.6 - 3D geometric model used in simulation. (a) Front view. (b) Isometric perspective view.

It is observed that the model presented in Figure 3.6 is a simplification, as only the most relevant components from the model in Figure 3.1 were considered in the simulation. Additionally, the coil was represented by a cylinder with the same length and diameter as the original coil, but with an adjusted thickness so that the cross-sectional area of the simulated coil (see Figure 3.7) is equivalent to the total area through which the current flows in the original

coil. This approach simplifies the simulation model while preserving the magnetic field and electrical conduction characteristics of the coil.

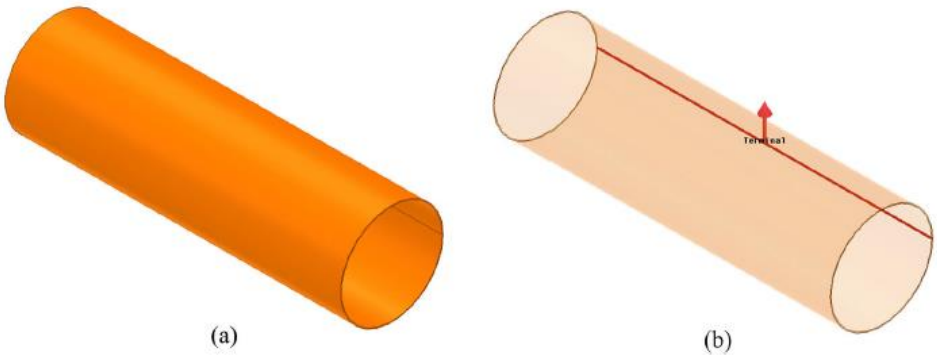


Figure 3.7 - Simulated coil. (a) Simplified model of the coil. (b) Detail of the excitation terminal of the coil.

Figure 3.7 presents the simulated model of the coil, showing in (a) the simplified cylindrical model and, in (b), the detail of the excitation terminal. The coil was excited with a sinusoidal current of 18.8 A at a frequency of 105 *kHz*. The terminal was also assigned a number of turns equal to 11. The material properties considered in the simulation model can be found in Table 3.2.

As shown in Table 3.2, the support, being made of a steel alloy, exhibits electromagnetic properties similar to those of iron. For the wire, the properties used are based on the characteristics considered in the analytical calculation discussed in Section 3.3.1. The coil, in turn, is made of copper wires. The surrounding environment was assumed to be air at normal temperature and pressure.

Table 3.2 - Electromagnetic properties considered in the simulated model.

	σ (S/m)	εr	μr
Coil	5.8×10^7	1	1
Support	1.03×10^7	1	4000
Wire	5.0×10^6	1	600

In Figure 3.8 (a), the finite element mesh generated over the simulation model can be seen. This mesh is more refined in critical components, such as the heating wire and the coil. Details of this mesh are shown in Figures 3.8 (b) and 3.8 (c).

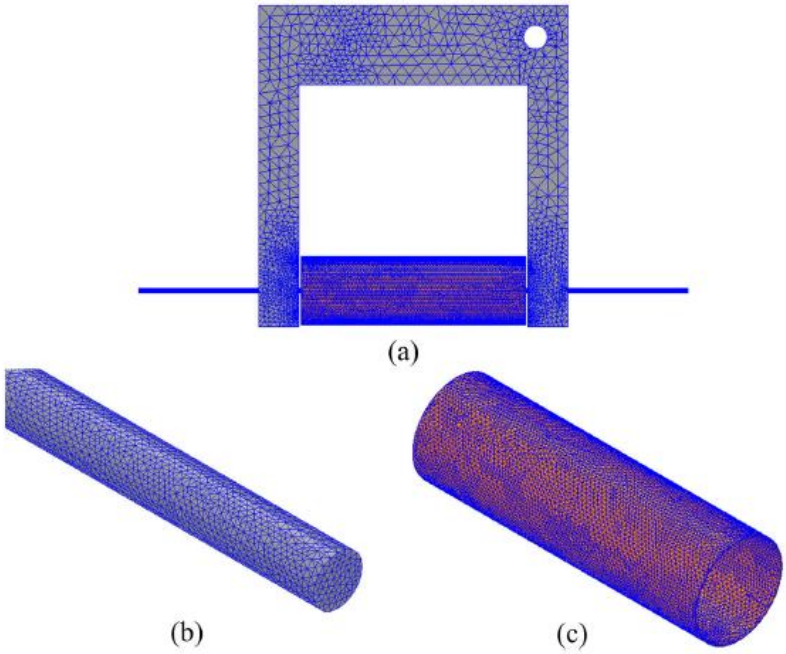


Figure 3.8 - Finite element mesh generated in the simulation model. (a) Mesh over the model. (b) Detail of the mesh generated on the heating wire. (c) Detail of the mesh generated on the coil.

The model was simulated using a frequency-domain magneto dynamic solution. This approach allows the determination of magnetic field values and induced currents generated by a coil as a function of frequency, considering the skin effect and eddy current losses [24].

3.4.2 Simulation results

The magnetic field distribution inside the coil and the induced current density in the heating wire were obtained by performing the simulation of the coil model. These distributions can be observed in Figures 3.9 (a) and 3.9 (b).

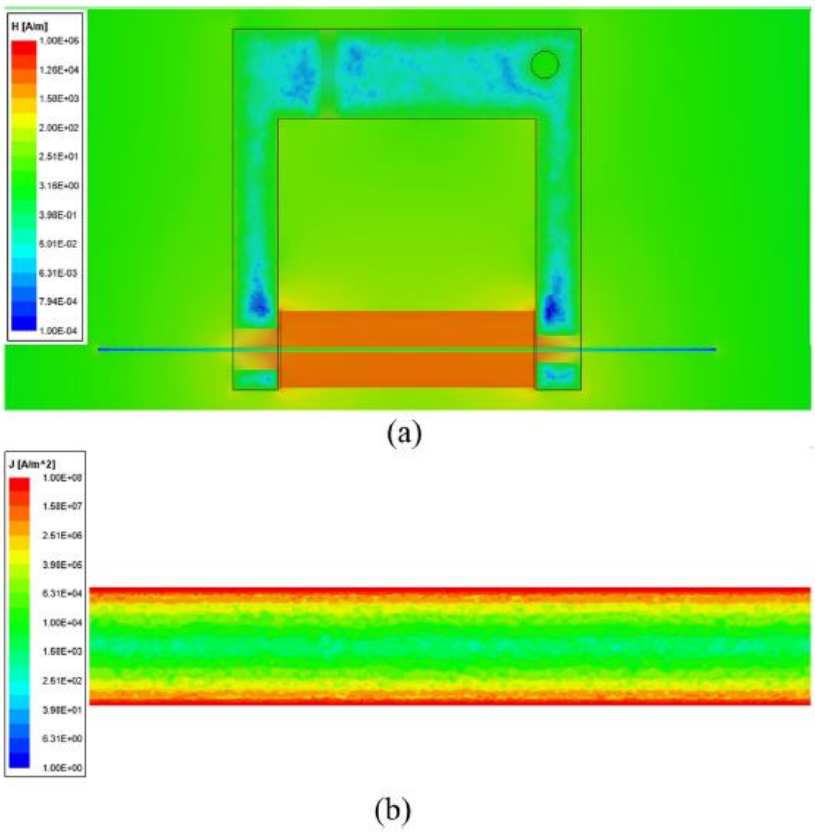


Figure 3.9 - Field in the simulation model. (a) Magnetic field distribution in the longitudinal section of the coil. (b) Induced electric current density in the longitudinal section of the heating wire.

In Figure 3.9 (a), the concentration of the magnetic field inside the coil is shown. It can be seen that the generated field has good uniformity, with an approximate value of 3628 *A/m*, corresponding to a magnetic induction of about 4.57 *mT*. In Figure 3.9 (b), it is observed that the induced electric current is concentrated in the outer layers of the wire, highlighting the skin effect of the current.

Furthermore, with the simulation model, it was possible to determine the resistance and inductance values of the coil at the frequency of 105 kHz, being 60.87 *mΩ* and 0.67 *μH*, respectively. These values are like those obtained by measurement, presented in Table 3.1. It is worth noting that the simplification used in the coil simulation model may influence these values.

Moreover, temperature variation affects the magnetic properties of the material, which in turn influence the electromagnetic behavior of the system. However, the software used for

the simulation does not effectively account for these temperature-dependent changes in magnetic properties, introducing another source of uncertainty in the results. Despite these limitations, it was possible, through simulation, to obtain an induced power in the wire of 8.5 *W*, a value similar to that found by applying Equation 3.4.

3.5 THERMAL ANALYSIS

To predict the heating capability of the coil, it is necessary to evaluate the thermal dynamics, including the temperature distribution and heat generation in the wire.

From the power dissipated in the wire, the wire's exit temperature from the coil can be calculated. This temperature is directly influenced by the energy converted into heat due to eddy currents. However, for a more accurate temperature estimate, it is essential to consider heat losses through conduction, convection, and radiation. Analyzing conduction also allows calculation of the temperature profile across the wire's cross-section, providing a detailed understanding of internal heat distribution. Conduction losses occur as heat transfers along the wire, convection results from heat exchange with the surrounding air, and radiation contributes to energy loss as thermal energy is emitted from the wire's surface. Accounting for these mechanisms leads to a more precise evaluation of the wire's temperature.

3.5.1 Heat dissipation by convection

Among these methods of heat dissipation, convection significantly influences the wire's temperature as it moves. This effect occurs due to the interaction between the heated wire and the surrounding air, which removes heat from the wire surface. It is influenced by factors such as wire velocity, ambient airflow, and temperature differences between the wire and its environment. As the heated wire exchanges energy with the surrounding fluid, primarily air, this process occurs through natural and forced convection. The heat transfer rate is governed by the Equation 3.5 [25]:

$$q_{conv} = h.A.\Delta T \qquad (3.5)$$

Where q_{conv} (W) is the heat transfer rate, h ($W/(m^2K)$) is the convection heat transfer coefficient, A (m^2) is the surface area of the wire exposed to airflow, and ΔT (K) is the temperature difference between the wire surface and the surrounding environment. For the calculation of the convective heat transfer coefficient h, the flow over a flat plate was considered, as the wire can be approximated as a cylinder. When the cylindrical shape is unfolded, it forms a flat surface, allowing the use of established correlations and models for heat transfer over flat plates. This approximation is commonly employed in cases where the geometry of the object is not perfectly flat but can be treated as such. By considering the wire as a cylinder and approximating it as a flat plate, h can be calculated by the Equation 3.6 [25].

$$h = \frac{Nu.k}{L} \qquad (3.6)$$

Where Nu is the dimensionless Nusselt number, k $(W/(mK))$ is thermal conductivity of the fluid and L (m) is the characteristic length, which will be taken as the total length of the wire within the coil. For a laminal flow over an isothermal flat plate [25], Nu can be calculated in Equation 3.7 by Reynolds number (Re) calculated in Equation 3.8.

$$Nu = 0.644 Re^{1/2} Pr^{1/2} \qquad (3.7)$$

$$Re = \frac{\rho_m.v.L}{\mu} \qquad (3.8)$$

To calculate Re, ρ_m (kg/m^3) represents the fluid density, v (m/s) is the fluid velocity in relation to the surface, L (m) is the characteristic length, and μ ($Pa.s$) is the fluid dynamic viscosity. In order to solve the problem, the air properties used will be based on air at 80 $\circ C$. This temperature is derived from previous experiments.

Calculating Reynolds number, ρ_m is 0.9994 kg/m^3, μ is 2.097×10^{-5}, and L is the coil length, being 0.056 m. The reference velocity, v, will be 0.0083 m/s, which is the one of the typical velocities at which the wire is deposited in L-DED processes during laboratory experiments. Thus, the Reynolds number obtained by Equation 3.8 is 22.24, indicating that the flow is laminar. Being Prandtl Number, $Pr = 0.72$, Nu is calculated by Equation 3.7 to be 2.80. For the thermal air conductivity of 0.03 $W/(mK)$, the convective heat transfer coefficient is calculated by Equation 3.6 to be 1.54 $W/(m^2K)$.

Using Equation 3.5, it is possible to calculate the heat dissipation by convection, considering the heat exchange area of the wire inside the coil as $2.11\times10^{-4}\ m^2$, an average wire temperature of 80 $\circ C$, and an ambient temperature of 21 $\circ C$. With these parameters, the power dissipated by convection in the wire is 0.018 W. Note that this calculation takes into account the instantaneous velocity of the wire, meaning that the greater the instantaneous velocity, the higher the heat dissipation due to convection. However, at this velocity level, the heat dissipation caused by convection is significantly lower than the heating power absorbed by the wire. As a result, while the wire remains inside the coil and exposed to the magnetic field, convection heat dissipation is not so relevant.

3.5.2 Heat dissipation by radiation

In addition to convection, radiative heat transfer plays a role in the overall thermal dissipation of the wire. Radiation occurs due to the emission of electromagnetic waves from the wire's surface, following Stefan-Boltzmann's law [26]. This mode of heat transfer is particularly significant at higher temperatures, as it depends on the fourth power of the absolute temperature difference between the wire and its surroundings. Unlike convection, which requires a fluid medium, radiation can occur in a vacuum and is influenced by factors such as the wire's emissivity and surface properties.

The heat dissipation by radiation can be quantified using the Stefan-Boltzmann equation, which describes the thermal energy emitted by a surface as electromagnetic radiation. The radiative heat transfer is given by the Equation 3.9.

$$q_{rad} = \varepsilon.\sigma.A.(T_S^4 - T_\infty^4) \qquad (3.9)$$

In this expression, q_{rad} (W) represents the radiative heat dissipation rate, while ε is the emissivity of the wire's surface, a dimensionless property that indicates the material's ability to emit thermal radiation compared to an ideal black body. The Stefan-Boltzmann constant, σ, has a value of $5.67\times10^{-8}\ W/(m^2K^4)$. The surface area of the wire is denoted by A, and the temperatures of the wire's surface and the ambient environment, both in Kelvin, are represented by T_S and T_∞, respectively [26]. This equation highlights the strong dependence of radiative heat dissipation on temperature, as the energy emitted increases exponentially with the

temperature difference between the wire and its surroundings. Additionally, the emissivity of the wire material plays a fundamental role, directly influencing the amount of heat transferred by radiation.

For this study, the emissivity of the wire material was considered to be 0.6, based on typical values for carbon steel surfaces under oxidized conditions. The heat exchange area was calculated as $2.11 \times 10^{-4}\ m^2$, corresponding to the portion of the wire inside the coil exposed to the magnetic field. The average surface temperature of the wire was estimated at 348.65 K (75.5 $\circ C$), while the ambient temperature was 294.15 K (21 $\circ C$). By substituting these values into the Stefan-Boltzmann equation, the radiative heat dissipation was calculated to be approximately 0.05 W.

3.5.3 Thermal balance and temperature elevation

The overall thermal balance of the wire heating system is determined by the power generated within the wire and the heat dissipation through convection and radiation. The heating process is primarily driven by Joule heating, where the electric current passing through the wire generates thermal energy. The total power generated was calculated to be 9.6 W, with convective heat dissipation estimated at 0.018 W and radiative heat loss at 0.05 W. The total energy responsible for heating the wire can be expressed by the following Equation 3.10.

$$Q_{total} = q_{gen} - q_{conv} - q_{rad} \qquad (3.10)$$

By comparing the total dissipated power with the generated power, it is evident that the heat losses represent a negligible portion of the total power input, at least while the wire is inside the coil. This balance confirms that the predominant effect of the generated power is the direct heating of the wire, with only minor contributions from heat dissipation mechanisms. The total energy is calculated to be 9.5 W. Once the wire leaves the coil and is no longer subjected to the magnetic field, it will continue to lose heat through radiation and convection. Consequently, the wire temperature will start to decrease after exiting the coil. The energy dissipation power in this stage is approximately 0.068 W.

To estimate the temperature, increase of the wire, the thermal equilibrium equation is applied, considering the total power available for heating, the mass of the wire, and the time of

exposure to the magnetic field. The energy balance can be written as shown in Equation 3.11 [27].

$$T_{out} = T_{in} + \frac{t.Q_{total}}{m.c} \qquad (3.11)$$

Where Q_{total} is calculated by Equation 3.10, m (kg) is the mass of the wire, c $(J/(kg{\circ}C))$ is the specific heat capacity of the wire material, T_{out} $({\circ}C)$ is the temperature of the wire exiting the coil, T_{in} $({\circ}C)$ is the temperature of the wire entering the coil, and can be assumed as equal to the ambient temperature. t (s) is the time of wire exposure to the magnetic field and is determined by the coil length divided by wire feed speed.

The specific heat capacity of carbon steel was considered as 690 $J/(kg{\circ}C)$. The mass of the wire segment exposed to the magnetic field was determined based on the wire length inside the coil, the wire density, and the wire diameter. The total mass was calculated as 4.98×10^{-4} kg. The exposure time of the wire to the magnetic field was estimated based on the same wire feed velocity used in Equation 3.8, resulting in 6.72 s. The ambient temperature was set at 21 ${\circ}C$ as the initial condition for the wire. According to the thermal balance described in Equation 3.11, the calculated outlet temperature is 207 ${\circ}C$. This result was compared with the experimentally measured temperature presented in previous work by the authors, which reached 219 ${\circ}C$ under maximum heating conditions [28]. The difference between the analytical prediction and the experimental measurement is approximately 5.5%, indicating good agreement and validating the accuracy of the developed thermal model. This comparison confirms that the inductive heating system provides reliable and predictable wire heating behavior, suitable for integration into the L-DED process.

The results indicate that the outlet temperature is directly proportional to the total power supplied and the exposure time, while inversely proportional to the mass and specific heat capacity of the wire. This approach provides a simplified yet effective method for predicting the thermal behavior of the wire during electromagnetic heating.

3.6 FINITE ELEMENT MODELING OF THE THERMAL DISSIPATION

In this work, the thermal analysis of the system composed of the coil and the solder wire was initially carried out using analytical calculations. However, to validate the obtained results and investigate effects that are difficult to model analytically, such as the temperature distribution within the conductor, a thermodynamic analysis based on the Finite Element Method was performed.

The thermal analysis of the system described in Section 3.2 was performed using Icepak, from Ansys' Electronics simulation platform [29].

3.6.1 Simulation setup

In the thermal simulation, the same 3D model presented in Figure 3.6 was used. The model is excited through the power distribution induced in the solder wire, the support, and the coil itself by the magnetic field. The data for this power distribution were imported from the electromagnetic simulation described in Section 3.3.2 Additionally, the simulation considers the same values used in the analytical calculations presented in Sections 3.4.1, 3.4.2, and 3.4.3, regarding the thermal properties of the materials composing the system and the surrounding environment.

The model was simulated using time-domain thermodynamic formulation [29], with the simulation run up to 7.2 *s* and a time step of 0.1 *s*.

3.6.2 Simulation results

By performing the thermodynamic simulation of the system, the temperature distribution on the surface of the solder wire was obtained, which can be seen in Figure 3.10.

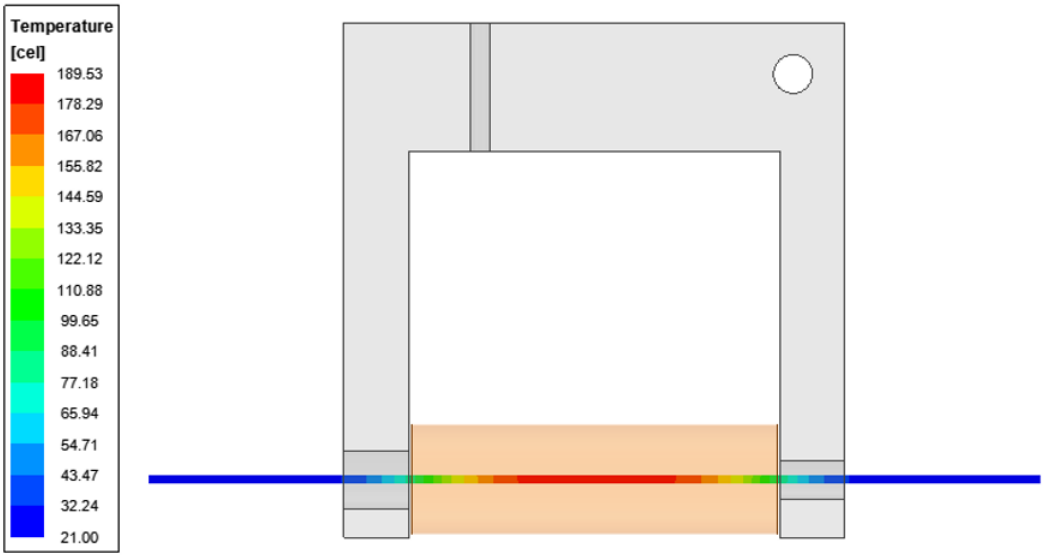


Figure 3.10 - Temperature distribution on the surface of the solder wire at 6.7*s*.

Figure 3.10 shows the temperature distribution on the surface of the solder wire at 6.7 *s*, corresponding to the same exposure time of the wire discussed in Section 3.4.3.

In Figure 3.11, a graph of the solder wire temperature obtained from the simulation as a function of time is shown. From the graph, there is no significant temperature variation between the center of the wire and its surface. Furthermore, the Temperature at 6.7 *s* is 189.42 $\circ C$.

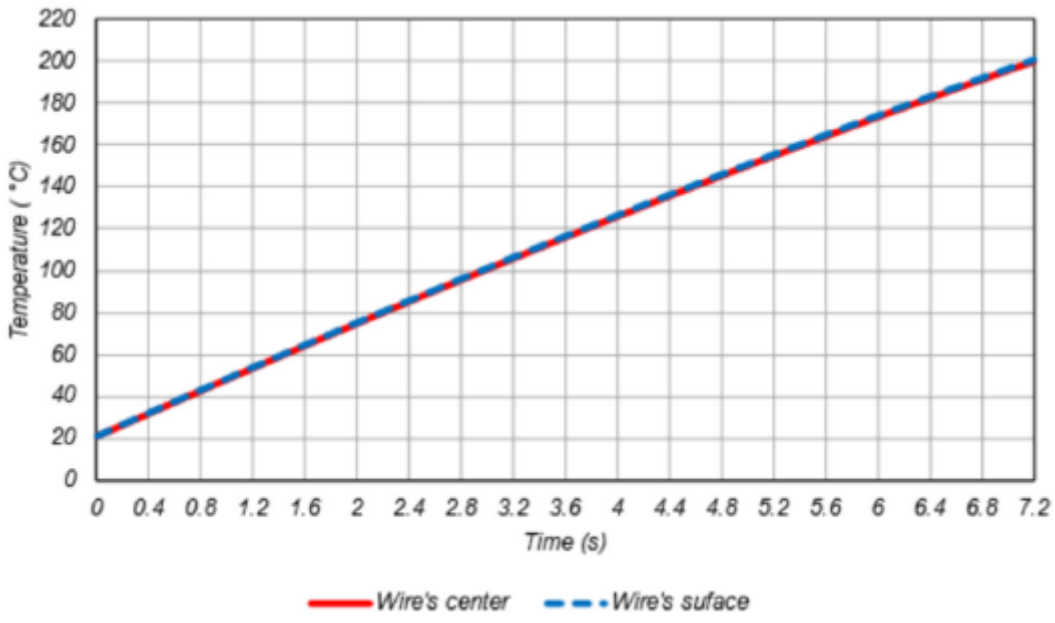


Figure 3.11 - Temperature at the center and on the surface of the wire as a function of simulation time.

3.7 CONCLUSIONS

This study provides an analytical and numerical assessment of an inductive coil for wire preheating in L-DED, predicting magnetic field intensity, current distribution, power dissipation and wire temperature.

The analytical approach predicted a magnetic field intensity of 3693 A/m and a magnetic flux density of 4.64 mT, closely matching the simulation results of 3628 A/m and 4.57 mT, respectively. Finite element analysis revealed a pronounced skin effect with a calculated skin depth of 0.024 mm, confining current density to the wire's surface an effect that directly governs heating efficiency at the operational frequency of 105 kHz. The power dissipated through induction was determined to be 9.6 W analytically and 8.5 W via simulation, reinforcing the reliability of the theoretical model. Moreover, impedance characterization revealed strong coherence between measured and simulated resistance (58.8 $m\Omega$ vs. 60.87 $m\Omega$) and inductance (0.93 μH vs. 0.67 μH), further validating the electromagnetic model.

Thermal analysis confirmed that the inductive heating system is highly effective, with the wire reaching an outlet temperature of 207 $\circ C$, closely aligned with the experimental measurement of 219 $\circ C$, yielding a deviation of only 5.5 %. In addition, the temperature simulation predicted a value of 189.42 °C, which further supports the strong agreement between the numerical and experimental results, confirming the accuracy of the thermal modeling and the efficiency of the inductive heating configuration. Convective and radiative losses were found to be marginal relative to the total input power, ensuring that in this experiment, the heating process is predominantly governed by electromagnetic induction rather than environmental dissipation.

The ability to develop analytical formulations for the electromagnetic and heat transfer phenomena involved in the wire preheating system designed in the laboratory is essential for a deep understanding of the physical mechanisms taking place during the preheating process. Moreover, by expressing these equations analytically, it becomes possible to integrate them into a control algorithm, enabling both open-loop and closed loop control strategies. This allows for real-time prediction and regulation of the wire's temperature before it enters the molten pool, based on key system inputs such as coil current and wire feed speed.

The outcomes of this research advance wire-based additive manufacturing by enabling thermal control and leveraging magnetic fields to influence melt pool dynamics, enhance Marangoni convection, and suppress instabilities.

In summary, this work establishes a validated modeling framework for designing and optimizing inductive heating in wire-based L-DED, providing advancements in process stability.

3.8 ACKNOWLEDGEMENTS

The authors acknowledge the Post-Graduate Program in Mechanical Engineering and the Post-Graduate Program in Electrical Engineering at the Federal University of Santa Catarina (UFSC) for their academic and institutional support. The authors also wish to thank the Laboratory of Electromagnetism and Electromagnetic Compatibility (MagLab/UFSC), the Precision Engineering Laboratory (LMP/EMC/UFSC), and the Welding and Mechatronics Institute (LABSOLDA/UFSC) for providing the experimental infrastructure and technical assistance essential for the development of this research. The authors also acknowledge the Brazilian National Council for Scientific and Technological Development (CNPq) for the doctoral scholarship support.

3.9 REFERENCES

[1] Sibisi TH, Shongwe MB, Tshabalala LC, Mathoho I (2023) Lam Additive Manufacturing: A fundamental review on mechanical properties, common defects, dominant processing variables, and its applications. The International Journal of Advanced Manufacturing Technology 128(7–8):2847–2861. https://doi.org/10.1007/s00170-023-12139-w

[2] Dai D, Li Y, Gu D, Zhao W, Long Y, Shi X, Zhang H, Lin K, Xi L (2024) Role of angular velocity on Marangoni convection shifting, heat accumulation, and microstructure evolution using laser directed energy deposition. J Appl Phys 135(5):1–17.https://doi. org/10.1063/5.0187045

[3] Kar A, Mazumder J (1995) Mathematical modeling of key-hole laser welding. J Appl Phys 78(11):6353–6360. https://doi.org/10.1063/1.360686

[4] Ding D, Pan Z, Cuiuri D, Li H (2015) Wire-feed additive manufacturing of metal components: technologies, developments and future interests. The International Journal of

Advanced Manufacturing Technology 81:465–481. https://doi.org/10.1007/s00170-015-7077-3

[5] Kisielewicz A, Pandian KT, Sthen D, Hagqvist P, Bermejo MAV, Sikström F, Ancona A (2021) Hot-Wire Laser-Directed Energy Deposition: Process Characteristics and Benefits of Resistive Pre-Heating of the Feedstock Wire. Metals 11(4):634. https://doi.org/10.3390/met11040634

[6] Zhong C, Pirch N, Gasser A, Poprawe R, Schleifenbaum J (2017) The Influence of the Powder Stream on High-Deposition-Rate Laser Metal Deposition with Inconel 718. Metals 7(10):443. https://doi.org/10.3390/met7100443

[7] Peng W, Jiguo S, Shiqing Z, Gang W (2015) Control of wire transfer behaviors in hot wire laser welding. The International Journal of Advanced Manufacturing Technology 83(9–12):2091–2100.https://doi.org/10.1007/s00170-015-7696-8

[8] Huang W, Xiao J, Chen S, Jiang X (2022) Control of wire melting behavior during laser hot wire deposition of aluminum alloy. Optics Laser Technol 150:107978. https://doi.org/10.1016/j.optlastec.2022.107978

[9] Zhao S, Xu S, Huang Y, Yang L (2021) Laser hot-wire cladding of Ni/WC composite coatings with a tubular cored wire. JMater Process Technol 298:117273. https://doi.org/10.1016/j.jmatprotec.2021.117273

[10] Gatzen M, Tang Z, Vollertsen F (2011) Effect of electromagnetic stirring on the element distribution in laser beam welding of aluminium with filler wire. Phys Procedia 12:56–65. https://doi.org/10.1016/j.phpro.2011.03.008

[11] Dutra MK, Pereira M, Lavaqui FAF, Faria TC (2023) Design, Implementation and Evaluation of a Wire Feeding System with Induction Heating Applied to L-DED. In: de Oliveira D, Ziberov M, Machado AR (eds), Proceedings of the 8th thematic conference on mechanical design of process machines, equipment and installations, pp 105–113. Springer Nature Switzerland, Cham. https://doi.org/10.1007/978-3-031-43555-3_10.

[12] Xu D, Liu X, Wang P, Yang J, Xu W, Fang H (2010) Dynamic evolution of welding residual stress field under noncontact electromagnetic force. J Appl Phys 107(5):053902. https://doi.org/10.1063/1.3319578

[13] VoigtAL, Cunha TV,Niño CE (2020) Conception, implementation and evaluation of induction wire heating system applied to hot wire GTAW(IHW-GTAW). J Mater Process Technol 281:116615.https://doi.org/10.1016/j.jmatprotec.2020.116615

[14] Gräf S, Staupendahl G, Seiser C, Meyer B-J, Müller FA (2010) Generation of a dynamic polarized laser beam for applications in laser welding. J Appl Phys 107(4):1–6. https://doi.org/10.1063/1.3295911

[15] Voigt AL, Cunha TV, Niño CE (2020) Conception. Implementation and evaluation of induction wire heating system applied to hot wire GTAW (IHW-GTAW). In: Journal of materials processing technology, 281:116615. https://doi.org/10.1016/j.jmatprotec.2020.116615.

[16] Rudnev V, Loveless D, Cook RL (2017) In: Handbook of Induction Heating, CRC Press, Boca Raton, 2nd edn, pp 51–69

[17] Mohan N, Undeland TM, Robbins WP (2003) Power Electronics – Converters, 3rd edn. Applications and Design. Wiley, Danvers

[18] Griffiths DJ (2013) Introduction to Electrodynamics. Pearson, New Jersey, 4th edn, pp 233–327

[19] Sadiku MNO (2015) Elements of Electromagnetics, 6th edn. Oxford University Press, New York

[20] Rudnev V, Loveless D, Cook RL (2017) Handbook of Induction Heating. CRC Press, Boca Raton, 2nd edn, pp 51–69

[21] Zinn S, Semiatin SL (1988) Elements of Induction Heating - Design. Novelty, Control and Applications. ASM International, pp 9–23

[22] Freda M, Macci F, D'Amanzo E, Colaneri A (2024) Santisteban VM Induction Heating Optimizing for Steel Billets: Advanced Electromagnetic-Thermal Modeling Approach. In: Proceedings of the COMSOL conference, Florence, COMSOL, pp 1–7

[23] Simpson PG (1960) Induction Heating Coil and System Design. McGrawHill, New Jersey, pp 33–35

[24] ANSYS (2021) Maxwell Help. ANSYS, Canonsburg

[25] Incropera FP, Dewitt DP, Bergman TL, Lavine AS (2017) External Flow. In: Fundamentals of heat and mass transfer, chapter 7, pp 401–452. Wiley, Hoboken, 6th edn

[26] Incropera FP, Dewitt DP, Bergman TL, Lavine AS (2017) Radiation: Process and Properties. In: Fundamentals of heat and mass transfer, chapter 12, pp 723–776. Wiley, Hoboken, 6th edn

[27] Çengel YA, Boles MA, Kanoglu M (2019) Energy Analysis of Closed Systems. In: Thermodynamics, an engineering approach, chapter 4, pp 161–194. McGraw-Hill, New York, 9th edn 2019

[28] Prujansky CL, Dutra MK, Pereira M (2025) Evaluation of Wire Temperatures and Power Control in Inductive Heating for Directed Energy DepositionWith Laser. In: Proceedings of the 13th Brazilian congress of manufacturing engineering – COBEF 2025, Salvador.
Brazilian Assoc Mech Eng Sci – ABCM

[29] ANSYS (2021) Icepak Help. ANSYS, Canonsburg

4 EFFECT OF THE MAGNETIC FIELD GENERATED BY COIL ON METAL TRANSFER BEHAVIOR IN WIRE-LASER DIRECTED ENERGY DEPOSITION

Manoel Kolling Dutra[1], Caio Linhares Prujansky[1], Milton Pereira[1],

Régis Henrique Gonçalves e Silva[1], Marcelo Pompermaier Okuyama[1], Adroaldo Raizer[2], Emanoel Pereira Elias[2]

[1]Department of Mechanical Engineering, Federal University of Santa Catarina, Delfino

Conti Street, Florianópolis, 88040-900, Santa Catarina, Brazil.

[2]Department of Electrical and Electronic Engineering, Federal University of Santa Catarina, Delfino

Conti Street, Florianópolis, 88040-900, Santa Catarina, Brazil.

Abstract

Wire-Laser Directed Energy Deposition (W-LDED) offers high deposition rates and efficient material utilization but is limited by unstable metal transfer, spatter formation, and excessive dilution, which reduce process robustness and deposit quality. This work investigates the influence of an electromagnetic field (EMF), generated by a custom-designed coil, on metal transfer dynamics and bead morphology in W-LDED. High-speed imaging at 1000 fps was employed to capture transient droplet melt pool interactions, while cross-sectional macrographs were analyzed to quantify bead geometry and dilution. The application of EMF stabilized the liquid-bridge transfer, reduced rupture frequency and spatter, and improved robustness under wire misalignment by redirecting droplets toward the melt pool. Quantitative analysis showed that EMF increased bead height from 0.81 to 0.97 mm, bead width from 2.50 to 2.60 mm, and cross-sectional area from 1.52 to 1.84 mm^2, while reducing dilution from 41.98% to 26.69%. These effects are attributed to Lorentz forces arising from the interaction between the applied magnetic field and electrically induced currents in the molten metal, which damp Marangoni-driven convection and promote a more uniform thermal distribution. The results demonstrate that electromagnetic assistance is a practical strategy to enhance metal transfer stability, bead quality, and process reliability in W-LDED.

Keywords: W-LDED, Electromagnetic Field, Metal Transfer, High-speed Imaging, Additive Manufacturing.

4.1 INTRODUCTION

Additive Manufacturing (AM) has become a key enabling technology for producing complex metallic components with improved material efficiency, design flexibility, and reduced lead times, particularly in high-value industrial applications such as aerospace, automotive, and energy sectors [1–3]. Among AM processes, Direct Energy Deposition (DED) has attracted considerable attention due to its capability of repairing and fabricating near-net-shape parts with high deposition rates [1]. When using wire as the feedstock, Wire Laser Energy Deposition (W-LDED) offers advantages such as higher material utilization efficiency, reduced contamination risks, and lower costs compared to powder based DED [2, 3]. These benefits make W-LDED particularly suitable for aerospace, automotive and energy applications. Despite the advantages, the process still faces critical challenges related to metal transfer dynamics and metal pool stability. Instabilities during the feeding and melting of the wire can result in irregular bead geometry, lack of fusion, and porosity [4, 5]. Therefore, understanding and controlling the metal transfer mechanisms are essential to improve process reliability and part quality. To this end, advanced monitoring techniques, including coaxial optical systems and high-speed imaging, have been employed to capture transient melt pool phenomena and droplet transfer dynamics [6–8]. High-speed videography, in particular, has proven to be a powerful tool to reveal the underlying mechanisms of liquid bridge formation, droplet detachment, and melt pool oscillations in real time [9]. Recent studies have also explored the application of auxiliary fields, such as magnetic or ultrasonic excitation, to control melt pool behavior and enhance deposition stability [10–13].

The introduction of an electromagnetic coil to generate a magnetic field constitutes a promising approach for controlling the magnetohydrodynamics of the melt pool. The application of a static electromagnetic field reduces oscillations of the internal forces within the melt pool as a result of electromagnetic forces associated with currents induced in the liquid metal and the interaction between the external magnetic field and electrical currents arising from temperature variations (thermoelectric currents). As a result, improved welding quality is achieved, with reduced surface roughness and a decreased need for subsequent machining

operations. Moreover, magnetic field control stands out among techniques for mitigating oscillations in the welding process as a non-contact solution, offering high controllability, precision, and robustness when compared to other techniques, such as the use of ultrasonic or mechanical vibrations [14].

Previous studies on magnetic-field-assisted laser welding have reported similar stabilization phenomena. Huang *et al.* [15] experimentally demonstrated that a transverse magnetic field suppresses porosity formation by stabilizing melt pool flow during laser welding of steels. Likewise, Wang *et al.* [16] investigated the influence of magnetic-field orientation on molten-pool behavior and showed that a Y-direction field can effectively modulate flow symmetry and improve weld uniformity. More recently, Lu *et al.* [17] performed laser penetration tests under different magnetic-field positions and confirmed that externally applied magnetic fields can significantly alter melt pool morphology and energy distribution. These findings support the hypothesis that static magnetic fields can control melt pool convection through Lorentz forces, motivating the present investigation of coil-assisted magnetic fields applied to wire-laser directed energy deposition.

Although electromagnetic-assisted laser welding and directed energy deposition (DED) processes have been extensively investigated, most existing studies focus on melt pool geometry, microstructural evolution, or numerical modeling of magnetohydrodynamic effects. In contrast, direct high-speed visual evidence of droplet transfer stabilization under electromagnetic field assistance in wire-laser directed energy deposition (WLDED) remains scarce. This study experimentally demonstrates, through high-speed imaging and quantitative geometric analysis, how a static electromagnetic field generated by a custom-designed coil stabilizes liquid-bridge transfer, delays droplet detachment, reduces spatter, and improves bead geometry and dilution in W-LDED.

The present work aims to fill this gap by investigating the influence of an electromagnetic coil on metal transfer behavior in W-LDED. Highspeed imaging was employed to capture transient droplet–melt pool interactions under coil assisted and reference conditions. By combining electromagnetic characterization of the coil with image-based analysis of metal transfer, this study provides new insights into the role of magnetic fields in stabilizing wire-fed DED processes. The findings contribute to a better understanding of process physics and pave the way toward more controlled and robust manufacturing strategies.

4.2 MAGNETIC FIELD GENERATION COIL

This section presents the design and construction of the electromagnetic coil developed to generate a controlled static magnetic field in the W-LDED system. The coil was specifically designed to provide a uniform magnetic flux around the wire–melt pool interaction zone, enabling the experimental evaluation of magnetic field influence on metal transfer dynamics and bead morphology. Analytical calculations, numerical simulations, and experimental measurements were performed to characterize its electromagnetic behavior.

4.2.1 Design Aspects of the Coil

The goal of the coil design is to establish a continuous magnetic field over the welding region. For this purpose, the coil was designed to operate at 24 V_{DC} and a current of 0.45 A. Enameled copper wire of 26 AWG was used, and, in order to generate a significant magnetic field, the coil was wound with 3300 turns around an air core.

Figure 4.1 shows the coil built for magnetic field generation, while Table 4.1 summarizes its main design characteristics.



Figure 4.1 - Coil designed for magnetic field generation.

Table 4.1 - Coil design characteristics.

Length	65 mm
Outer Diameter	52 mm
Inner Diameter	22 mm
Number of Turns	3300
Wire Gauge	26 AWG

The DC electrical resistance of this coil can be estimated based on its design features using Equation 4.1, whereas the inductance can be estimated using Equation 4.2 [18].

$$R = \frac{2.\pi.r.N_{coil}}{\sigma.S_{wire}} \quad (4.1)$$

$$L = \frac{\mu_0.N^2.\pi.r_{coil}^2}{L_{coil}} \quad (4.2)$$

Where R is the coil resistance (Ω), r_{coil} is the mean radius of the coil (m), N is the number of turns, σ is the conductivity of copper (S/m), S_{wire} is the cross-sectional area of the copper wire (m^2), L is the coil inductance (H), μ_0 is the magnetic permeability of free space ($4\pi \times 10^{-7}$ H/m) and l_{coil} is the length of the coil (m) [18].

The magnetic field generated inside this coil can be estimated based on Ampère's Law using Equation 4.3, and the magnetic flux density can be obtained from Equation 4.4 [18].

$$H = \frac{N.I}{L_{coil}} \quad (4.3)$$

$$B = \mu.H \quad (4.4)$$

Where H is the magnetic field (A/m), N is the number of turns of the coil, l_{coil} is the length of the coil (m), I is the electric current flowing through the coil (A), B is the magnetic flux density (T), and μ is the magnetic permeability inside the coil (H/m). It is important to note that this expression derives from the assumption of an infinitely long solenoid, where the field is considered uniform inside the coil. In this case, the coil length-to-radius ratio is not very large, so edge effects are relevant and cause deviations from the idealized value, particularly near the coil ends [18].

4.2.2 Electromagnetic Simulation

A computational simulation of the field generation coil was performed using the Finite Element Method (FEM) with a magnetodynamic solution [19]. The aim of this simulation was to evaluate the design aspects presented in Section 4.2.1, as well as the distribution of the magnetic field around the coil. The software used to develop the simulation model was Ansys Maxwell, version 2022 R1 [19].

The simulation model was developed based on the dimensions presented in Table 4.1, with the coil represented as a copper tube, as illustrated in Figure 4.2 (a). In the simulation, the electrical conductivity of copper was set to 5.8×10^7 S/m, and the relative magnetic permeability was assumed to be unity. The excitation was applied by injecting a DC current of 0.45 A into the coil section, as shown in Figure 4.2 (b). Figure 4.2 (c) shows the finite element mesh generated for the coil structure.

Furthermore, the thickness of the tube used to represent the coil was adjusted to preserve the same conductive cross-section as the constructed coil shown in Figure 1. In this way, it is ensured that the simulation model maintains the current carrying characteristics of the real coil.

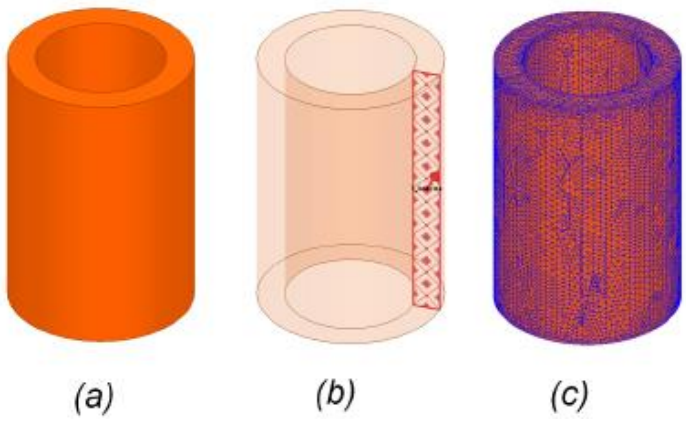


Figure 4.2 - Simulation model of the coil. (a) Coil body model. (b) Excitation section with current. (c) Finite element mesh generated on the coil.

4.2.3 Electromagnetic Characterization of the Field Generation Coil

Based on the design aspects of the coil and the analytical equations presented in Section 4.2.1, the main electromagnetic characteristics of the coil were determined analytically. Additionally, these characteristics were obtained using the simulation model described in Section 4.2.2. The corresponding results are summarized in Table 4.2. Table 4.2 presents the electromagnetic parameters of the coil determined both analytically and through simulation, namely: the electrical resistance (R), the inductance (L), the magnetic field inside the coil (H), and the corresponding magnetic flux density (B). For validation purposes, the resistance and

inductance of the actual coil, shown in Figure 4.1, were measured using an impedance analyzer operating at 20 Hz. These values are also included in Table 4.2.

Table 4.2 - Electromagnetic Characteristics of the Field Generation Coil.

	Analytical	***Simulation***	***Measurement***
R (Ω)	51.34	51.32	50.61
L (mH)	226.37	156.58	138.75
H (kA/m)	22.84	19.84	-
B (mT)	28.71	24.93	-

Figure 4.3 shows the magnetic field distribution estimated using the simulation model described in Section 4.2.2.

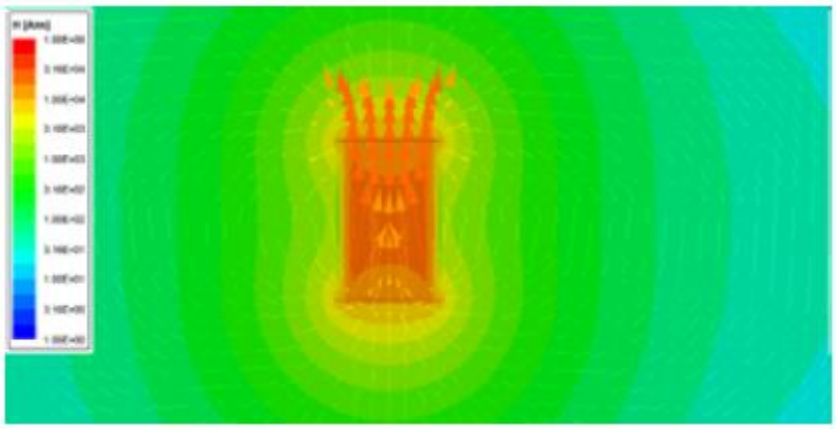


Figure 4.3 - Magnetic field distribution in the simulated coil.

4.3 HIGH-SPEED VIDEOGRAPHY ANALYSIS OF METAL TRANSFER

High-speed imaging was employed to capture transient phenomena of wire–melt pool interaction during Wire-Laser Directed Energy Deposition (W-LDED). The experiments were conducted using a Photron FASTCAM Nova S9 high-speed camera, operating at a frame rate of 1000 fps with a resolution of 1024 × 1024 pixels. A Canon EF 180 mm macro lens was used in combination with an EF 2× III extender, providing enhanced magnification of the interaction zone. The exposure time was 10 μs, and a bandpass filter (810 ± 12 nm, Ø 50 mm) was mounted

to suppress background radiation from the melt pool and laser reflections. Illumination was provided by a Cavilux-HF laser system, delivering 810 ± 10 nm wavelength at 500 W.

This setup ensured high-contrast visualization of the melt pool and droplet dynamics under the intense radiation environment of the laser process. The combined optical arrangement enabled the real-time observation of liquid bridge formation and behavior, droplet detachment, and melt pool oscillations under both reference (no coil) and electromagnetic coil-assisted conditions.

Experiments were carried out using a fiber laser (IPG Photonics YLS 10000) operating at 1.3 kW, with a deposition speed of 300 mm/min and wire feed rate of 0.85 m/min. The feedstock material was ER70S-6 (Ø 1.2 mm) wire deposited on SAE 1020 steel substrates. The electromagnetic coil was integrated around the wire path to generate a static magnetic field acting directly on the melt pool. The experimental setup can be seen in Figure 4.4.

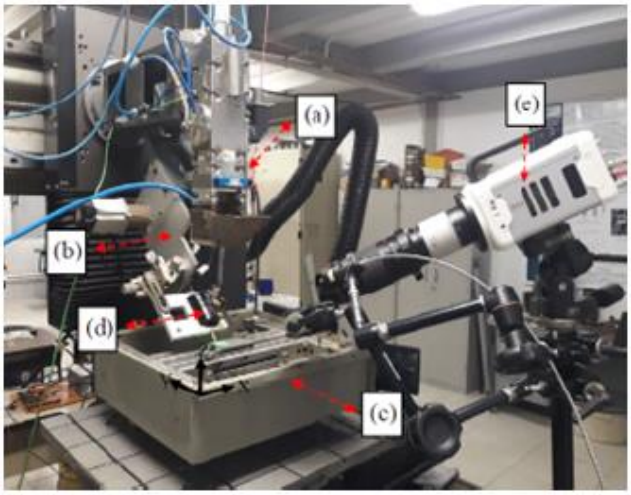


Figure 4.4 - Experimental setup for high-speed imaging of the W-LDED process with electromagnetic coil assistance. Where a) Laser head, b) Wire feeder, c) Processing chamber, d) Electromagnetic coil developed for the experiments, e) High-speed camera.

For each experimental condition investigated in this study (with and without electromagnetic field assistance), a single deposition track was produced and recorded using high-speed imaging. This approach was intentionally adopted to ensure a controlled and direct comparison of transient metal transfer behavior under identical processing parameters. Due to the high data rate and experimental complexity associated with high-speed videography, the

analysis focused on detailed frame-by-frame evaluation of melt pool and droplet dynamics within individual deposition events, rather than statistical comparison across multiple tracks.

Figure 4.5 presents a schematic representation of the experimental setup, highlighting the welding region in greater detail. The illustration shows that the electromagnetic coil is positioned along the wire at a fixed distance of approximately 40 mm from the laser melt pool interaction zone. This configuration was adopted to allow the magnetic field to directly influence the metal transfer and molten pool dynamics without mechanically interfering with the deposition process.

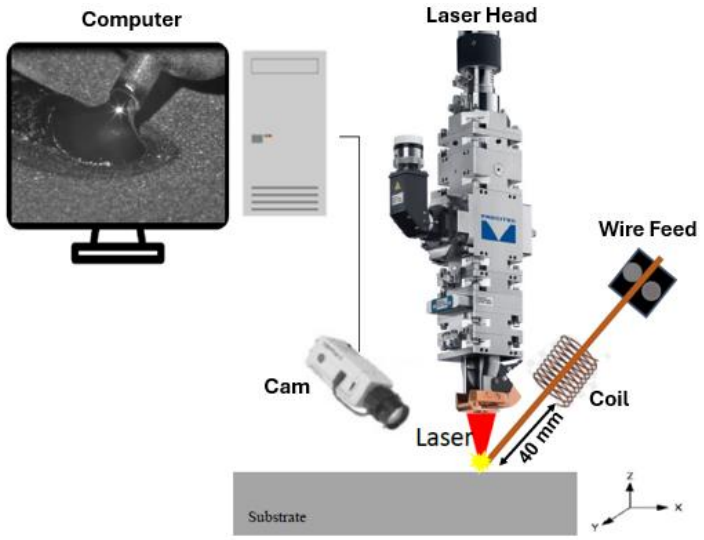


Figure 4.5 - Schematic of the experimental setup used in the W-LDED process, showing the laser head, wire feeding system, electromagnetic coil, and imaging system. The coil is positioned along the wire at a fixed distance of approximately 40 mm from the laser–melt pool interaction zone.

In Figure 4.6, a close-up view of the experimental setup is presented, in which the welding area, the magnetic field generation coil, and the illumination laser used for the high-speed image acquisition system are highlighted.

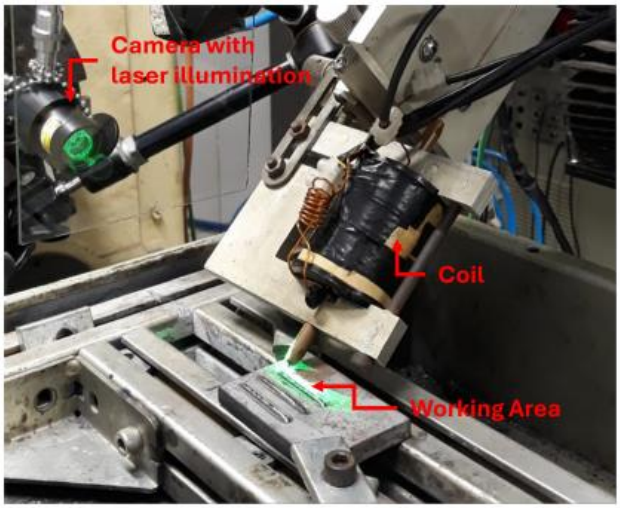


Figure 4.6 - Close-up view of the experimental setup.

4.3.1 Metal Transfer without EMF Assistance

In the absence of electromagnetic assistance, the metal transfer was dominated by liquid-bridge dynamics, where the molten wire maintained a short but highly unstable neck connection to the substrate (see Supplementary Video S1[2]). This instability was characterized by rapid oscillations of the molten neck thickness and irregular variations in droplet volume, caused by fluctuations in heat input and Marangoni-driven convection at the wire tip. High-speed imaging in Figure 4.7 shows that the molten region at the wire tip expanded non-uniformly from approximately 0.14 mm^2 to 1.55 mm^2 reflecting sudden increases in melt volume followed by partial contraction. These transient enlargements led to intermittent rupture of the liquid bridge [20] and sporadic ejection of spatter, which in turn caused measurable variations in bead geometry and dilution.

The molten region areas reported in Figure 4.7 were quantified using the ImageJ software by manually segmenting the contour of the molten metal visible at the wire tip in each frame. For this analysis, three independent measurements were performed on consecutive high-speed images acquired during a single deposition track. The reported values correspond to average areas obtained from these measurements. The relatively small variation observed between frames reflects transient fluctuations inherent to the liquid bridge dynamics rather than variability among independent deposition experiments. Therefore, these measurements are

[2] Supplementary Video S1 can be accessed online at: Video S1

representative of instantaneous metal transfer behavior under the investigated conditions and are used here to illustrate the characteristic instability of the non-assisted process.

The oscillations observed in the molten metal contour arise not only from Marangoni-driven convection and thermocapillary flows naturally present in the melt pool, but also from the interaction with the laser-induced plasma plume. The plasma exerts both a localized pressure on the molten surface and a shear-drag effect due to vapor flow, which together with surface-tension gradients promote fluctuating fluid motion and amplify instabilities when no external control is applied [21–24]. Previous studies confirm that variability in metal transfer and molten pool oscillations remain critical challenges in W-LDED [4, 5].

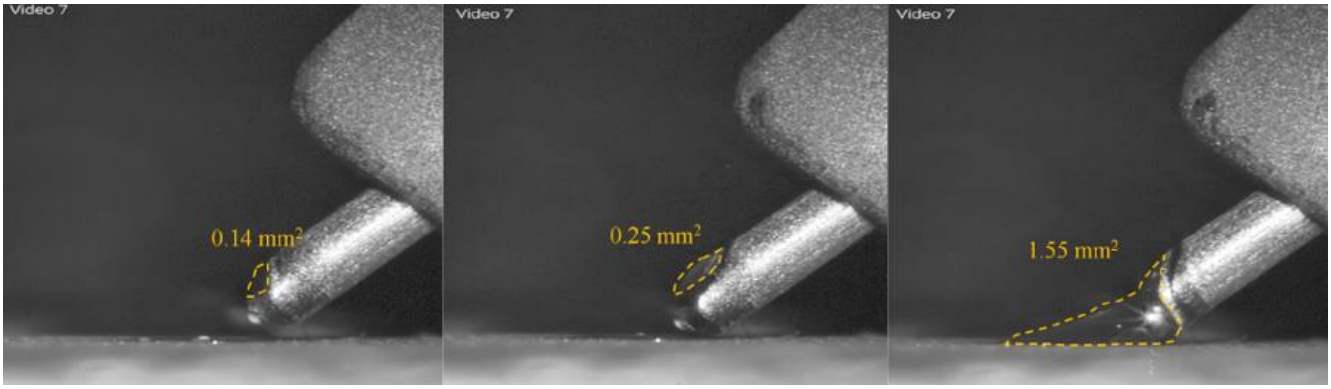


Figure 4.7 - High-speed image sequence of metal transfer in WLDED without coil assistance.

4.3.2 Metal Transfer with EMF Assistance

High-speed imaging revealed that when the electromagnetic coil was activated (20–30 mT; corroborated by finite-element simulation), the metal transfer dynamics exhibited significant changes compared to the no-EMF condition (see Supplementary Video S2[3]). It is important to emphasize that the wire feed rate (0.85 m/min), laser power (1.3 kW), and scanning speed (300 mm/min) were kept constant in both cases (with and without coil assistance). Therefore, the observed differences in droplet retention, liquid bridge stability, and bead geometry can be attributed to the influence of the applied magnetic field. As shown in Figure 4.8, the molten region at the wire tip exhibited a steadier and more uniform increase in size,

[3] Supplementary Video S2 can be accessed online at: Video S2

ranging from approximately 1.68 mm^2 to 2.98 mm^2, which indicates a delayed and more controlled droplet detachment under the influence of the applied magnetic field. Unlike the no assisted condition, where the molten volume fluctuated irregularly, the EMF assisted case showed a consistent enlargement rate between consecutive frames, evidencing improved thermal and geometric stability of the liquid bridge. This longer retention of the molten metal at the wire tip produced a larger molten region confined to the wire end and promoted a more stable and repeatable liquid-bridge formation, with reduced fluctuation in neck thickness and detachment timing compared to the non-assisted condition. From a physical standpoint, these experimentally observed changes can be interpreted based on magnetohydrodynamic interactions between the applied magnetic field and the electrically conductive molten metal, as detailed below.

The molten region areas reported in Figure 4.8 were quantified using the ImageJ software by segmenting the visible molten metal contour at the wire tip in each high-speed frame. For this analysis, three independent measurements were performed on consecutive frames acquired during a single deposition track under electromagnetic field (EMF) assistance. The reported values correspond to average areas obtained from these measurements. The relatively uniform growth of the molten region and the reduced frame to frame variability reflect the stabilizing effect of the applied magnetic field on liquid bridge dynamics, rather than statistical variability among independent deposition experiments.

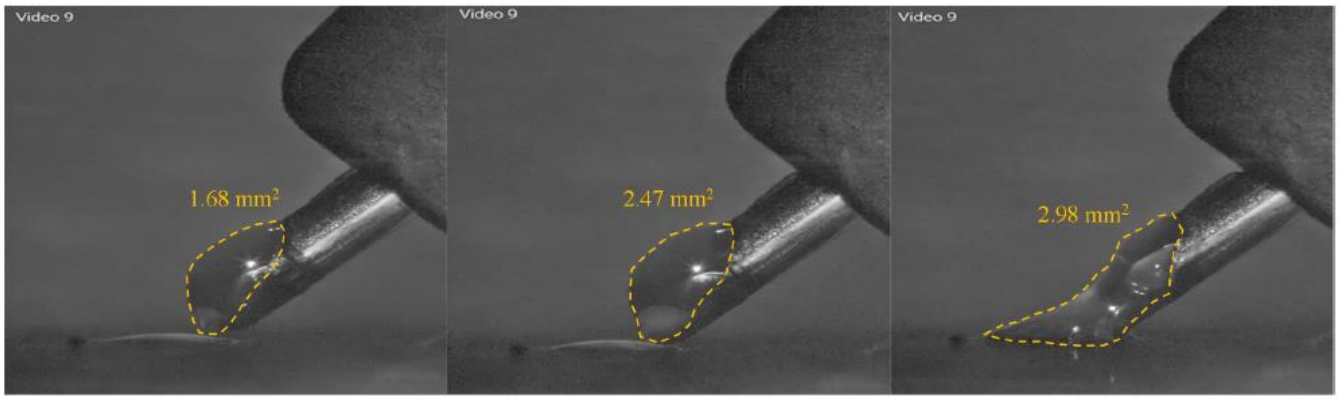


Figure 4.8 - High-speed image sequence of metal transfer in WLDED with electromagnetic coil assistance.

The observed behavior can be explained by the action of Lorentz forces arising from the interaction between the applied static magnetic field (B) and the electrical currents (J) naturally present in the conductive molten metal. These currents originate from thermal gradients, fluid motion, and the laser–wire interaction. The electromagnetic force acting on an elemental molten volume can be expressed by Equation 4.5.

$$dF = J.B.dV \qquad (4.5)$$

where dF is the infinitesimal force acting on a volume element dV . Equivalently, the volumetric force density is defined by Equation 4.6.

$$f = J.B \qquad (4.6)$$

This volumetric force introduces an upward component that counteracts gravity, effectively "holding" the droplet longer at the wire tip. Such a formulation, consistent with magnetohydrodynamic descriptions of molten metal flow [14], explains the observed delay in droplet detachment. Figure 4.9 schematically represents this balance of forces, showing gravity driving the droplet downward and the resultant Lorentz force acting upward against it.

In the welding process, the application of an external magnetic field induces current densities in the electrically conductive liquid metal through motional induction mechanisms (u × B), resulting from the relative motion of the molten droplet across the magnetic field lines. In addition, electrical currents also circulate within the molten droplet due to thermoelectric effects associated with spatial gradients of temperature and chemical composition. These current densities (J), present in both the molten droplet and the melt pool, interact with the external magnetic field (B) generated by the coil, giving rise to volumetric Lorentz forces (f = J × B). As the magnetic field is oriented along the coil axis, the resulting Lorentz force exhibits a significant upward component within the molten region, partially counterbalancing gravitational forces and acting as an electromagnetic braking mechanism that suppresses instabilities in the liquid metal flow. Consequently, droplet detachment is delayed, the geometry of the melt pool is moderately modified, and metal transfer occurs in a smoother and more controlled manner, characterized by reduced spatter and diminished oscillatory behavior. This

electromagnetic damping mechanism, schematically illustrated in Figures 4.9–4.11, demonstrates the effectiveness of electromagnetic-field-assisted processing in promoting weld bead uniformity [22, 25–27].

It is important to note that the filler wire used in this study (ER70S-6) exhibits ferromagnetic behavior at room temperature and is therefore magnetically responsive prior to melting. However, the primary stabilization mechanism observed under electromagnetic field (EMF) assistance is governed by Lorentz forces resulting from the interaction between electrically induced currents (J) in the conductive molten metal and the externally applied magnetic field (B). This magnetohydrodynamic effect does not require ferromagnetic material behavior and remains active as long as the molten metal is electrically conductive. Once the wire and melt pool reach elevated temperatures during deposition, the magnetic permeability of ferromagnetic steels decreases significantly, approaching that of nonferromagnetic materials. Under these conditions, the Lorentz-force-driven interaction (J×B) dominates over magnetization effects. Consequently, a similar qualitative influence of electromagnetic field assistance is expected for fully austenitic (non-ferromagnetic) wires, although differences in electrical conductivity, melt viscosity, and thermal gradients may alter the magnitude of the stabilization effect. A systematic comparison between ferromagnetic and austenitic filler materials represents an important direction for future work.

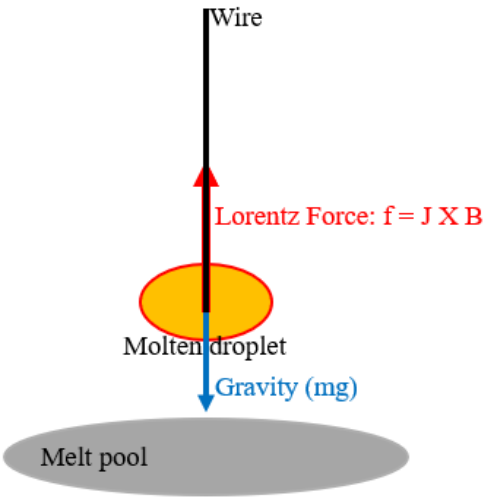


Figure 4.9 - Schematic of forces before droplet detachment.

Once the droplet touches the molten pool, the entire pool also becomes subjected to the applied magnetic field. Both high-speed imaging and schematic analysis suggest that the pool is slightly elevated under the influence of the electromagnetic field, reducing the effective distance between the wire and the molten pool. Although a mild convexity of the pool surface also appears without EMF primarily due to surface tension and plasma-induced pressure the elevation is notably enhanced when the electromagnetic field is applied. Quantitatively, the average pool height increased from approximately 0.81 mm (without EMF) to 0.97 mm (with EMF), confirming the upward action of the Lorentz force that counteracts gravity and concentrates molten material above the fusion line. This geometric modification promotes earlier and more consistent contact, which stabilizes the liquid bridge transfer and reduces spattering and interruptions. Figure 4.10 illustrates this effect, where the raised melt pool is closer to the wire tip, favoring coalescence.

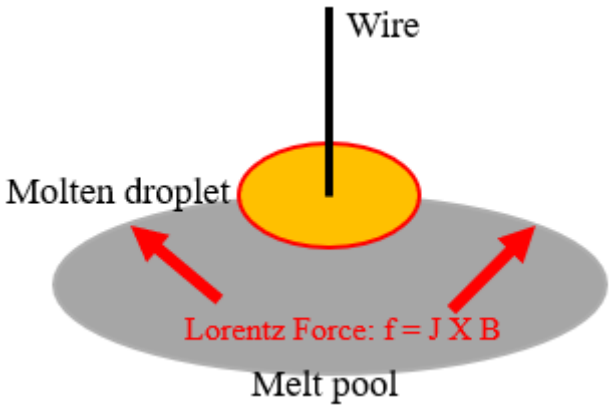


Figure 4.10 - Schematic of raised melt pool after droplet contact.

The melt pool height was quantified using ImageJ by measuring the vertical distance between the pool apex and the fusion line on high-speed images. For each condition, three independent measurements were performed on consecutive frames acquired during a single deposition track, and the reported values correspond to mean values. Without electromagnetic field (EMF) assistance, the average melt pool height was 0.81 ± 0.05 mm, whereas under EMF assistance it increased to 0.97 ± 0.04 mm. The reported standard deviations reflect frame-to-frame variability associated with transient melt pool dynamics rather than variability among independent deposition experiments.

These findings are consistent with previous reports that external electromagnetic fields can modify droplet trajectory, suppress spattering, and stabilize melt pool dynamics in wire-fed deposition [25, 28, 29]. Moreover, the role of Lorentz forces in damping turbulent Marangoni convection and redistributing thermal energy has been discussed in comprehensive review [10, 11]. The present experimental evidence provides new insight into how static coil-assisted fields stabilize metal transfer in W-LDED by delaying droplet detachment, enlarging the molten wire tip, and elevating the melt pool to facilitate earlier contact.

4.3.3 Discussion of Physical Mechanisms

The stabilization effect observed can be attributed to the interaction between induced currents and the applied magnetic field, resulting in localized Lorentz forces acting on the conductive liquid, as illustrated schematically in Figure 4.11.

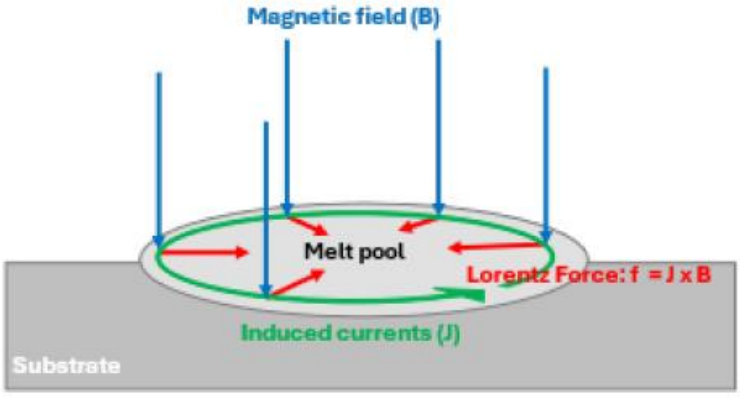


Figure 4.11 - Schematic illustration of Lorentz forces acting within the melt pool under electromagnetic field assistance. Induced currents (J, green arrows) circulate in a coherent pattern within the conductive molten metal under the applied magnetic field (B, blue arrows), which is oriented along the coil axis. The resulting Lorentz forces (F = J×B, red arrows) generate an upward and symmetric distribution that counteracts gravity and resists irregular fluid motion, thereby damping oscillations and stabilizing the liquid bridge between the molten wire and the pool.

These forces oppose irregular flow, effectively damping oscillations and reducing turbulence in the melt pool. Consequently, the liquid bridge connecting the molten wire to the pool remains more stable, and droplet detachment occurs under more predictable conditions. Such findings are consistent with theoretical predictions of electromagnetic field influence on liquid metal dynamics [14, 25, 30]. Importantly, the high-speed imaging approach provides

direct experimental validation of these mechanisms, offering insights not captured by purely analytical or numerical studies.

4.3.4 Melt pool behavior under electromagnetic field assistance

High-speed imaging provided additional insight into the effect of the electromagnetic field on melt pool dynamics. Representative frames are shown in Figure 4.12, with ImageJ-based measurements of the melt pool area under conditions without and with EMF.

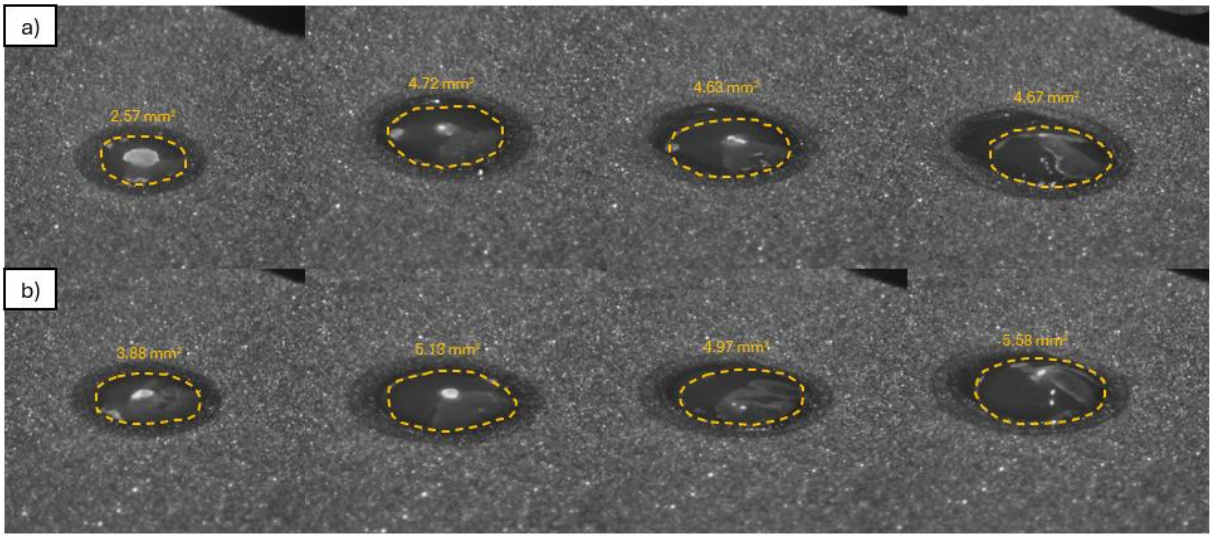


Figure 4.12 - High-speed imaging of the melt pool area with and without electromagnetic field (EMF) assistance. (a) Without EMF (b) With EMF.

Without EMF, the melt pool area fluctuated between 2.57 and 4.72 mm^2 throughout the exposure period (see Supplementary Video S3[4]). These values correspond to sequential frames captured during a single deposition test (laser power of 1.3 kW and deposition speed of 300 mm/min), in which the substrate was initially at room temperature. The observed dispersion ($\Delta A \approx \pm 0.9$ mm^2) reflects transient thermal fluctuations as the pool gradually expands before reaching a quasi-steady state, rather than variations among independent repetitions. This dispersion indicates unstable molten pool flow, consistent with turbulent convection and oscillatory behavior. In contrast, when EMF was applied, the melt pool area increased to 3.88 5.58 mm^2, with an average of 4.89 mm^2 and lower variability of $\pm$ 0.7 mm^2 (see Supplementary Video S4[5]). The increase in average area reflects the action of Lorentz forces opposing gravity and slightly elevating the pool, thereby concentrating molten material above the fusion line. At

[4] Supplementary Video S3 can be accessed online at: Video S3
[5] Supplementary Video S4 can be accessed online at: Video S4

the same time, the reduction in variability demonstrates that these forces dampen oscillations and suppress irregular flow, resulting in a more thermally stable molten pool.

The stabilizing effect of EMF observed in these high-speed images is consistent with previous reports that electromagnetic fields modify melt pool geometry, reduce turbulence, and promote more controlled energy distribution [2, 10, 11]. The elevated and more stable pool favors earlier contact between the wire and the molten metal, contributing to the establishment of a stable liquid bridge and improved transfer predictability.

4.4 RESULTS AND DISCUSSION

The following results analyze the influence of the applied electromagnetic field (EMF) on the metal transfer behavior and the resulting bead morphology in the W-LDED process. High-speed imaging was correlated with cross sectional macrographs to interpret droplet dynamics, liquid-bridge stability, and dilution changes. These analyses provide experimental evidence of how electromagnetic interaction modifies melt pool geometry and improves process stability.

For clarity, a concise summary of the main qualitative observations and quantitative results obtained with and without electromagnetic field (EMF) assistance is provided in Table 4.3. This table highlights the key improvements in metal transfer stability, melt pool geometry, bead dimensions, and dilution, enabling a direct and comprehensive comparison between both processing conditions.

Table 4.3 - Summary of key experimental observations and quantitative results obtained without and with electromagnetic field (EMF) assistance in W-LDED.

Parameter	***Without EMF***	***With EMF***	***Measurement***
Metal transfer mode	Unstable liquid bridge	Stabilized liquid bridge	Reduced rupture frequency and spatter
Molten region area at wire tip (mm^2)	0.14–1.55	1.68–2.98	Larger and more stable molten region
Melt pool area (mm^2)	2.57–4.72 (avg. ≈ 3.65)	3.88–5.58 (avg. ≈ 4.89)	Increased area with reduced variability
Melt pool height (mm)	0.81 ± 0.05	0.97 ± 0.04	Elevated pool due to Lorentz forces

Bead width (mm)	2.50	2.60	Slight increase
Bead height (mm)	0.81	0.97	Increased bead reinforcement
Cross-sectional area (mm2)	1.52	1.84	Higher deposition efficiency
Dilution (%)	41.98	26.69	Significant reduction
Process robustness under misalignment	Poor	Improved	Droplet redirection toward melt pool

4.4.1 Wire Misalignment and Melt Pool Interaction

High-speed videography was also performed under conditions where the wire did not directly impinge on the melt pool, simulating process misalignment or feeding irregularities as can be seen in Figure 4.13. This scenario provides additional insight into the role of the electromagnetic field in stabilizing the transfer and the trajectory of molten droplets.

High-speed sequences comparing metal transfer without (a) (see Supplementary Video S5[6]) and with EMF assistance (b) (see Supplementary Video S6[7]) reveal distinct differences in stability. Without EMF, liquid bridge transfer is characterized by elongated necks, irregular rupture, and occasional spattering, reflecting strong Marangoni-driven oscillations. With EMF, Lorentz forces delay droplet detachment and simultaneously elevate the molten pool, reducing the wire–pool distance. This dual effect stabilizes liquid bridge formation, suppresses spattering, and enables more predictable coalescence, leading to improved bead uniformity

These results indicate that coil assistance can partially mitigate misalignment effects, increasing tolerance to realistic disturbances in industrial environments where perfect wire positioning is not always guaranteed.

[6] Supplementary Video S5 can be accessed online at: Video S5
[7] Supplementary Video S6 can be accessed online at: Video S6

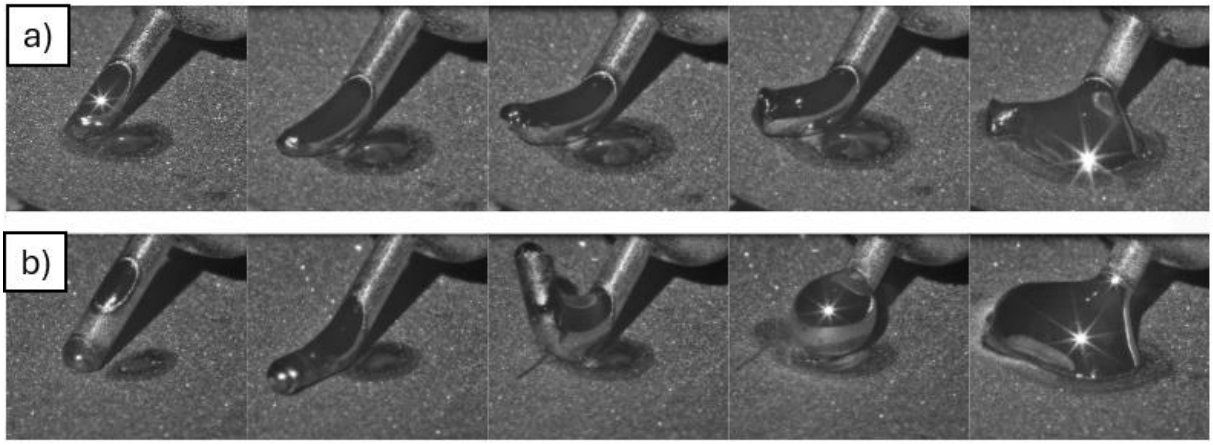


Figure 4.13 - High-speed image sequences under wire misalignment: (a) without EMF (b) with EMF.

The applied magnetic field appears to correct the trajectory of the molten wire, effectively “pulling” it toward the melt pool. This interaction promotes a more stable metal transfer mechanism, leading to a more precise and controlled deposition process. The presence of the magnetic field significantly reduces the failure events observed under non-assisted conditions, highlighting its role in improving overall process stability.

As described in Section 4.3.3 Discussion of Physical Mechanisms, the interaction between induced electrical currents in the molten metal and the externally applied magnetic field generates Lorentz forces that act as an electromagnetic damping mechanism. In the present experiments, this effect manifested as a clear stabilization of the liquid bridge, with reduced oscillatory behavior, delayed droplet detachment, and suppressed spattering. The attenuation of Marangoni-driven convection resulted in a smoother melt pool surface and a more uniform pool geometry, directly improving transfer predictability and bead consistency. Similar stabilization effects under electromagnetic assistance have been reported by Zhou *et al.* [31], who observed suppression of melt pool turbulence, and by Wang *et al.* [24], who demonstrated improved deposition precision and dimensional accuracy. Furthermore, the review by Tan *et al.* [11] highlights that electromagnetic assistance systematically enhances process robustness, reducing spatter formation and mitigating misalignment-induced defects.

In this way, the magnetic field not only stabilizes the transfer dynamics but also increases tolerance to perturbations, providing a scalable route to achieve higher deposition

quality and reliability in wire-laser directed energy deposition (W-LDED). The beads depositions can be seen in Figure 4.14.



Figure 14 - Macroscopic comparison of deposited beads: (a) without EMF and (b) with EMF. Both conditions were produced under identical parameters (laser power = 1.3 kW, deposition speed = 300 mm/min, wire feed rate = 0.85 m/min) using ER70S-6 wire (Ø1.2 mm) on SAE 1020 substrate.

In the bead deposited without (a) electromagnetic field assistance, an irregular morphology was observed, with visible interruptions and defects that indicate unstable and imprecise metal transfer. Such behavior is consistent with unassisted W-LDED processes, where oscillatory melt pool dynamics and uncontrolled liquid bridge rupture often result in uneven bead geometry and lack-of-fusion defects [2, 5].

In contrast, the bead produced under electromagnetic field application exhibited a more uniform and continuous morphology, demonstrating enhanced control and precision of the metal transfer process. The stabilization promoted by the magnetic field can be mechanistically attributed to Lorentz forces ($F = J \times B$), which act at two levels: (i) locally, by suppressing turbulent Marangoni convection and mitigating oscillations within the molten pool, and (ii) globally, by exerting an upward component that counteracts gravity and slightly elevates the molten pool as a whole. This dual action promotes earlier contact between the wire and the pool, leading to more efficient fusion, improved bead consistency, and reduced defect formation [32]. Similar improvements in bead stability and quality under electromagnetic assistance have been reported in both experimental and review studies, where EMF was shown to reduce dilution, minimize spatter, and enhance dimensional accuracy [10, 24, 28, 31]. Overall, the application of electromagnetic field resulted in a more efficient fusion process and higher-

quality deposited beads, confirming its role as a practical strategy for improving process robustness and deposit reliability in wire-laser directed energy deposition.

4.5 BEAD GEOMETRY AND DILUTION

Cross-sectional macrographs provided further confirmation of EMF effects. Without EMF, the bead presented a width of 2.50 mm, height of 0.81 mm, cross-sectional area of 1.52 mm^2, and dilution of 41.98%. With EMF, the bead width increased slightly to 2.60 mm, height rose to 0.97 mm, area increased to 1.84 mm^2, and dilution dropped to 26.69%. The reduced dilution can be attributed to the action of Lorentz forces [33] on the molten pool. Besides damping turbulent convection and reducing heat penetration, the upward component of the electromagnetic force opposes gravity and slightly elevates the pool as a whole. This effect concentrates energy and molten material above the fusion line, thereby reducing dilution.

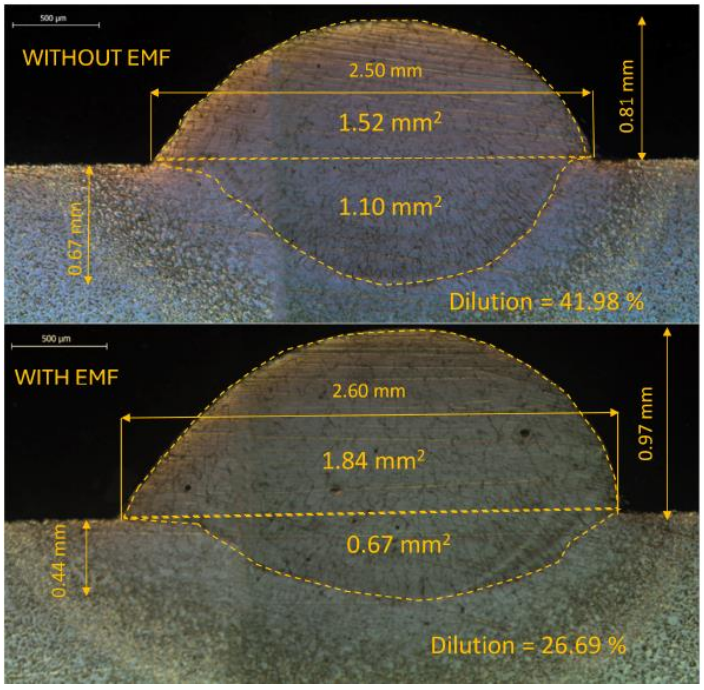


Figure 4.15 - Cross-sectional macrographs of deposited beads: (top) without EMF, showing higher dilution and deeper penetration; (bottom) with EMF, showing reduced dilution, higher bead height, and increased deposition area.

These findings align with Zeng *et al.* [10], who reviewed EMF-assisted AM and confirmed its role in reducing dilution, and with Fan *et al.* [28], who reported improved

dimensional accuracy with compound magnetic fields. The increased bead convexity also suggests improved wettability and stability, which are key for multilayer deposition.

4.6 CONCLUSIONS

This study provided a comprehensive assessment of electromagnetic field (EMF) assistance in Wire-Laser Directed Energy Deposition (WLDED), with emphasis on the mechanistic role of Lorentz forces in stabilizing metal transfer and bead formation. High-speed imaging and cross-sectional analysis revealed that, without EMF, metal transfer is dominated by unstable liquid bridge, irregular droplet detachment, and spattering, producing heterogeneous bead morphology.

When EMF was applied through a custom designed coil, two distinct but complementary mechanisms were observed. First, Lorentz forces acted locally within the molten pool, damping turbulent Marangoni convection and mitigating oscillatory flows. Second, a global upward force component opposed gravity, slightly elevating the melt pool and effectively reducing the wire-pool distance.

This dual action delayed droplet detachment, promoted earlier and more consistent wire-pool contact, and suppressed spatter, ultimately leading to improved bead uniformity and reduced dilution (41.98% → 26.69%). Beyond clarifying the physics of EMF melt pool interactions, these findings highlight electromagnetic assistance as a practical strategy to enhance process robustness.

Although the present study provides direct experimental evidence of electromagnetic-field assisted stabilization of metal transfer in WLDED, it is limited to single-track depositions and a specific material and process parameter set. Subsequent studies will extend this approach to multilayer builds, longer deposition times, and different filler materials, including non-ferromagnetic alloys, in order to assess the scalability, long-term stability, and broader industrial applicability of electromagnetic field assistance.

By increasing tolerance to wire misalignment, controlling dilution, and improving deposition stability, coil-assisted EMF extends the reliability of W-LDED toward industrial implementation.

From an application perspective, the stabilization of metal transfer and the reduction of

dilution achieved through electromagnetic field assistance are particularly relevant for multilayer builds and larger components, where cumulative thermal effects, wire misalignment, and process instabilities are more pronounced. By improving liquid-bridge stability and tolerance to perturbations without modifying laser power or wire feed rate, coil-assisted electromagnetic fields offer a scalable strategy to enhance process robustness, dimensional consistency, and metallurgical control in industrial W-LDED applications.

From an industrial perspective, the stabilization of metal transfer and reduction of dilution are particularly advantageous for applications that require controlled alloy chemistry and minimal substrate alteration, such as the repair or additive manufacturing of aerospace and tooling components.

Furthermore, the improved robustness against misalignment and wire-feeding variations increases process reliability, supporting the adoption of W-LDED with electromagnetic assistance in production environments.

In future work, the model will enable the evaluation of contributions to the welding process associated with variations in the imposed magnetic field through control of the electrical current in the coil. In addition, it will be important to carry out a detailed analysis of the electromagnetic and thermal characteristics of the coil during the welding process, considering its exposure to the heat generated by the laser source.

4.7 ACKNOWLEDGEMENTS

The authors acknowledge the Post-Graduate Program in Mechanical Engineering and the Post-Graduate Program in Electrical Engineering at the Federal University of Santa Catarina (UFSC) for their academic and institutional support. The authors also wish to thank the Laboratory of Electromagnetism and Electromagnetic Compatibility (MagLab/UFSC), the Precision Engineering Laboratory (LMP/EMC/UFSC), and the Welding and Mechatronics Institute (LABSOLDA/UFSC) for providing the experimental infrastructure and technical assistance essential for the development of this research. The authors also acknowledge the Brazilian National Council for Scientific and Technological Development (CNPq) for the doctoral scholarship support.

4.8 REFERENCES

[1] D. Svetlizky, M. Das, B. Zheng, A. L. Vyatskikh, S. Bose, A. Bandyopadhyay, J. M. Schoenung, E. J. Lavernia, and N. Eliaz," Directed energy deposition (DED) additive manufacturing: Physical characteristics, defects, challenges and applications," Materials Today, vol. 49, pp. 271–295, 2021.

[2] T. DebRoy, H. L. Wei, J. S. Zuback, T. Mukherjee, J. W. Elmer, J. O. Milewski, A. M. Beese, A. Wilson-Heid, A. De, and W. Zhang," Additive manufacturing of metallic components – Process, structure and properties," Progress in Materials Science, vol. 92, pp. 112–224, 2018.

[3] N. Ghanadi and S. Pasebani," A review on wire-laser directed energy deposition: Parameter control, process stability, and future research paths," Journal of Manufacturing and Materials Processing, vol. 8, no. 2, p. 84, 2024.

[4] D. Ding, Z. Pan, D. Cuiuri, and H. Li," Wire-feed additive manufacturing of metal components: Technologies, developments and future interests," International Journal of Advanced Manufacturing Technology, vol. 81, pp. 465–481, 2015.

[5] Y. Cai, Y. Wang, H. Chen, and J. Xiong," Molten pool behaviors and forming characteristics in wire-laser directed energy deposition with beam oscillation," Journal of Materials Processing Technology, vol. 326, p. 118326, 2024.

[6] R. Cunningham, C. Zhao, N. Parab, C. Kantzos, J. Pauza, K. Fezzaa, T. Sun, and A. D. Rollett," Keyhole threshold and morphology in laser melting revealed by ultrahigh-speed x-ray imaging," Science, vol. 363, no. 6429, pp. 849–852, 2019.

[7] M. Kahnert, K. Dilger, and J. P. Bergmann," Laser metal deposition with coaxial wire feeding for the automated and reliable buildup of solid metal parts," Journal of Manufacturing and Materials Processing, vol. 6, no. 4, p. 96, 2022.

[8] C. Zhao, K. Fezzaa, R. W. Cunningham, H. Wen, F. De Carlo, L. Chen, A. D. Rollett, and T. Sun," High-speed synchrotron X-ray imaging of melt-pool dynamics in directed energy deposition," Journal of Materials Processing Technology, vol. 283, p. 116707, 2020.

[9] C. Zhao, K. Fezzaa, R. W. Cunningham, H. Wen, F. De Carlo, L. Chen, A. D. Rollett, and T. Sun," Real-time monitoring of laser powder bed fusion process using high-speed x-ray imaging," Scientific Reports, vol. 7, p. 3602, 2017.

[10] C. Zeng, J. Xue, Y. Jia, S. Luo, F. Huang, X. Liu, and Y. Du," A review of additive manufacturing of metallic materials assisted by electromagnetic field technology," Journal of Manufacturing Processes, vol. 131, pp. 920–946, 2024.

[11] C. Tan, R. Li, J. Su, D. Du, B. Attard, Y. Chew, H. Zhang, E. J. Lavernia, Y. Fautrelle, and A. Dong," Review on field assisted metal additive manufacturing," International Journal of Machine Tools and Manufacture, vol. 189, p. 104032, 2023.

[12] Z. Hu, P. Zhang, X. Lin, and W. Huang," Process stability and molten pool control strategies in laser-based DED: A review," Journal of Materials Processing Technology, vol. 305, p. 117590, 2022.

[13] M. K. Dutra, C. L. Prujansky, M. Pereira, R. H. G. e Silva, A. Raizer, and E. P. Elias, Evaluation of magnetic field behavior and heating efficiency of an inductive preheating coil for wire-based laser directed energy deposition (L-DED), International Journal of Advanced Manufacturing Technology, vol. 141, pp. 1879–1892, 2025. doi:10.1007/s00170-025-16829-5.

[14] S. Xie, K. Jiang, L. Wang, and J. Yao," A study on the dynamic evolution mechanism of the steady magnetic field on the internal flow behavior of a laser melting pool," Metals, vol. 13, no. 4, p. 720, 2023.

[15] L. Huang, J. Wang, X. Liu, Y. Chen, and H. Zhang," Experimental research on formation mechanism of porosity in magnetic field assisted laser welding of steel," Journal of Manufacturing Processes, vol. 50, pp. 596–602, 2020.

[16] Z. Wang, Y. Liu, K. Chen, J. Zhou, and H. Zhang," Influence mechanisms of Ydirection magnetic field on molten pool behavior in laser welding," Journal of Manufacturing Processes, vol. 146, pp. 264–272, 2025.

[17] Y. Lu, N. Gou, X. Jiang, Z. Zhang, H. Chen, and C. Li, Laser penetration tests simulating composite plate laser welding at different positions in a magnetic field, International Journal of Advanced Manufacturing Technology, 2025.doi:10.1007/s00170-025-16005-9.

[18] M. N. O. Sadiku, Elements of Electromagnetics, 6th ed., Oxford University Press, 2015.

[19] ANSYS," Maxwell Help," ANSYS, 2021.

[20] L. Liu, J. Yang, B. Liu, Y. Wang, and H. Chen," Melt-pool behavior and droplet dynamics in wire-laser directed energy deposition," Journal of Materials Processing Technology, vol. 295, p. 117157, 2021.

[21] N. Kouraytem, X. Li, R. Cunningham, C. Zhao, N. Parab, T. Sun, A. D. Rollett, A. D. Spear, and W. Tan," Effect of Laser-Matter Interaction on Molten Pool Flow and Keyhole Dynamics," Physical Review Applied, vol. 11, 2019.

[22] Y. Wang, J. Chen, X. Wu, P. Li, L. Xu, and H. Zhang," External compound magnetic field assisted laser metal deposition for improving deposition efficiency and dimensional accuracy," Journal of Manufacturing Processes, vol. 87, pp. 144–156, 2023.

[23] W. Meng, Z. Li, J. Huang, Y. Wu, and R. Cao," Effect of gap on plasma and molten pool dynamics during laser lap welding for T-joints," The International Journal of Advanced Manufacturing Technology, vol. 69, pp. 1105–1112, 2013.

[24] Y. Wang, J. Chen, X. Wu, M. Chen, X. Huang, S. Li, and Z. Xu,” Investigation on high-deposition-rate directed energy deposition of Al-5%Mg alloy via external compound magnetic fields,” Additive Manufacturing, vol. 61, p. 103299, 2022.

[25] X. Meng and L. Chen,” Anisotropic Lorentz force effects on the Marangoni convection in liquid metal systems for fusion applications,” Scientific Reports, vol. 15, p. 11234, 2025.

[26] W. Niu, B. Song, J. Han, H. Yang, Z. Yao, H. Chen, and X. Lin,” Effect of static magnetic field on microstructure and mechanical property of AlSi10Mg alloy by laser directed energy deposition,” Journal of Materials Research and Technology, vol. 34, pp. 2392–2402, 2025.

[27] C. Liu, Y. Wu, J. Zhou, Y. Wen, L. Wang, and L. Xie,” Effect of in situ electromagnetic field manipulation on the microstructure and hardness of titanium alloy during laser melting deposition,” Materials Science in Additive Manufacturing, vol. 4, no. 1, p. 8332, 2025.

[28] X. Fan, T. G. Fleming, D. T. Rees, Y. Huang, S. Marussi, C. L. A. Leung, R. C. Atwood, A. Kao, A. J. Bodey, and P. D. Lee,” Thermoelectric magnetohydrodynamic control of melt pool flow during laser directed energy deposition additive manufacturing,” Additive Manufacturing, vol. 71, p. 103587, 2023.

[29] W. Niu, R. Li, H. Tan, Y. Zhang, and C. Guo,” Static magnetic field effects on microstructure and molten-pool behavior in laser processing,” Journal of Materials Processing Technology, vol. 330, p. 118622, 2024.

[30] W. Niu, B. Song, J. Han, H. Yang, Z. Yao, H. Chen, and X. Lin,” Effect of static magnetic field on microstructure and mechanical property of AlSi10Mg alloy by laser directed energy deposition,” Journal of Materials Research and Technology, vol. 34, pp. 1–13, 2025.

[31] H. Zhou, C. Song, Y. Yang, D. Wang, Z. Liu, Y. Xiao, M. Wang, J. Yu, K. Huang, Z. Deng, and S. Fan, ”Effect of axial static magnetic field on microstructure evolution, performance, and melt pool signals of AlSi10Mg fabricated by laser powder bed fusion, Optics and Laser Technology, vol. 163, p. 109316, 2023.

[32] Wang, X., Liu, Y., Chen, J., Zhou, Y.: Dimensional accuracy enhancement in wire-laser DED via controlled melt-pool dynamics. Journal of Materials Processing Technology 318, 117533 (2023). doi:10.1016/j.jmatprotec.2023.117533

[33] H. Sun, X.Wang, Z. Chen, Z. Xu, and Y. Qin,”Heat-balance control and dilution behavior in wire-laser additive manufacturing, ”Journal of Materials Processing Technology, vol. 318, p. 118330, 2023.

5 INFLUENCE OF DYNAMIC WIRE FEEDING ON METAL TRANSFER IN LASER-DIRECTED ENERGY DEPOSITION (L-DED)

Manoel Kolling Dutra[1], Caio Linhares Prujansky[1], Milton Pereira[1],
Régis Henrique Gonçalves e Silva[1], Marcelo Pompermaier Okuyama[1]
[1]Department of Mechanical Engineering, Federal University of Santa Catarina, Delfino Conti Street, Florianópolis, 88040-900, Santa Catarina, Brazil.

Abstract

Dynamic wire feeding has recently emerged as a promising strategy to improve control over melt-pool dynamics and energy distribution in wire-laser directed energy deposition (WL-DED). Unlike conventional continuous feeding, where the wire maintains a stable liquid-bridge transfer, dynamic feeding introduces periodic advancement and retraction of the wire, enabling active modulation of local heat input and wetting behavior. In this study, high-speed imaging and quantitative analyses of melt-pool area, contact angle, and bead cross-sections were performed to compare continuous and dynamic feeding conditions. Continuous feeding provided stable melt-pool geometry and uniform bead morphology, while dynamic feeding introduced controlled fluctuations that allowed tailoring of energy density and interfacial stability. Frequency modulation revealed that lower oscillation frequencies favored pool expansion, whereas higher frequencies reduced energy accumulation, defining an operational window between stability and adaptability. Contact angle analysis confirmed that dynamic feeding actively altered wettability, and bead cross-sections showed narrower geometries with increased dilution under dynamic conditions. These results demonstrate that dynamic wire feeding is not a substitute but a complementary strategy to continuous feeding, offering new opportunities for adaptive control of melt-pool dynamics and deposition quality in WL-DED.

Keywords: Laser Metal Deposition (LMD), L-DED, Oscillating Wire Feeding, Reciprocating Wire Feeding, Dynamic Wire Oscillation, Metal Transfer Mechanisms, Melt-pool behavior.

5.1 INTRODUCTION

Laser Directed Energy Deposition with wire feed (WL-DED) has emerged as a promising additive manufacturing technique due to its high material efficiency, reduced contamination risks, and potential for near-net-shape fabrication and repair applications. Compared to powder-fed systems, wire feed offers advantages such as higher deposition efficiency and cleaner processing, which have been extensively highlighted in recent reviews of the technology's development and industrial adoption [1–3]. Despite these advantages, challenges remain regarding process stability, particularly in controlling metal transfer dynamics and ensuring consistent bead morphology [4, 5].

Metal transfer in WL-DED involves complex interactions between the laser beam, molten pool, and feeding wire. Depending on the process conditions, the transfer may occur through liquid bridge formation, droplet detachment, or unstable spattering events [6–8]. High-speed imaging studies have revealed that small variations in process parameters such as laser power, scanning speed, and wire feed rate significantly affect energy absorption, droplet trajectories, and melt pool dynamics, which in turn influence porosity, dilution, and surface quality [9–11]. Consequently, achieving robust and reproducible metal transfer remains a critical challenge for industrial implementation.

Several approaches have been proposed to mitigate instabilities, including the use of coaxial nozzles, process monitoring, and hybrid deposition techniques [12, 13]. However, most investigations to date rely on constant wire feed rates, neglecting the potential benefits of temporal modulation. Recent exploratory studies suggest that actively controlling the mechanical presentation of the wire can improve liquid bridge stability and reduce spattering, but systematic understanding of such mechanisms is still limited [14, 15].

Dynamic wire feeding defined as periodic oscillation or modulation of the feed rate—has recently been introduced as a potential method to synchronize metal delivery with melt pool dynamics. Preliminary results indicate that this technique may suppress liquid bridge rupture, stabilize droplet capture, and enhance deposition quality [16–18]. Nevertheless, there is still a lack of systematic frameworks connecting modulation frequency and amplitude to transfer regimes and bead characteristics such as height, width, and dilution. Bridging this gap requires experimental evaluation combining high-speed imaging of transient transfer events with quantitative analysis of final bead geometry.

This study aims to provide a comprehensive evaluation of the influence of dynamic wire feeding on metal transfer stability in WL-DED. By correlating high-speed videography with cross-sectional macrography, the work investigates how frequency of feeding oscillations affects (i) persistence or rupture of the liquid bridge, (ii) droplet emission and capture, and (iii) bead morphology. The outcomes contribute to a mechanistic understanding of dynamic feeding in WL-DED and offer operational guidelines for designing more robust process windows.

5.2 DYNAMIC WIRE FEEDING SYSTEM

The dynamic wire feeding (DWF) setup was implemented through a custom-built servo-driven wire feeder capable of oscillatory modulation of the feed rate. The system was designed with a rigid modular frame made of 30 × 30 mm square steel tubes, welded to minimize vibrations and structural deformation. A 3 mm steel plate was mounted on the frame as a base for the assembly of the feeding unit, servo motor, and guiding mechanisms. This robust configuration ensured mechanical stability during high frequency oscillations. The feeding mechanism enabled forward–backward oscillations of the wire at controlled frequencies in the range of 5–20 Hz, with a positioning error below 1%. The oscillatory motion was imposed directly on the pulling system, allowing precise synchronization of wire advance and retraction with the laser-melt pool interaction. The feeding frequency was programmable through the servo driver controller, making it possible to investigate the effect of different modulation regimes on metal transfer and bead morphology. To better illustrate the integration between the mechanical and control subsystems, a schematic of the dynamic wire feeding architecture is presented in Figure 5.1.

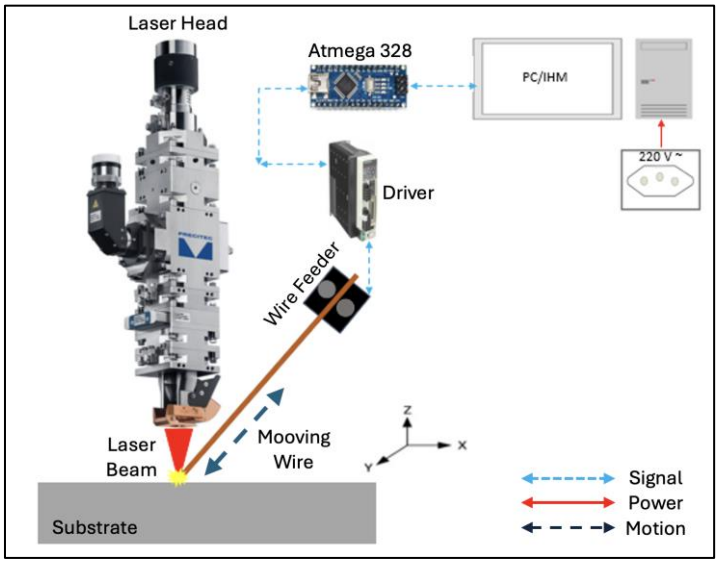


Figure 5.1 - Schematic of the dynamic wire feeding system integrated with the L-DED setup: (a) laser head, (b) substrate, (c) servo-driven wire feeding mechanism, (d) driver, (e) Atmega 328 controller, (f) PC/HMI interface, and (g) 220 V power supply. Signal and power connections are indicated.

Figure 5.1 shows the integration between the laser head, servo-driven feeding unit, electronic driver, Atmega 328 controller, and PC/HMI interface. The complete feeding unit assembled on the laser deposition test bench is shown in Figure 5.2, highlighting the servo motor and the pulling mechanism responsible for generating the oscillatory motion.

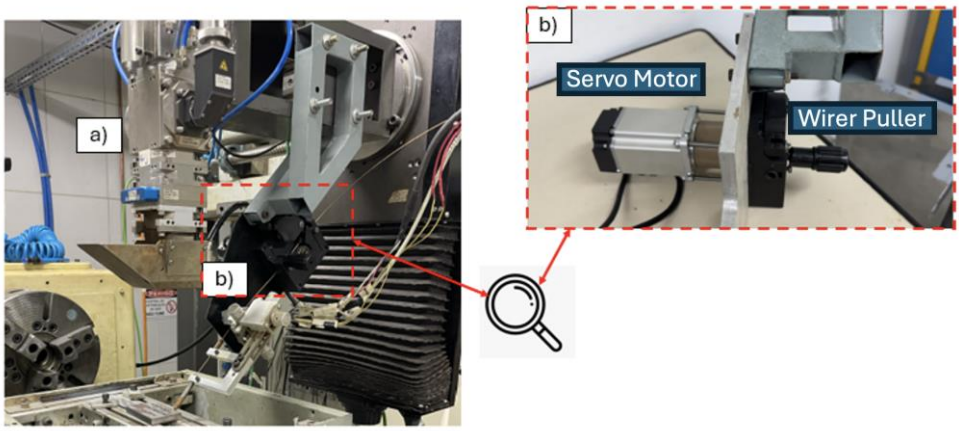


Figure 5.2 - Experimental setup of the L-DED system: (a) laser deposition head; (b) dynamic wire feeding system, with an enlarged detail showing the servo motor and the wire puller responsible for oscillatory wire motion control.

The servo-driven feeding unit utilizes an AC servo motor, rated at 400 W, paired with a compatible servo drive. Wire motion is controlled via step-and-direction signals generated by

an ATMega328P microcontroller, where the STEP signal defines rotational increments through pulse frequency, and the DIR signal sets the rotation direction. This setup allows control of wire advancement and retraction. The linear wire speed is calculated based on the 30 mm diameter of the feeding roller, converting rotational motion into linear displacement. Approximately 10,280 pulses correspond to one full revolution of the motor, equivalent to a linear feed of roughly 94.2 mm of wire. The combination of motor, drive, and microcontroller provides a versatile and accurate platform for exploring the effects of dynamic feeding on laser-deposited bead morphology.

In the dynamic wire feeding mode, each oscillation cycle is composed of two distinct phases: wire advancement and retraction. The total cycle time is defined by the oscillation frequency, and each phase occupies half of this period. During the advance phase, the wire moves forward at a higher instantaneous speed to compensate for the subsequent retraction, ensuring that the desired net feed rate is maintained over time. The retraction phase occurs at its own defined velocity, determined by the retraction distance and the duration of half the cycle. In addition to these two primary phases, each reversal of motion introduces short transition intervals associated with deceleration, stopping, and re-acceleration of the wire. These secondary timing components slightly modify the effective duration of each phase and influence the instantaneous interaction between the wire tip and the melt pool. By adjusting the oscillation frequency, retraction distance, and resultant feed rate, it is possible to control both the instantaneous wire speeds and the dynamic interaction between the wire and the melt pool.

5.2.1 Bench Experiments of the Dynamic Wire Feeder

To validate that the feed rates modeled in the control software could be accurately delivered by the servo motor and driver assembly, a series of positioning experiments were conducted. Experiments evaluated the performance of the system under dynamic feeding conditions, in which the wire alternates between forward and backward motion. Figure 5.3 shows the setup for the bench experiments.

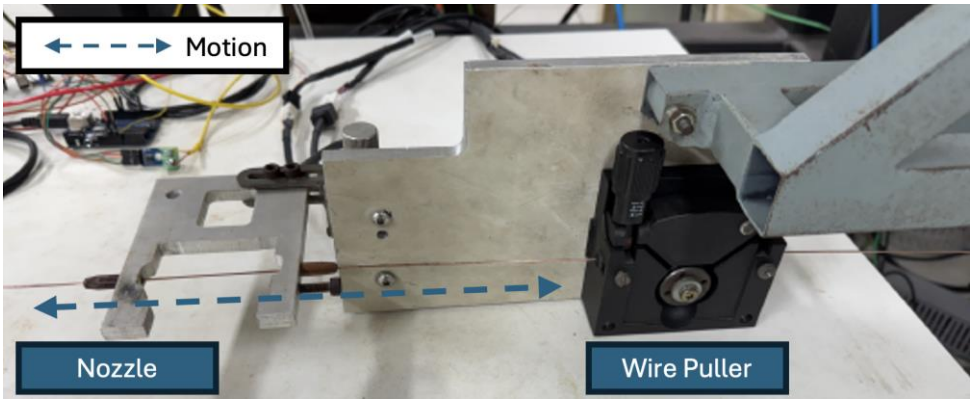


Figure 5.3 - Bench experiments of the wire feeder setup.

Tests were conducted at four oscillation frequencies (5, 10, 15, and 20 Hz) and four target resultant feed rates (0.50, 0.85, 1.20, and 1.55 m/min), totaling 16 experiments. For each combination of frequency and feed rate, the actual displacement of the wire was measured using the tip of the nozzle as reference. With a measuring tape, the length between the tip of the nozzle and the end of the wire was measured., The actual speed was calculated and compared to the commanded value to determine the absolute error. Figure 5.4 shows a chart with the compiled results of the absolute speed error.

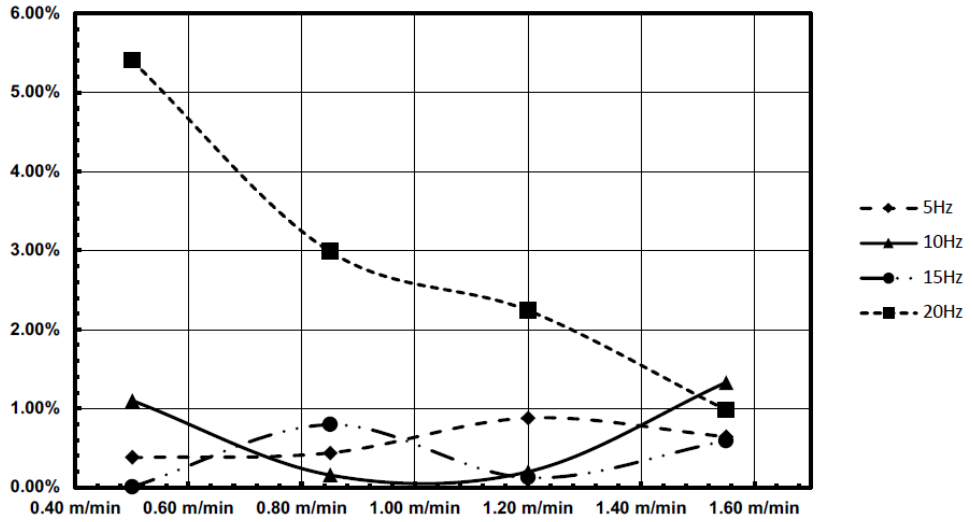


Figure 5.4 - Absolute speed error for different feed rates and frequencies.

The results for oscillation frequencies of 5, 10, and 15 Hz can be considered satisfactory, as the measured errors remained below 1% for most feed rates. However, at 20 Hz

the system begins to exhibit noticeably higher positioning errors, particularly at the lowest feed rate of 0.50 m/min, where deviations exceeded 5%. The average error across all dynamic feeding tests was approximately 1.1%, which is significantly higher than the 0.28% average error observed in continuous feeding for speeds above 0.5 m/min. This indicates that, although dynamic feeding achieves acceptable accuracy for most conditions, high oscillation frequencies introduce additional challenges that should be considered.

5.3 HIGH-SPEED VIDEOGRAPHY ANALYSIS OF METAL TRANSFER

High-speed imaging was employed to capture transient phenomena of wire–melt pool interaction during Wire-Laser Directed Energy Deposition (WL-DED). The experiments were conducted using a Photron FASTCAM Nova S9 high-speed camera, operating at a frame rate of 1000 fps with a resolution of 1024 × 1024 pixels. A Canon EF 180 mm macro lens was used in combination with an EF 2× III extender, providing enhanced magnification of the interaction zone. The exposure time was 10 s, and a bandpass filter (810 ± 12 nm, Ø 50 mm) was mounted to suppress background radiation from the melt pool and laser reflections. Illumination was provided by a Cavilux-HF laser system, delivering 810 ± 10 nm wavelength at 500 W.

This optical arrangement ensured high contrast visualization of the melt pool, wire tip, and transient droplet dynamics under the intense radiation environment of the laser process. The methodology enabled direct observation of liquid bridge formation and rupture, droplet detachment, and melt pool oscillations under dynamic feeding conditions.

Experiments were carried out using a fiber laser source (IPG Photonics YLS 10000) operating at 1.3 kW, with a scanning speed of 300 mm/min and a wire feed rate of 0.85 m/min. These process parameters were kept constant throughout all trials, while only the oscillation frequency of the dynamic wire feeding system was varied. This strategy enabled direct comparison with continuous wire feeding conditions, allowing the influence of feeding modulation on metal transfer behavior to be systematically evaluated. Although the electromagnetic coil was physically mounted around the wire path as part of the same experimental bench used in other studies, it remained deenergized during all tests described in this work. Thus, no magnetic field was applied, and the coil served only as a passive structural component. The experimental setup is shown in Figure 5.5.

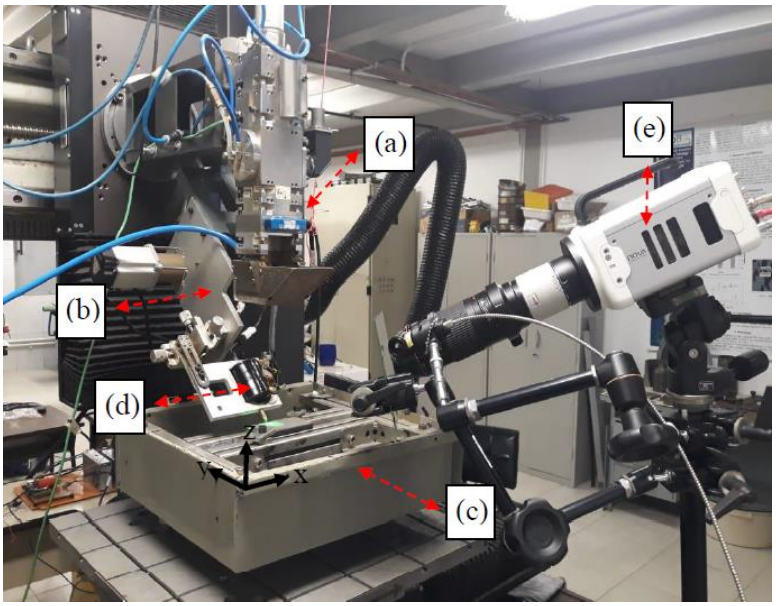


Figure 5.5 - Experimental setup for high-speed imaging of the WL-DED process. The electromagnetic coil (d) was part of the experimental bench but remained de-energized during the tests reported in this study. (a) Laser head, (b) Wire feeder, (c) Processing chamber, (d) Electromagnetic coil (off), (e) High-speed camera.

5.3.1 Continuous Wire Feeding

In the continuous wire feeding mode, the wire tip remains in uninterrupted contact with the melt pool, sustaining a liquid bridge that ensures stable transfer (see Supplementary Video S1[8]). As shown in Figure 5.6, the cross-sectional areas of the melt pool varied only slightly (7.30–8.93 mm²), reflecting quasi-steady heat input and uniform bead morphology. Similar stabilization of melt pool geometry under continuous feeding has been reported in recent reviews on wire-laser directed energy deposition (WL-DED) [18, 19].

[8] Supplementary Video S1 is available at: Video S1

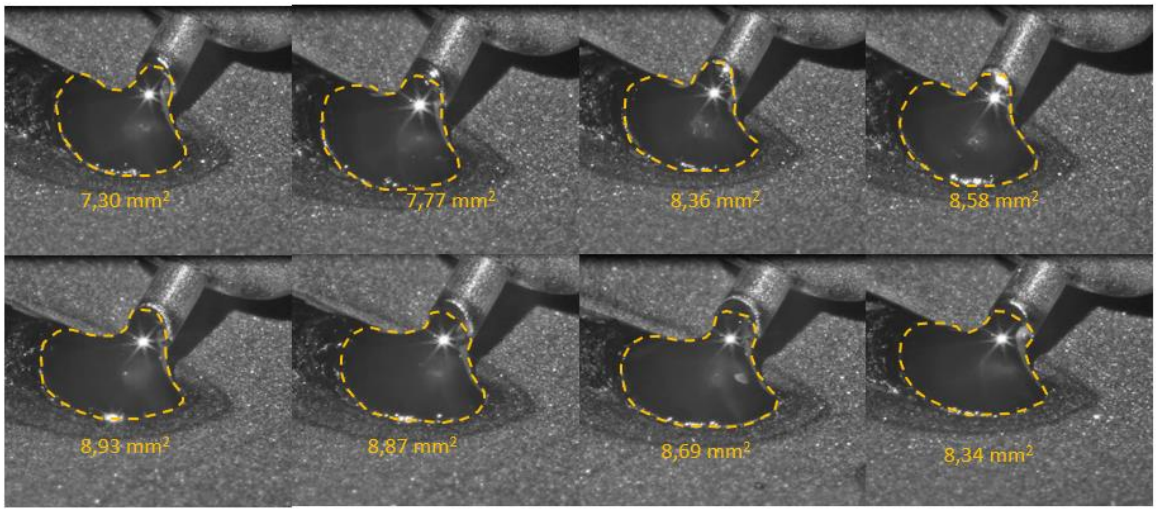


Figure 5.6 - High-speed image sequence of metal transfer in WL-DED in continuous wire feeding mode.

The main mechanism involved is the liquid bridge transfer, which surface tension maintains the droplet cohesion, while capillary forces generated at the liquid bridge promote the droplet attraction toward the melt pool. This regime favors predictable bead width and height, as well as moderate dilution levels adequate for metallurgical bonding without excessive penetration. Recent investigations demonstrated that continuous feeding reduces oscillations of the melt pool and avoids pendant-droplet instabilities, improving both deposition efficiency and geometric repeatability [20–22].

However, continuous feeding inherently limits local modulation of heat input and control over melt-pool oscillations. In contrast, dynamic wire feeding introduces periodic advancement and retraction of the wire, intermittently altering the fraction of laser energy absorbed by the wire and the substrate. This cyclic interaction produces a controllable modulation of local heat input, enabling transient redistribution of energy density within the melt pool and thereby influencing oscillation amplitude and thermal gradients [15, 23, 24]. As emphasized in shape-control studies, continuous feeding is robust and reproducible but lacks flexibility compared to oscillatory or dynamic feeding strategies, which deliberately introduce controlled perturbations to tune bead geometry and solidification conditions [23].

Therefore, continuous wire feeding represents a stable baseline condition for WL-DED, where energy distribution and transfer are consistent, and it provides the necessary reference

for evaluating advanced approaches such as dynamic feeding (to be discussed in Section 5.3.2 Dynamic Wire Feeding).

5.3.2 Dynamic Wire Feeding

Unlike the continuous mode, dynamic wire feeding introduces periodic advancement and retraction of the wire, intermittently breaking the liquid bridge between the wire tip and the melt pool (see Supplementary Video S2[9]). This behavior is evident in Figure 5.7, where the melt-pool area exhibits a wider fluctuation range (5.61–9.33 mm²) compared to the steady profile obtained under continuous feeding (Section 5.3.1 Continuous Wire Feeding). The periodic detachment of the wire reduces the fraction of laser energy absorbed by the wire itself, momentarily concentrating heat input on the substrate and melt pool, which increases local energy density and alters pool geometry.

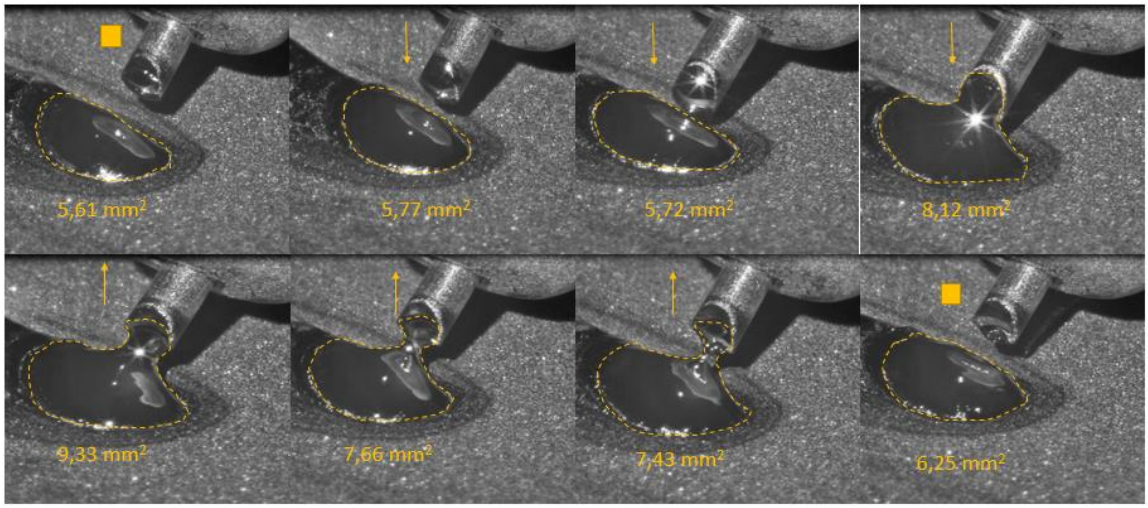


Figure 5.7 - High-speed image sequence of metal transfer in WL-DED with dynamic wire feeding.

These dynamic variations in heat input and liquid bridge stability create cyclical transitions between bridge transfer and free-surface laser pool interaction. Similar behavior has been reported in recent studies, showing that dynamic feeding can deliberately induce oscillations in the melt pool, which in turn modifies fluid flow and solidification conditions [20–22]. By intermittently removing the energy sink represented by the wire, the process

[9] Supplementary Video S2 is available at: Video S2

enhances pool convection and increases dilution during the retraction phase, while advancing phases promote droplet feeding and stabilization of bead build-up [21].

The key advantage of dynamic feeding is the added flexibility to tailor deposition geometry and mitigate instability. Oscillatory or modulated feeding strategies have been highlighted as promising approaches to control bead shape, influence Marangoni convection, and homogenize solute distribution, especially in multi-layer builds [19–23].

However, this flexibility comes at the cost of higher variability in cross-sectional areas, as observed in Figure 5.7, and requires precise synchronization of wire motion with laser parameters to avoid spatter, underfill, or excessive dilution. Thus, while continuous feeding provides a robust and repeatable baseline, dynamic wire feeding enhances process controllability at the expense of geometric stability, enabling new opportunities to fine-tune transfer dynamics and microstructure evolution in advanced WL-DED processes.

5.3.3 Effect of Dynamic Feeding Frequency

The application of dynamic wire feeding at different oscillation frequencies introduces an additional level of control over the melt-pool dynamics. In this study, three representative frequencies 5, 10, and 15 Hz were selected based on the operational limits defined in Section 5.2.1. These values represent the range where the servo-driven wire feeder can maintain stable reciprocating motion without excessive delay (low-frequency limit) or wire–pool decoupling (high-frequency limit).

Figure 5.8 shows the melt pool areas measured for each condition: 10.51 mm² at 5 Hz, 10.06 mm² at 10 Hz, and 9.71 mm² at 15 Hz. Compared to the continuous feeding regime (Section 5.3.1), where the melt-pool area fluctuated within a narrow band (≈ 7.3–8.9 mm^2), the dynamic mode with frequency modulation results in larger mean areas, reflecting the additional pool expansion when the wire is retracted. At lower frequencies (5 Hz), the pool has sufficient time to absorb the increased energy density during retraction, leading to a larger molten cross-section. As frequency increases, the period of wire–pool detachment shortens. Although the advance and retraction phases each occupy half of the oscillation cycle, higher frequencies reduce the absolute duration of both phases. Consequently, the retraction interval becomes too short for significant energy accumulation in the melt pool, leading to smaller molten areas and attenuated thermal oscillations [24, 26, 27].

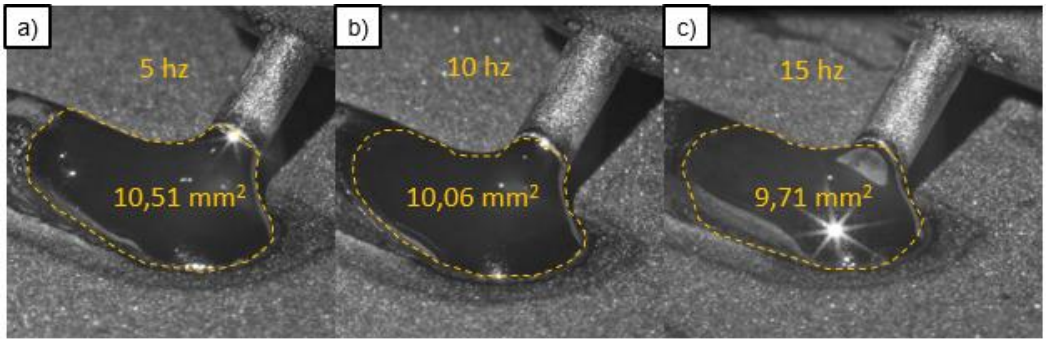


Figure 5.8 - Melt-pool cross sections under dynamic wire feeding at different oscillation frequencies: (a) 5 Hz, (b) 10 Hz, and (c) 15 Hz. The measured areas were 10.51 mm², 10.06 mm², and 9.71 mm², respectively. Lower frequency (5 Hz) favored larger molten areas due to longer retraction intervals and increased local energy density, whereas higher frequencies (10–15 Hz) reduced the available interaction time, limiting pool expansion.

These results are consistent with recent findings that oscillatory or pulsed wire-feeding strategies can modulate the heat balance and convection patterns in the melt pool, enabling tailored control of bead geometry and dilution [24, 25]. Lower frequency modulation tends to amplify melt-pool oscillations and enhance Marangoni-driven circulation, while higher frequencies can suppress large-scale fluctuations but reduce the effectiveness of energy redistribution [26]. This trade-off indicates that frequency selection is critical: too low may destabilize droplet transfer, while too high may limit the benefits of dynamic modulation [27].

Importantly, when compared with the results in Section 5.3.2, it becomes clear that frequency tuning in dynamic feeding serves as a fine adjustment knob: continuous feeding ensures stability, dynamic feeding introduces oscillatory control, and frequency variation further refines the balance between melt-pool size, dilution, and transfer stability. Thus, frequency-controlled feeding emerges as a pathway toward adaptive deposition strategies, enabling on-demand tailoring of bead characteristics depending on layer geometry or desired metallurgical outcomes.

5.3.4 Contact Angle Behavior under Dynamic Wire Feeding

Dynamic wire feeding not only influences melt pool size and oscillations (Sections 5.3.2–5.3.3), but also affects wetting dynamics and contact angle behavior, which are critical indicators of interfacial stability and bead geometry. Figure 5.9 illustrates the contact angles

measured during deposition under oscillatory wire motion, with values ranging from 35.29° to 52.74°.

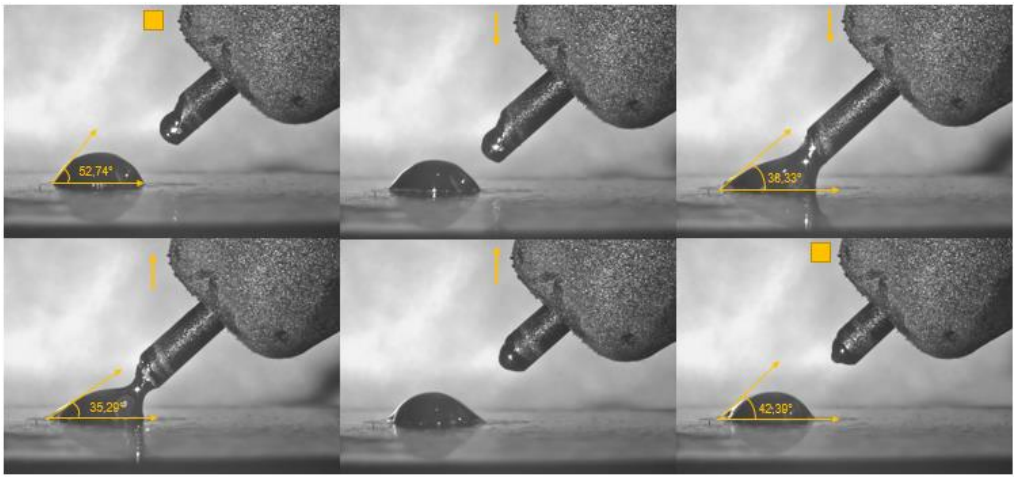


Figure 5.9 - Contact angle evolution during dynamic wire feeding. Values ranged from 52.74° to 35.29°, showing reduced spreading during retraction and enhanced wetting during wire advancement.

During dynamic wire feeding, the observed variations in contact angle are mainly governed by the mechanical interaction between the feed wire and the molten pool. When the wire advances and contacts the pool, adhesion between the molten metal and the wire tip pulls the liquid laterally, deforming the pool surface and reducing the apparent contact angle (see Supplementary Video S3[10]). Conversely, during the retraction phase, this adhesive pulling effect disappears, allowing surface tension to restore a more rounded profile, which increases the measured angle. Therefore, the oscillations in contact angle primarily reflect dynamic deformation induced by wire adhesion rather than intrinsic changes in wetting properties [24, 25, 27].

The cyclical fluctuation of contact angles caused by dynamic feeding highlights its role as a modulator of surface tension driven flows and wetting forces. Such oscillations can promote homogenization of melt-pool temperature and composition, while simultaneously enabling more controlled transitions between bridge transfer and free-surface laser pool interaction. Recent investigations have emphasized that frequency and amplitude modulated wire feeding strategies improve bead regularity, reduce porosity, and enhance metallurgical

[10] Supplementary Video S3 is available at: **Video S3**

bonding by actively controlling wetting and spreading behavior [25–27]. Therefore, dynamic wire feeding emerges not only as a method to control melt-pool geometry but also as a powerful tool for tailoring wetting conditions and interfacial stability, providing additional design flexibility for advanced WL-DED applications.

5.4 RESULTS AND DISCUSSION

This section presents and discusses the experimental results obtained in this study. The influence of the dynamic wire feeding on metal transfer stability, droplet dynamics and bead morphology.

5.4.1 Melt-Pool Geometry and Stability

The comparison between continuous and dynamic wire feeding highlights fundamental differences in melt-pool stability. Under continuous feeding, the melt-pool area remained within a narrow band (7.30–8.93 mm²), demonstrating stable liquid-bridge transfer and uniform energy distribution between wire and substrate. This regime minimizes oscillations, ensuring repeatable bead morphology, as also observed in recent investigations of WL-DED stability [20–22].

In contrast, dynamic feeding introduced wider fluctuations in melt-pool area (5.61–9.33 mm²), directly linked to the alternating phases of wire advancement and retraction. During advancement, the liquid bridge stabilized transfer and expanded pool area, while retraction phases redirected laser energy to the substrate, leading to localized heating and transient pool growth. This dual behavior illustrates the inherent trade-off between stability and controllability when moving from continuous to dynamic feeding. Figure 5.10 illustrates the difference between continuous wire deposition and dynamic wire deposition.

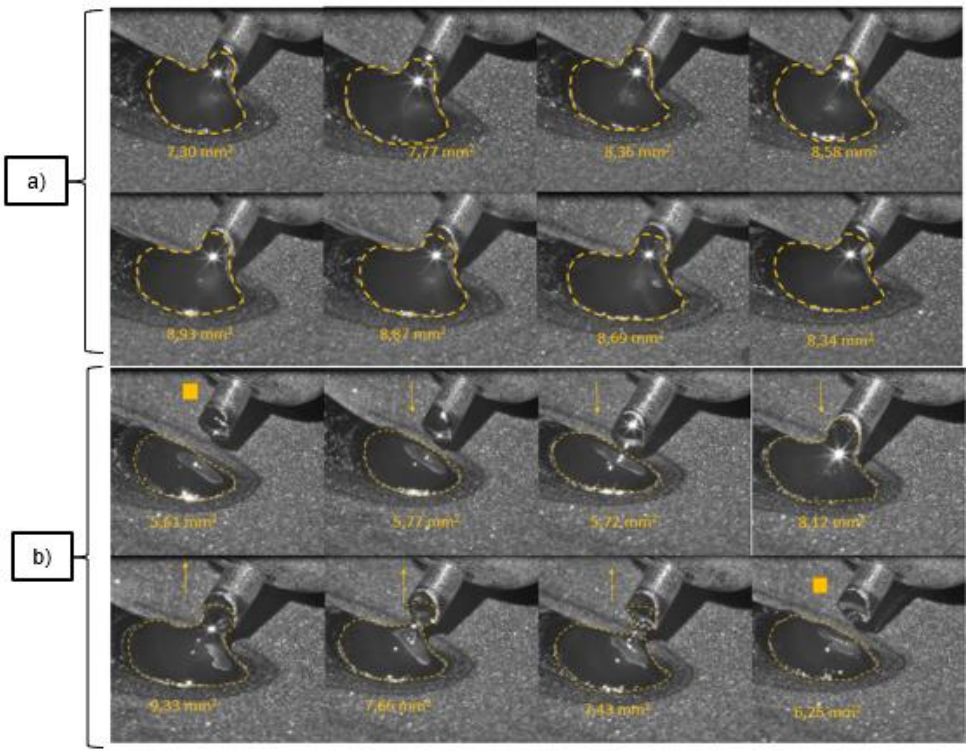


Figure 5.10 - Melt-pool evolution under (a) continuous and (b) dynamic wire feeding. Continuous feeding produced stable areas (7.30–8.93 mm²), while dynamic feeding showed larger fluctuations (5.61–9.33 mm²) due to alternating wire advancement and retraction.

5.4.2 Influence of Feeding Frequency

Frequency modulation added a further layer of control over pool dynamics. At 5 Hz, the melt-pool reached the largest area (10.51 mm²), reflecting sufficient retraction time for energy accumulation and pool expansion. At 10 Hz, the pool size slightly decreased (10.06 mm²), representing a balance between energy input and stability. At 15 Hz, the area reduced further (9.71 mm²), as shorter retraction times limited the heat accumulation capacity.

These findings are consistent with reports that lower frequencies enhance pool oscillations and Marangoni-driven circulation, whereas higher frequencies dampen fluctuations but reduce effective energy redistribution [25, 26]. The present results suggest the existence of an optimal frequency window in which deposition geometry can be tailored without compromising process stability.

5.4.3 Contact Angle and Wetting Behavior

Dynamic wire feeding also modulated wetting conditions, as shown by the measured contact angles ranging from 35.29◦ to 52.74◦. Higher angles corresponded to retraction phases, where reduced wire–pool interaction concentrated laser energy in the pool and increased surface tension dominance, thereby decreasing wettability. Conversely, lower angles were observed during advancement phases, when the wire contributed additional molten material, reducing surface tension gradients and enhancing spreading.

These oscillations in contact angle illustrate how dynamic feeding periodically shifts the balance between surface tension and wetting forces, offering a mechanism to influence bead morphology and substrate bonding. Recent studies corroborate that active modulation of wetting dynamics through pulsed or oscillatory feeding can reduce porosity, improve bead uniformity, and enhance metallurgical bonding [25, 27].

5.4.4 Comparative Discussion

Taken together, the results demonstrate a clear progression of control strategies:

- Continuous feeding provides a stable baseline with minimal pool fluctuation, suited for applications prioritizing robustness.
- Dynamic feeding introduces controlled variability, enabling modulation of melt-pool geometry and interfacial conditions.
- Frequency tuning refines this modulation, defining an operational window where stability and flexibility are balanced.
- Contact angle analysis reveals that dynamic feeding actively modulates wettability, a critical factor for adhesion and bead quality.

This framework shows that dynamic wire feeding is not merely an alternative to continuous feeding but a tool for adaptive control of energy distribution, wetting behavior, and transfer stability in W-LDED.

5.4.5 Bead Geometry with and without Dynamic Feeding

The influence of dynamic wire feeding on the final bead geometry is clearly evidenced in Figure 5.11, which compares cross-sections of tracks deposited without DWF and with DWF. In the absence of dynamic feeding, the bead exhibited a width of 1.10 mm and a cross-sectional

area of 10.64 mm². In contrast, when DWF was applied, the bead became narrower (0.86 mm) and its cross-sectional area was significantly reduced to 4.08 mm².

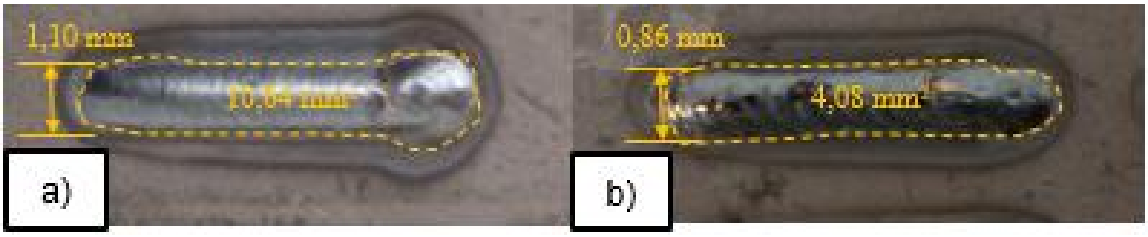


Figure 5.11 - Bead geometry without (a) and with (b) dynamic feeding. The introduction of AD reduced bead width (1.10 → 0.86mm) and area (10.64 → 4.08mm2), highlighting the effect of intermittent wire–pool detachment on energy concentration and dilution.

These results confirm that dynamic feeding not only modulates melt-pool dynamics in real time (Sections 5.4.2–5.4.3), but also translates into measurable changes in final bead geometry and dilution balance. The reduction in bead width and area with DWF indicates that intermittent wire retraction leads to moments when laser energy is concentrated on the substrate, thereby increasing dilution and reducing the volumetric efficiency of deposition. Similar findings have been reported in recent studies of oscillatory wire feeding, where modulation of wire–pool interaction was shown to influence dilution depth and bead uniformity [19–25].

While continuous feeding maximizes deposition volume and stability, dynamic feeding demonstrates the ability to tailor bead morphology, particularly when narrow or controlled geometries are desired. This reinforces the concept that dynamic wire feeding should not be viewed as a replacement for continuous feeding, but rather as a complementary strategy that enables adaptive control of geometry, surface quality, and energy distribution depending on process requirements.

5.5 CONCLUSIONS

This study investigated the effect of continuous and dynamic wire feeding strategies on melt pool behavior, wetting dynamics, and final bead geometry in wire–laser directed energy deposition (W-LDED). High-speed imaging, contact angle measurements, and bead cross-sectional analysis enabled a systematic comparison of transfer stability, energy distribution, and deposition efficiency. The following conclusions can be drawn:

1. Continuous wire feeding promoted stable liquid-bridge transfer, with melt-pool areas ranging from 7.30 to 8.93mm2. This regime ensured uniform energy distribution and reproducible bead morphology, representing a robust baseline condition for W-LDED.

2. Dynamic wire feeding introduced controlled fluctuations in melt-pool size (5.61–9.33 mm^2), caused by alternating wire advancement and retraction. While this increased variability, it provided greater flexibility in tailoring energy input and melt-pool dynamics.

3. Feeding frequency significantly influenced melt pool geometry. At 5 Hz, the largest pool area (10.51 mm^2) was obtained due to longer retraction intervals and increased local energy density. At 15 Hz, shorter retraction times reduced pool size (9.71 mm^2). These results suggest the existence of an operational frequency window that balances stability and controllability.

4. Contact angle measurements (35.29°- 52.74°) revealed that dynamic feeding actively modulates wetting behavior. Wire advancement reduced angles and enhanced spreading, while retraction increased angles and decreased wettability. This demonstrates that AD can be used to tune interfacial stability and bead adhesion.

5. Bead geometry analysis confirmed the macroscopic impact of AD. Compared to continuous feeding (width = 1.10 mm, area = 10.64 mm^2), dynamic feeding reduced bead width (0.86 mm) and area (4.08 mm^2), indicating increased dilution and localized energy concentration.

Overall, the results demonstrate that dynamic wire feeding should not be regarded as a replacement for continuous feeding, but rather as a complementary strategy that enables adaptive control of melt-pool dynamics, wetting, and bead morphology. By combining the stability of continuous feeding with the flexibility of dynamic modulation, W-LDED can be tailored for different applications, ranging from high-deposition efficiency to precision-controlled geometries.

Future work should explore the correlation between these process dynamics and resulting microstructural features and mechanical properties, as well as the integration of closed-loop control strategies to exploit dynamic feeding as an adaptive tool for next-generation additive manufacturing.

5.6 ACKNOWLEDGEMENTS

The authors acknowledge the Post-Graduate Program in Mechanical Engineering at the Federal University of Santa Catarina (UFSC) for their academic and institutional support. The authors also wish to thank the Precision Engineering Laboratory (LMP/EMC/UFSC), and the Welding and Mechatronics Institute (LABSOLDA/UFSC) for providing the experimental infrastructure and technical assistance essential for the development of this research. The authors also acknowledge the Brazilian National Council for Scientific and Technological Development (CNPq) for the doctoral scholarship support.

5.7 REFERENCES

[1] D. Ding, Z. Pan, D. Cuiuri, and H. Li, "Wirefeed additive manufacturing of metal components: technologies, developments and future interests," International Journal of Advanced Manufacturing Technology, vol. 81, no. 1–4, pp. 465–481, 2015. DOI: 10.1007/s00170-015- 7077-3.

[2] W. E. Frazier, "Metal additive manufacturing: a review," Journal of Materials Engineering and Performance, vol. 23, no. 6, pp. 1917–1928, 2014. DOI: 10.1007/s11665- 014-0958-z.

[3] S. M. Thompson, L. Bian, N. Shamsaei, and A. Yadollahi, "An overview of direct laser deposition for additive manufacturing," Additive Manufacturing, vol. 8, pp. 36–62, 2015. DOI: 10.1016/j.addma.2015.07.001.

[4] A. J. Pinkerton, "Advances in the modeling of laser direct metal deposition," Journal of Laser Applications, vol. 27, no. S1, S15001, 2015. DOI: 10.2351/1.4906084.

[5] DebRoy, T., Wei, H.L., Zuback, J.S., Mukherjee, T., Elmer, J.W., Milewski, J.O., Beese, A.M., Wilson-Heid, A., De, A., Zhang, W. "Additive manufacturing of metallic components – process, structure and properties," Progress in Materials Science, vol. 92, pp. 112–224, 2018. DOI: 10.1016/j.pmatsci.2017.10.001.

[6] A. Heralic, A. K. Christiansson, and B. Lennartson, "Height control of laser metalwire deposition based on iterative learning control and 3D scanning," Optics and Lasers in Engineering, vol. 50, no. 9, pp. 1230–1241, 2012. DOI: 10.1016/j.optlaseng.2012.03.003.

[7] Cunningham, R., Narra, S.P., Montgomery, C., Beuth, J., Rollett, A.D. "Keyhole threshold and morphology in laser melting revealed by ultrahigh-speed X-ray imaging," Science, vol. 363, no. 6429, pp. 849–852, 2019. DOI: 10.1126/science.aav4687.

[8] Y. Zhao, J. Chen, M. Zhou, and C. Zhang, "Influence of wire feeding direction on droplet transfer and bead formation in laser wire additive manufacturing," Optics and Laser Technology, vol. 126, 106106, 2020. DOI: 10.1016/j.optlastec.2020.106106.

[9] E. W. Teichmann, J. Kelbassa, A. Gasser, S. Tarner, and J. H. Schleifenbaum, “Effect of wire feeder force control on laser metal deposition process using coaxial laser head,” Journal of Laser Applications, vol. 33, no. 1, 012041, 2021. DOI: 10.2351/7.0000304.

[10] N. Ghanadi and S. Pasebani, “A Review on Wire-Laser Directed Energy Deposition: Parameter Control, Process Stability, and Future Research Paths,” Journal of Manufacturing and Materials Processing, vol. 8, no. 2, 84, 2024. DOI: 10.3390/jmmp8020084.

[11] Abuabiah, M., Tammas-Williams, S., Todd, I., Prangnell, P.B. “Advancements in Laser Wire-Feed Metal Additive Manufacturing: A Brief Review,” Materials, vol. 16, no. 5, 2030, 2023. DOI: 10.3390/ma16052030.

[12] C. Bernauer, T. Merk, A. Zapata, and M. Zaeh, “Laser metal deposition with coaxial wire feeding for the automated and reliable build-up of solid metal parts,” Key Engineering Materials, vol. 926, pp. 65–79, 2022. DOI: 10.4028/p-ob7dg7.

[13] Y. Zhang and F. Liou, “Adaptive control of laser metal deposition processes,” IEEE Transactions on Automation Science and Engineering, vol. 4, no. 2, pp. 234–244, 2007. DOI: 10.1109/TASE.2007.898853.

[14] K. Zhang, H. Li, and Z. Chen, “Droplet transfer behavior in laser wire additive manufacturing with oscillating wire feeding,” Optics and Laser Technology, vol. 138, 106870, 2021. DOI: 10.1016/j.optlastec.2021.106870.

[15] R. Li, W. Chen, X. Zhao, and M. Song, “Process stabilization by periodic modulation of wire feeding in laser additive manufacturing,” Journal of Materials Processing Technology, vol. 301, 117458, 2022. DOI: 10.1016/j.jmatprotec.2021.117458.

[16] Y. Song, Q. Zhu, R. Xu, and L. He, “Effect of dynamic wire feeding on melt pool behavior and deposition stability in wire-laser additive manufacturing,” Additive Manufacturing, vol. 63, 103025, 2023. DOI: 10.1016/j.addma.2022.103025.

[17] Y. Song, Q. Zhu, and R. Xu, “Effect of dynamic wire feeding on melt pool behavior and droplet transfer in laser DED,” Additive Manufacturing, vol. 63, 103025, 2023. DOI: 10.1016/j.addma.2023.103025.

[18] Tran, T.Q., Nguyen, V.T., Le, T.D., Nguyen, T.T. “An assessment of wire laser additive manufacturing with focus on characteristics, research progress and quality improvement,” International Journal of Additive Manufacturing Technologies, vol. 1, 12, 2025. DOI: 10.1007/s44245-025-00133-3.

[19] M. Ghasempour-Mouziraji, D. Afonso, and R. A. Sousa, “A short review on the wire based directed energy deposition of metals: mechanical and microstructural properties and quality enhancement,” Applied Sciences, vol. 14, no. 21, 9921, 2024. DOI: 10.3390/app14219921.

[20] Y. Fu, X. Chen, L. Zhang, and M. Zhang, “Fundamental investigation into mass transfer of wire-based laser DED,” Science and Technology of Welding and Joining, vol. 29, no. 2, pp. 167–177, 2024. DOI: 10.1080/13621718.2024.2297459.

[21] F. Caiazzo, A. Caggiano, and V. Alfieri, “Additive manufacturing by means of laseraided directed metal deposition of titanium wire,” International Journal of Advanced Manufacturing Technology, vol. 96, pp. 2699– 2707, 2018. DOI: 10.1007/s00170-018-1760-0.

[22] Y. Ai, X. Liu, Y. Yan, and S. Han, “Investigation of molten pool dynamic behaviors in laser additive manufacturing by numerical simulation,” Journal of Laser Applications, vol. 33, no. 4, 042041, 2021. DOI: 10.2351/7.0000496.

[23] Y. Mao, H. Chen, and J. Xiong, “In situ microalloying of Al-Cu-Sc alloy manufactured by beam oscillating wire laser directed energy deposition: Grain refinement and properties improvement,” Additive Manufacturing, vol. 93, 104419, 2024. DOI: 10.1016/j.addma.2024.104419.

[24] P. Wang, Z. Shen, and X. Yao, “Real time monitoring of melt pool behaviors in laser additive manufacturing,” International Journal of Advanced Manufacturing Technology, vol. 116, pp. 1421–1433, 2022. DOI: 10.1007/s00170-021-07999-5.

[25] C. Li, X. Ren, H. Yu, and Z.Wang, “Influence of pulsed wire feeding on melt pool geometry and microstructure in laser-DED,” Optics and Laser Technology, vol. 173, 110397, 2024. DOI: 10.1016/j.optlastec.2024.110397.

[26] L. Zhao, Q. Wang, Y. Zhang, and F. Li, “Tailoring melt pool dynamics by frequency modulated wire feeding in hybrid laserwire processes,” Materials Science and Engineering A, vol. 878, 145545, 2024. DOI: 10.1016/j.msea.2024.145545.

[27] M. B. Rodrigues, R. G. N. Silva, M. Pereira, R. H. G. e Silva, and E. W. Teichmann, “Effect of dynamic wire feeding on deposition quality in laser cladding process,” Journal of Laser Applications, vol. 32, no. 2, 022065, 2020. DOI: 10.2351/7.0000097.

6 CONCLUSIONS

This doctoral thesis investigated the effects of inductive hot-wire preheating, electromagnetic field assistance, and dynamic wire feeding on metal transfer stability, melt-pool behavior, and bead geometry in wire-fed Laser Directed Energy Deposition (W-LDED). The study was structured around specific objectives, which were systematically addressed through three scientific articles. The main findings are summarized below by explicitly relating each objective to the corresponding experimental and analytical outcomes.

Objective I – Development and characterization of an inductive hot-wire system

This objective was addressed in **Article I**, where an inductive heating system was designed, implemented, and experimentally validated.

The results demonstrated that the hot-wire technique effectively modifies the thermal balance of the process by reducing the fraction of laser energy required to melt the filler wire. This thermal assistance promotes a reduction in the temperature gradient between the wire and the melt pool, leading to:

- Stabilization of liquid-bridge transfer
- Reduction of droplet detachment events
- Decrease in bead height and increase in penetration

Therefore, it is concluded that inductive preheating is an effective strategy for enhancing thermal efficiency and promoting more stable metal transfer conditions in W-LDED.

Objective II – Evaluation of the influence of electromagnetic field on melt-pool behavior

This objective was investigated in **Article II**, where a dedicated electromagnetic coil was developed and integrated into the deposition system.

The application of a static magnetic field was shown to significantly influence melt-pool dynamics through the action of Lorentz forces. The main observed effects include:

- Suppression of Marangoni-driven instabilities
- Reduction of spatter formation
- Increased stability of liquid-bridge transfer
- Improved uniformity of bead geometry

The results confirm that electromagnetic field assistance acts as a non-contact stabilization mechanism, improving process robustness and reducing sensitivity to disturbances.

Objective III – Investigation of dynamic wire feeding effects on metal transfer

This objective was addressed in **Article III**, which introduced a servo-driven dynamic wire feeding system capable of controlled forward–backward oscillations.

The results demonstrated that dynamic wire feeding enables active modulation of mass and energy transfer, directly influencing melt-pool behavior. Key findings include:

- Control of melt-pool area through oscillation frequency
- Influence on contact angle and wetting behavior
- Reduction of heat accumulation during retraction phases
- Improved adaptability of the process to transient conditions

It was also observed that an optimal frequency range exists, where the balance between stability and flexibility is maximized.

Thus, dynamic wire feeding is confirmed as an effective kinematic control strategy for W-LDED.

Objective IV – Analysis of the effects of the three techniques

The combined application of hot-wire preheating, electromagnetic field assistance, and dynamic wire feeding was not experimentally investigated within a single integrated setup in this work. However, a comparative analysis of the individual effects observed in Articles I, II, and III allows the evaluation of their potential interaction.

The results obtained for each technique demonstrate complementary mechanisms of action:

- Hot-wire preheating modifies the thermal balance, reducing the energy required for wire melting;
- Electromagnetic field assistance stabilizes melt-pool flow through Lorentz-force-induced damping;
- Dynamic wire feeding introduces temporal modulation of mass and energy transfer.

Based on these individual findings, it is expected that the integration of these techniques would produce synergistic effects, combining thermal, electromagnetic, and kinematic control of the process. Such integration is likely to result in:

- Enhanced stability of metal transfer;
- Improved control of melt-pool geometry;
- Reduction of spatter and process instabilities;
- Expansion of the operational window.

Therefore, although the combined application was not experimentally validated in the present work, the analysis of the individual mechanisms indicates a strong potential for synergistic interaction, suggesting that an integrated approach may provide a more robust and controllable W-LDED process.

Objective V – Correlation between physical mechanisms and bead geometry

Through high-speed imaging and cross-sectional analysis, a direct relationship between physical phenomena and bead geometry was established. The results showed that:

- Thermal control (hot-wire) influences energy distribution and penetration
- Electromagnetic forces modify melt-pool flow and stability
- Dynamic feeding controls wetting behavior and melt-pool size

These mechanisms directly impact bead height, width, penetration, and dilution, confirming that process physics can be actively controlled through the proposed techniques.

Despite the positive outcomes achieved, the implementation of the proposed techniques involved technical challenges and limitations that should be considered. The integration of inductive hot-wire preheating required careful control of electrical parameters to avoid overheating and ensure stable thermal conditions. The application of the electromagnetic field demanded precise positioning and calibration of the coil, as well as consideration of potential electromagnetic interactions with surrounding components. Dynamic wire feeding introduced additional system complexity, requiring accurate synchronization between wire motion and process conditions to avoid instabilities such as excessive detachment or insufficient material transfer. Furthermore, the combination of these techniques increases the number of process variables, making parameter optimization more complex. These aspects highlight the need for

careful system design, calibration, and control strategies, and should be considered in future developments to ensure robust and reproducible operation.

Final Remarks

The central hypothesis of this thesis was validated. The application of inductive hot-wire preheating, electromagnetic field assistance, and dynamic wire feeding promotes a more stable metal transfer regime by:

- Reducing thermal gradients
- Damping fluid-flow instabilities
- Synchronizing mass and energy transfer

This combined approach significantly enhances process stability, reduces sensitivity to disturbances, and improves deposition quality.

From a scientific perspective, this work contributes to a deeper understanding of the physical mechanisms governing metal transfer in W-LDED, particularly under liquid-bridge transfer conditions. From a technological perspective, the developed hybrid system demonstrates strong potential for industrial application, enabling more robust and controllable wire-based additive manufacturing processes. Additionally, it is important to highlight that this work resulted in the conception, design, and construction of an innovative research infrastructure capable of integrating inductive hot-wire preheating, electromagnetic field assistance, and dynamic wire feeding within a single experimental platform. This infrastructure enables advanced experimental investigation of metal transfer mechanisms and melt-pool behavior under combined thermal, electromagnetic, and kinematic control, significantly expanding the research capabilities in wire-based L-DED. The availability of such an integrated system opens new avenues for future studies, allowing the exploration of phenomena and process control strategies that were previously not accessible.

6.1 SUGGESTIONS FOR FUTURE WORK

Based on the findings and limitations identified throughout this doctoral research, several directions for future work are proposed:

a. Multilayer and three-dimensional deposition studies:

Extend the application of the integrated hot-wire, EMF, and dynamic wire feeding system to multilayer and complex three-dimensional builds, evaluating thermal accumulation, interlayer bonding, and geometric stability.

b. Closed-loop process control:

Develop real-time closed-loop control strategies by integrating high-speed imaging, thermal sensing, and electrical measurements to actively regulate wire motion, electromagnetic excitation, and thermal input during deposition.

c. Microstructural and mechanical characterization:

Investigate the influence of the hybrid control strategies on microstructure evolution, grain morphology, residual stresses, and mechanical properties of deposited materials.

d. Expanded material systems:

Apply the proposed hybrid W-LDED approach to different alloys, including aluminum, stainless steels, and nickel-based superalloys, assessing material-specific responses to thermal and electromagnetic assistance.

e. Electromagnetic field modulation strategies:

Explore the effects of time-varying or pulsed magnetic fields synchronized with dynamic wire feeding to further enhance melt-pool control and metal transfer stability.

f. Process scalability and industrial validation:

Evaluate the scalability of the developed system for higher deposition rates, larger components, and industrial-grade laser systems, including long-duration operational stability.

g. Numerical Multiphysics modeling:

Develop coupled thermal–fluid–electromagnetic numerical models to quantitatively predict melt-pool behavior and support the optimization of hybrid control parameters.

These future investigations will further consolidate the scientific foundation established in this thesis and contribute to the advancement of robust, adaptive, and industrially viable wire-based laser additive manufacturing processes.

7 COMPLEMENTARY REFERENCES

Considering that this thesis is structured in the format of scientific articles, all references used to support the theoretical foundation, experimental methodology, and discussion of results are fully presented within each respective article. Therefore, no additional complementary references are required beyond those already listed in Articles I, II, and III.

APPENDIX A – SYSTEM DESCRIPTION AND SCHEMATIC REPRESENTATION

A.1 General overview of the developed system

This appendix presents a description of the wire-feeding system developed in this doctoral research for application in Wire-Laser Directed Energy Deposition (W-LDED). The system was conceived to overcome limitations commonly observed in conventional wire feeders, particularly those related to mechanical rigidity, lack of wire conditioning, and limited control over the interaction between the filler wire and the melt pool.

The developed device integrates three advanced techniques into a single platform: inductive wire preheating (hot-wire), external electromagnetic field assistance (EMF), and dynamic wire feeding through controlled forward–backward oscillations. The primary objective of this integrated design is to provide enhanced control over mass and energy transfer during deposition, enabling improved process stability, robustness, and geometric consistency of deposited beads.

The system was designed to be modular and mechanically robust, allowing straightforward integration with an L-DED laser head while maintaining precise control of wire positioning relative to the laser beam and the melt pool. A schematic representation of the integrated system is shown in Figure A.1, illustrating the relative positioning of the laser head, wire feeder, inductive coil, electromagnetic coil, and substrate.

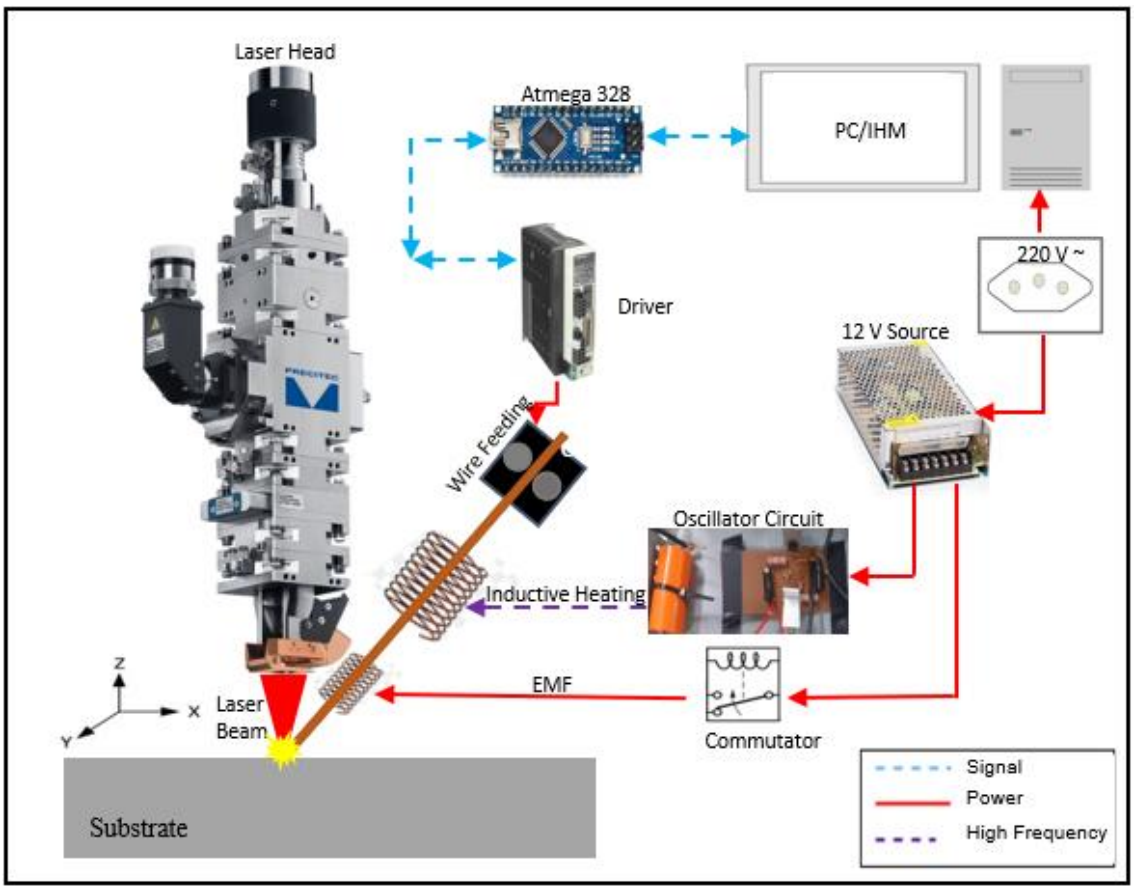


Figure A.1 - Schematic of the wire-fed L-DED system integrating dynamic wire feeding, inductive hot-wire preheating, and electromagnetic field (EMF) assistance. The setup includes the laser head, servo-driven wire feeder controlled by an ATmega328 microcontroller, inductive heating coil, electromagnetic coil, oscillator circuit, and power supply. Control signals, power lines, and high-frequency connections are indicated by different line styles.

A.2 Functional architecture of the system

The developed system is composed of four main subsystems:

1. **Dynamic wire feeding subsystem**, responsible for imposing controlled oscillatory motion of the wire;
2. **Inductive wire preheating subsystem (hot-wire)**, designed to increase wire temperature prior to interaction with the melt pool;
3. **Electromagnetic field application subsystem**, responsible for generating a static magnetic field in the deposition region;

4. **Mechanical integration and support structure**, ensuring rigidity, alignment, and repeatability.

A.3 Dynamic wire feeding subsystem

The dynamic wire feeding subsystem was implemented using a custom-built servo-driven wire feeder capable of modulating the wire feed rate through periodic forward and backward motion. The mechanical structure consists of a rigid modular frame manufactured from welded 30 × 30 mm square steel tubes, designed to minimize vibrations and structural deformation during operation. A 3 mm thick steel base plate supports the feeding mechanism, servo motor, and guiding components.

Wire motion is generated by an AC servo motor coupled to a wire pulling mechanism. The servo motor is driven by a dedicated servo drive and controlled via step-and-direction signals generated by a microcontroller-based control unit. The STEP signal defines the rotational increments through pulse frequency, while the DIR signal determines the direction of rotation, enabling precise control of wire advancement and retraction.

The linear wire displacement is calculated from the rotational motion of the feeding roller, which has a diameter of 30 mm. Approximately 10,280 pulses correspond to one full motor revolution, resulting in a linear wire displacement of approximately 94.2 mm. This configuration provides high positional accuracy and repeatability, with measured positioning errors below 1% for most operating conditions.

In dynamic feeding mode, each oscillation cycle is composed of two main phases: wire advancement and wire retraction. The total cycle time is defined by the oscillation frequency, and each phase occupies approximately half of this period. During the advancement phase, the wire is fed at a higher instantaneous speed to compensate for the subsequent retraction, ensuring that the desired net feed rate is maintained over time. Short transition intervals associated with deceleration, stopping, and re-acceleration occur at each reversal of motion and slightly influence the instantaneous interaction between the wire tip and the melt pool.

A.4 Inductive wire preheating subsystem (Hot-Wire)

The inductive wire preheating subsystem was designed to thermally condition the filler wire prior to its interaction with the laser-induced melt pool. The system consists of a copper induction coil positioned concentrically around the wire path, upstream of the deposition zone. Alternating current supplied to the coil generates a time-varying magnetic field, inducing eddy currents within the metallic wire and promoting Joule heating.

The coil geometry, number of turns, and positioning were selected to ensure efficient electromagnetic coupling with the wire while avoiding physical interference with the laser beam or the wire feeding mechanism. The inductive heating system operates independently of the dynamic feeding subsystem, allowing flexible adjustment of wire temperature without altering the mechanical feeding parameters.

The integration of inductive preheating aims to reduce the fraction of laser energy required to melt the wire, thereby modifying the thermal balance of the process and promoting more stable metal transfer conditions.

A.5 Electromagnetic field application subsystem

An electromagnetic field application subsystem was incorporated into the system to enable controlled interaction between an externally generated magnetic field and the molten metal during deposition. This subsystem consists of a dedicated electromagnetic coil positioned around the wire path and oriented such that the generated magnetic field intersects the melt pool region.

The coil was designed to generate a predominantly static magnetic field during operation, with its magnitude controlled by the applied current. The mechanical integration of the electromagnetic coil ensures stable positioning relative to the melt pool while maintaining electrical isolation from other subsystems.

Although the electromagnetic field parameters are discussed in detail in the main body of the thesis, this appendix focuses on the physical integration and functional role of the coil within the overall system architecture.

A.6 Integration with the L-DED process

The complete system was mounted on the laser deposition test bench and mechanically integrated with the L-DED laser head. Careful attention was given to the relative positioning of

the wire, laser beam, inductive coil, and electromagnetic coil to ensure consistent interaction conditions during deposition.

The modular design of the system allows rapid assembly and disassembly, reducing setup time and minimizing the risk of misalignment. Mechanical rigidity and precise guidance of the wire were prioritized to ensure reproducible deposition conditions across different experimental campaigns.

Overall, the developed system provides a versatile experimental platform for investigating advanced wire feeding strategies in L-DED, enabling systematic evaluation of the effects of dynamic feeding, inductive preheating, and electromagnetic field assistance on metal transfer behavior and bead geometry.